2008

Design And Experimental Study Of An Integrated Vapor Chamber -" Thermal Energy Storage System

Krishna Kota
University of Central Florida

DESIGN AND EXPERIMENTAL STUDY OF AN INTEGRATED VAPOR CHAMBER – THERMAL ENERGY STORAGE SYSTEM

by

KRISHNA M. KOTA
M.S. University of Central Florida, 2005
B. Tech. Jawaharlal Nehru Technological University, 2002

A dissertation submitted in partial fulfillment of the requirements
for the degree of Doctor of Philosophy in Mechanical Engineering
in the Department of Mechanical, Materials and Aerospace Engineering
in the College of Engineering and Computer Science
at the University of Central Florida
Orlando, Florida

Summer Term
2008

Major Professors: Louis Chow
Jay Kapat

ABSTRACT

Future defense, aerospace and automotive technologies involve electronic systems that release high pulsed waste heat like during high power microwave and laser diode applications in tactical and combat aircraft, and electrical and electronic systems in hybrid electric vehicles, which will require the development of an efficient thermal management system. A key design issue is the need for fast charging so as not to overheat the key components. The goal of this work is to study the fabrication and technology implementation feasibility of a novel high energy storage, high heat flux passive heat sink. Key focus is to verify by theory and experiments, the practicability of using phase change materials as a temporary storage of waste heat for heat sink applications. The reason for storing the high heat fluxes temporarily is to be able to reject the heat at the average level when the heat source is off.

Accordingly, a concept of a dual latent heat sink intended for moderate to low thermal duty cycle electronic heat sink applications is presented. This heat sink design combines the features of a vapor chamber with rapid thermal energy storage employing graphite foam inside the heat storage facility along with phase change materials and is attractive owing to its passive operation unlike some of the current thermal management techniques for cooling of electronics employing forced air circulation or external heat exchangers.

In addition to the concept, end-application dependent criteria to select an optimized design for this dual latent heat sink are presented. A thermal resistance concept based design tool/model has been developed to analyze and optimize the design for experiments. The model showed that it is possible to have a dual latent heat sink design capable of handling 7 MJ of

thermal load at a heat flux of 500 W/cm^2 (over an area of 100 cm^2) with a volume of 0.072 m^3 and weighing about 57.5 kg. It was also found that with such high heat flux absorption capability, the proposed conceptual design could have a vapor-to-condenser temperature difference of less than 10 ^{0}C with a volume storage density of 97 MJ/m^3 and a mass storage density of 0.122 MJ/kg.

The effectiveness of this heat sink depends on the rapidness of the heat storage facility in the design during the pulse heat generation period of the duty cycle. Heat storage in this heat sink involves transient simultaneous laminar film condensation of vapor and melting of an encapsulated phase change material in graphite foam. Therefore, this conjugate heat transfer problem including the wall inertia effect is numerically analyzed and the effectiveness of the heat storage mechanism of the heat sink is verified. An effective heat capacity formulation is employed for modeling the phase change problem and is solved using finite element method. The results of the developed model showed that the concept is effective in preventing undue temperature rise of the heat source.

Experiments are performed to investigate the fabrication and implementation feasibility and heat transfer performance for validating the objectives of the design i.e., to show that the VCTES heat sink is practicable and using PCM helps in arresting the vapor temperature rise in the heat sink. For this purpose, a prototype version of the VCTES heat sink is fabricated and tested for thermal performance. The volume foot-print of the vapor chamber is about 6”X5”X2.5”. A custom fabricated thermal energy storage setup is incorporated inside this vapor chamber. A heat flux of 40 W/cm^2 is applied at the source as a pulse and convection cooling is used on the condenser surface. Experiments are done with and without using PCM in the thermal

energy storage setup. It is found that using PCM as a second latent system in the setup helps in lowering the undue temperature rise of the heat sink system. It is also found that the thermal resistance between the vapor chamber and the thermal energy storage setup, the pool boiling resistance at the heat source in the vapor chamber, the condenser resistance during heat discharging were key parameters that affect the thermal performance. Some suggestions for future improvements in the design to ease its implementation and enhance the heat transfer of this novel heat sink are also presented.

This work is dedicated to Lord Sri Venkateswara without whose miraculous blessings, I would not have made it this far.

TABLE OF CONTENTS

LIST OF FIGURES

LIST OF TABLES

NOMENCLATURE

A	surface area of foam (m^2)
A_H	area of the heat source (cm^2)
a	vapor chamber long side (m)
a_s	specific surface area of the porous medium (m^2/m^3)
b	vapor chamber short side (m)
Bi	Biot number
c_p	effective specific heat of PCM and foam composite (J/kg.K)
c_{pf}	specific heat of foam (J/kg.K)
c_{pl}	specific heat of liquid phase of PCM (J/kg.K)
c_{pm}	latent heat of fusion of PCM averaged over the melting range (J/kg.K)
c_{ps}	specific heat of solid phase of PCM (J/kg.K)
c_{pw}	specific heat of TES unit column wall (J/kg.K)
D	thermal duty cycle
d_p	pore diameter (micrometers)
g	acceleration due to gravity (m/s^2)

h	convection heat transfer coefficient ($W/m^2.K$)
h_{int}	foam ligament and PCM interfacial heat transfer coefficient ($W/m^2.K$)
h_{lv}	latent heat of vaporization (J/kg)
h_{sf}	latent heat of fusion of the PCM (J/kg)
h_{sfo}	latent heat of fusion of the PCM in the operating temperature range (J/kg)
Ja	Jakob number
k	effective thermal conductivity tensor for PCM and foam composite (W/m.K)
k_{air}	thermal conductivity of air (W/m.K)
k_b	thermal conductivity of the bond/epoxy filling the contact air gap (W/m.K)
k_c	thermal conductivity of condensate (W/m.K)
k_{eff}	effective thermal conductivity of the foam and PCM composite (W/m.K)
k_{fe}	effective out-of-plane thermal conductivity of foam ligaments (W/m.K)
k_{foam}	thermal conductivity of the foam ligaments (W/m.K)
k_{fy}	foam thermal conductivity in Y-direction (W/m.K)

k_{fz}	foam thermal conductivity in Z-direction (W/m.K)
k_l	thermal conductivity of liquid phase of PCM (W/m.K)
k_{PCM}	typical thermal conductivity of PCM (W/m.K)
k_s	thermal conductivity of solid phase of PCM (W/m.K)
k_w	thermal conductivity of TES unit column wall (W/m.K)
k_{wl}	thermal conductivity of the working fluid in liquid state (W/m.K)
k_{yy}	effective thermal conductivity of PCM and foam composite in Y-direction (W/m.K)
k_{zz}	effective thermal conductivity of PCM and foam composite in Z-direction (W/m.K)
L	height of PCM and foam composite (m)
M	molecular weight of the working fluid
m_{PCM}	total mass of PCM present in the VCTES system (kg)
m_{tot}	total mass of VCTES heat sink (kg)
N	number of fins per unit inch; Boolean NO
Nu_p	pore Nusselt number

$\boldsymbol{n}$	unit normal
n	number of columns
p	ratio of total mass of PCM to the total mass of the VCTES expressed as a percentage
pc	assumed critical value for the ratio of total PCM mass to total VCTES mass expressed as a percentage
P_{sat}	normal pressure (gage)/vapor saturation pressure (atm) (=P)
Pr	Prandtl number
Q	total heat absorption capacity of the VCTES heat sink (MJ)
Q_m	heat storage capacity per unit mass (MJ/kg)
Q_v	heat storage capacity per unit volume (MJ/m3)
q	heat flux (W/m^2)
q_C	heat flux on the condenser (W/cm^2)
q_{colf}	column maximum heat flux absorption capability with foam inside columns (W/cm^2)
q_H	heat flux from the heater (W/cm^2)
q_i	heat flux on each column (W/cm^2)

R_u	universal gas constant (J/kg.K)
r	ratio of used PCM mass to the total PCM mass expressed as percentage
rc	assumed critical value for the ratio of used PCM mass to the total PCM mass expressed as percentage
T	temperature field in PCM and foam composite (K)
T_0	initial temperature of the transient problem (K)
T_C	Condenser surface temperature (K)
T_H	heater surface temperature (K)
T_{inf}	ambient temperature (K)
T_m	melting temperature of the PCM (K)
T_{PCM}	PCM temperature (K)
T_{sat}	actual value of vapor saturation temperature (K)
T_v	vapor temperature (K); guess value of vapor saturation temperature (K)
T_w	temperature field in column wall (K)
T_{wall}	column outside wall (on the vapor side) temperature (K)
Time	temporal variable at which a numerical solution is stored (s)

t	temporal variable (s)
t_{air}	thickness of the air gap (m)
t_b	thickness of a thermal conductive bond/epoxy filling the contact air gap (m)
t_c	vapor chamber plate thickness (mm)
t_p	pulse heat load on time (s)
t_w	thickness of the solid walls of the column (m) (= t_{wall})
U	set of initial guess variables
$\boldsymbol{V}$	result set
V	volume of foam (m^3)
v_{lv}	specific volume change during phase change (m^3/kg)
W	width of the foam filled PCM composite (m)
x	spatial coordinate in the Cartesian X-direction (m)
x	length of the TES column (m)
Y	Boolean YES
y	spatial coordinate in the Cartesian Y-direction (m)

y	width of the TES column (mm)
z	spatial coordinate in the Cartesian Z-direction (m)
z	height of the TES column (m)
δ	condensate film thickness (m)
ΔT_{VC}	temperature difference between vapor and condenser (K)
ΔT_{VPCM}	temperature difference between vapor and PCM (K)
ΔT_{PCM}	temperature difference between PCM and condenser surface (K)
ΔTc_{VC}	assumed critical temperature difference between vapor and condenser (K)
δT	PCM melting range (K)
δT_o	operating temperature range of VCTES heat sink within PCM melting range (K)
ε	foam porosity
ρ	effective density of PCM and foam composite (kg/m^3)
ρ_c	density of condensate (kg/m^3)
ρ_f	density of foam (kg/m^3)
ρ_l	density of liquid phase of PCM (kg/m^3)

ρ_s	density of solid phase of PCM (kg/m^3)
ρ_v	density of vapor (kg/m^3)
ρ_w	density of TES unit column wall (kg/m^3)
ρ_{wl}	density of the working fluid in liquid state (kg/m^3)
ρ_{wv}	density of the working fluid in vapor state (kg/m^3)
σ	accommodation coefficient
σ_{max}	maximum stress developed in any of the vapor chamber walls (MPa)
σ_y	yield strength of the vapor chamber material (MPa)
μ_l	viscosity of the working fluid in liquid state (Pa.s)
v	Poisson's ratio for the vapor chamber material

CHAPTER ONE: INTRODUCTION

Future electronic systems will involve small size, lightweight and compact components that release very high waste heat in a pulse. Miniaturization of such systems will generate large heat fluxes during the pulse time, which will require the development of an efficient thermal management system.

A key design issue is the need for fast charging so as not to overheat the pulse heat generating electronic device. In conventional passive latent heat sinks employing either thermal energy storage (TES) using phase change materials or using the heat pipe phenomenon, the heat transfer path comprising of heat absorption, storage and discharge each will have either high thermal resistance or a low rate of heat transfer. For instance, a latent solid-liquid phase change TES facility, if employed as a heat sink cannot provide for rapid heat absorption since most of the available solid-liquid phase change materials (PCMs) have extremely low thermal conductivities and since heat transfer occurs by diffusion. Inability of heat sink to quickly absorb heat from the heat source would result in rapid temperature rise of the heat source material and thus will eventually cease its functioning. This degradation of the performance of the heat source or component being cooled will be even faster if the heat fluxes that it generates are very high. Hence, most of the latent TES devices employing phase change materials are designed as heat spreaders with a large size both at the heat absorption end and at the heat dissipation end. Low thermal conductivities of phase change materials also hamper the swiftness of heat storage in solid-liquid phase change heat storage facilities. Liquid-vapor latent phase change heat sinks like heat pipes always have the limitations of critical heat flux of the working fluid and evaporator dry-out at high heat fluxes.

Suggestions were made by prior researchers to improve the rapidity of heat storage process in solid-liquid phase change heat sinks and successful attempts have been made along those lines. Some of them include using fins and metal [1] or graphite [2] foams along with a phase change material (PCM) enclosed in a container or mixing thermal conductive metal particles or adding liquid metal in the phase change material to form a colloidal suspension [1]. Of these, employing porous graphite foam to enhance the heat transfer of a TES system proved very effective and successful [2]. Even on improving the thermal conductivity of PCMs, it is not possible to use them for high heat flux applications owing to their inherently low latent heat values compared to the liquid-vapor phase process, the latent heat of which is more suitable for absorbing high heat fluxes.

This work presents the concept of a dual latent heat sink intended for low thermal duty cycle, high heat flux electronic heat sink applications. This new heat sink design combines the features of a vapor chamber with rapid thermal energy storage employing graphite foam inside the heat storage facility along with phase change materials. A vapor chamber acting as a heat spreader enables for more uniform temperature distribution along the surface of the device being cooled while incorporating the rapid liquid-vapor phase change heat absorption feature at the heat source. Hence, the vapor chamber feature elevates the system thermal conductivity by about hundred to thousand times that of pure metallic copper. This feature coupled with the rapid TES facility in the design makes this integrated system an interesting and useful one for multiple thermal management applications. The focus of this work is to use phase change materials as a temporary storage of waste heat for heat sink applications. The reason for storing the high heat fluxes temporarily is to be able to reject the heat at the average level when the heat source is off.

If heat has to be rejected in real time, the condenser has to be very large. The current design incorporates all the attractive features like fast charging ability for moderate-to-high heat fluxes, compactness, reliability and lightweight.

Potential application areas include, but are not limited to, temperature control of IGBTs and MOSFETs, laser diode cooling, actuator and avionics cooling in aircraft, thermal management of electronics in directed-energy weapon (DEW) systems and their subsystems, smartphones cooling and battery thermal management for electric or hybrid vehicles., thus covering a wide gamut of heat flux applications.

The following sections briefly describe the fundamentals of vapor chamber phenomenon and thermal energy storage followed by the integration concept of vapor chamber and thermal energy storage (VCTES) with phase change materials.

Vapor Chamber Phenomenon

A heat pipe (Figure 1) is essentially a closed tube internally lined with a porous wick structure. The wick is saturated with a proper amount of working fluid. When a portion of the heat pipe is exposed to heat, the fluid in the heated portion vaporizes picking up thermal energy. It flows to the condenser portion and releases the thermal energy. Condensed fluid is returned by capillary action in the wick back to the hotter portion.

This thermodynamic cycle continues as the thermal energy is transferred from one end to the other. The key phenomenon that makes the heat pipe a very efficient heat transfer device is its near isothermal operation. Heat pipes do not have a specific value for thermal conductivity like solid materials due to the two-phase heat transfer. A heat pipe's effective thermal

conductivity (usually 1000 W/m.K to 50000 W/m.K) will change with the amount of power being transferred, the evaporator and condenser sizes, and the transport distance.

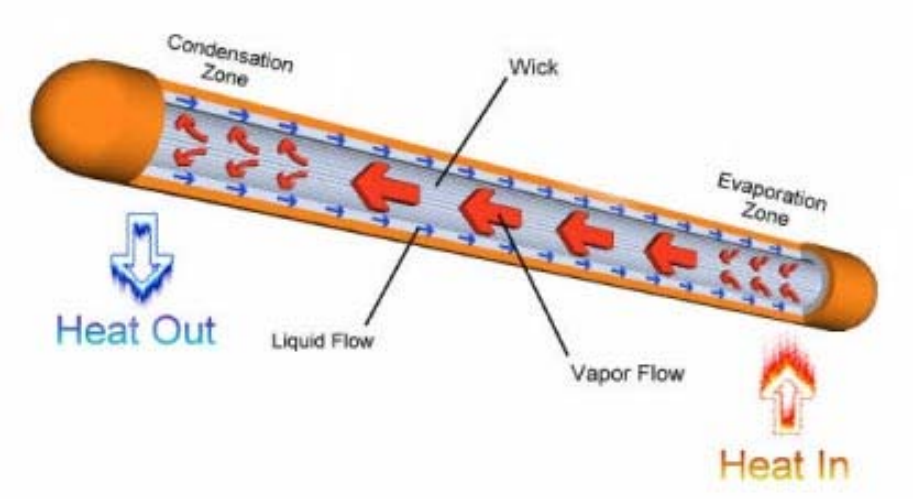

Figure 1: Heat pipe phenomenon [3]

Heat pipes are totally passive heat transfer systems having no moving parts, and they require no external means of energy to operate. They can be manufactured in a number of shapes and sizes. Their lightweight and compact size also makes them the ideal choice for space-constrained applications.

A vapor chamber is essentially a heat pipe but used more in the context of a heat spreader i.e., the same device is termed as a heat pipe if its primary operation is transfer of heat from one place to another and is termed as a vapor chamber if it is used for distributing heat from a concentrated source over a large area. Therefore, by virtue of their application, heat pipes are usually long with small lateral dimensions whereas vapor chambers are short with big lateral

dimensions. One variety of heat pipes are also proposed where they are used for heat spreading and are termed as flat heat pipes [4].

Thermal Energy Storage

For many energy technologies, storage is a crucial aspect. Energy can be stored in many forms like classified in Figure 2.

TES can be defined as the temporary storage of high- or low-temperature energy for a later use. Thermal energy can be stored either by elevating or lowering (as in cold TES where the cooling capacity is stored by lowering the temperature) the temperature of a substance i.e., by altering its sensible heat, or by changing the phase of the substance i.e., by altering its latent heat or by a combination of the two. A prominent example of TES is solar energy storage, where the solar energy collected and stored during day is used for future use. TES, specifically in the current work differs from this in the sense that the energy stored here is pulsated waste heat from a heat source that can be rejected over a long period and is not intended for future use. This temporary storage of high-pulsated heat coupled with lethargic discharging can considerably lower the heat sink size, which forms an attractive aspect for thermal management applications.

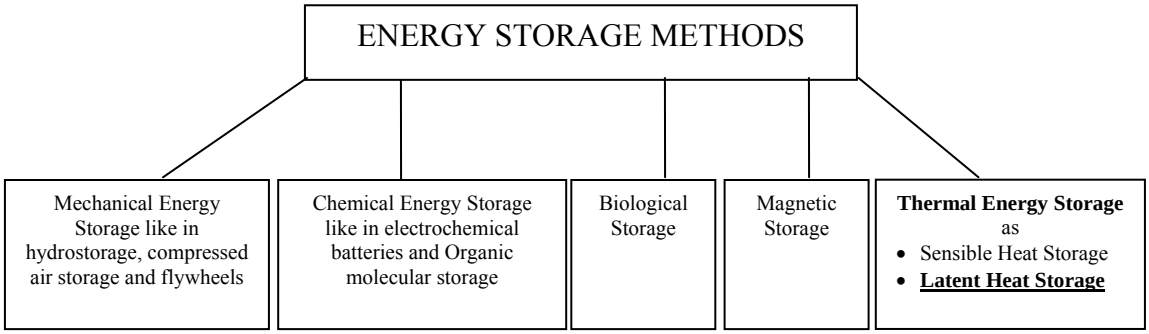

Figure 2: A classification of energy storage methods [5]

The main advantage of latent TES over sensible TES is the energy storage density (ESD), which is comparatively more for latent heat storage systems than sensible heat storage systems because the latent heat change is usually much higher than the sensible heat change for a given medium, which is related to its specific heat. Latent TES offers the operational advantage of a nearly isothermal storage and hence is a readily acceptable method for coupling with a vapor chamber phenomenon. Latent TES systems also are more compact and light-weight over sensible TES devices again because of more energy storage density.

Of the possible isothermal phase transitions involving absorption or release of latent heat for TES, the most suitable ones are the solid-liquid and solid-solid [6,7] transitions. Solid-vapor and liquid-vapor transitions (even though can involve the highest energy storage density) present the disadvantage of very large volume changes.

Any latent heat TES system should have the following three components – a heat storage medium (phase change material) that undergoes a phase transition within the desired operating temperature range and the bulk of heat added is stored as latent heat, containment (encapsulation

material) for the storage substance to prevent mixing with other working fluids in the same system, a heat exchange substance (conducting phase change media/fluid in the vapor chamber) for transferring heat from the heat source to the storage medium and from the latter to the heat sink.

The most important criteria to be met by the storage material for latent TES in which the material undergoes a solid-liquid or a solid-solid phase transition are as follows:

- High transition enthalpy per unit mass,
- Ability to fully reverse the transition,
- Adequate transition temperature,
- Chemical passivity with the vapor chamber material,
- Transition with a minimal volumetric change,
- Non-toxicity, and
- Low cost concerning the application for which it is intended for use.

Concept of Integrated Vapor Chamber – Thermal Energy Storage (VCTES) System

Figure 3 shows the concept of integrated VCTES system used as a heat sink in spray cooling application. It consists of a solid container with a liquid-vapor phase change conducting fluid/Heat Transfer Fluid (HTF). Columns/containers, which are adequately spaced are attached to the top of the container and encapsulate a high thermal conductivity foam infiltrated with phase change material for thermal energy storage.

When the heat load is on, the working fluid in the spray-cooling chamber (or any other heat source) absorbs the heat and changes its phase from liquid to vapor and the vapor spreads in

the VCTES container. Once the vapor contacts the cold surfaces of the columns, it condenses and the PCM inside the columns absorbs the heat from the vapor and melts. The condensate then drips down because of gravity. When the heat load is off, the encapsulated phase change material (EPCM) refreezes by conducting heat laterally through the VCTES walls, which is the condenser portion of the vapor chamber, and then the heat is discharged to the ambient. This process of charging during heat ON time and discharging during heat OFF time repeats periodically over the thermal duty cycle (Figure 4).

As shown in Figure 4, during the heat load OFF time, the heat flux from the heat source may not be zero. In some applications, there may still be some very low heat flux emanating from the source during the non-peak period/heat OFF time. Since most/all of the PCM may be in a molten state at the end of heat ON time and has to discharge heat during the heat OFF time, it may not be able to absorb any more heat (since most/all of it is in liquid phase). In this case, the condenser surface can directly participate in such applications and discharge the small non-peak period heat to the ambient. The rate of discharge can be increased by including condenser fins.

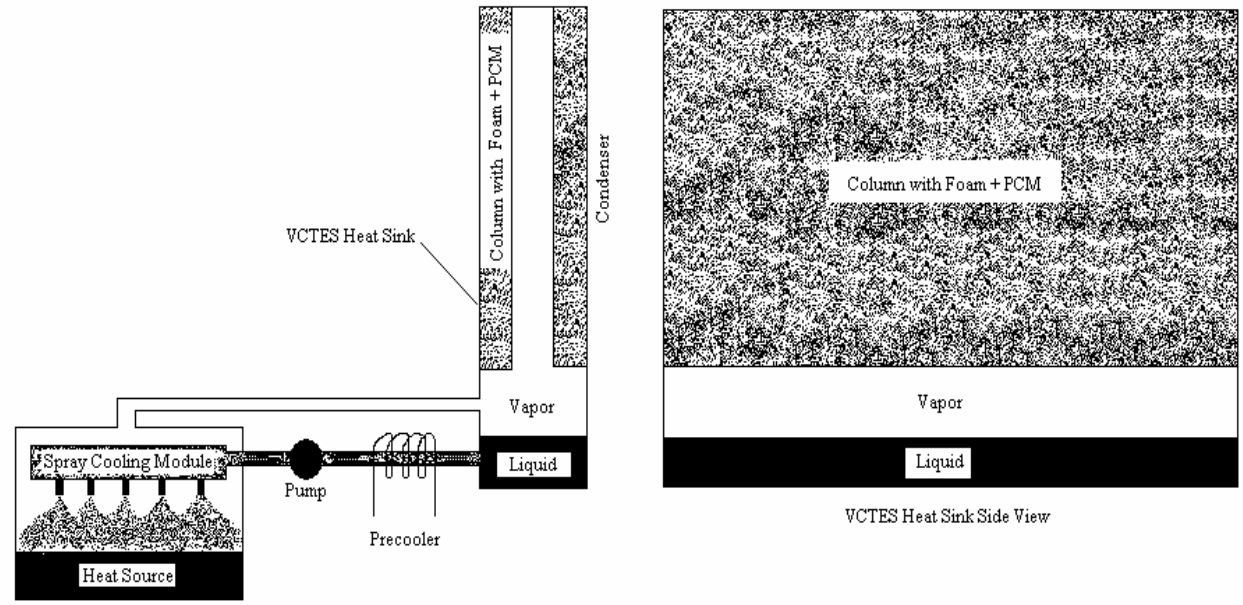

Figure 3: Concept of integrated VCTES system (applied to a spray-cooling module)

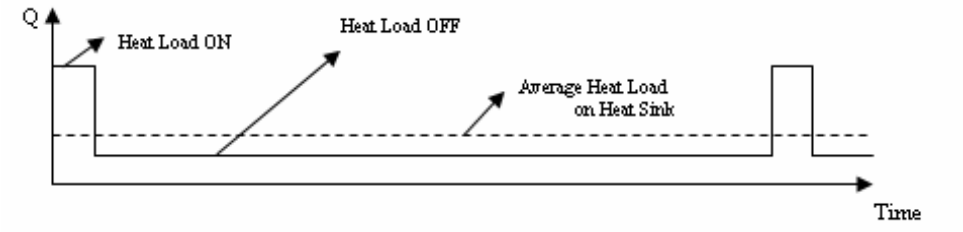

Figure 4: Pulsated heat load diagram

A key advantage of this design comes from using liquid-vapor phase change for heat absorption and using solid-liquid phase change as an intermediate condenser unlike most heat sinks where either one of PCM or a heat pipe is directly used to absorb and dissipate heat. Since liquid-vapor phase change is much faster compared to diffusion in a PCM, it is advantageous to first absorb pulse heat from the heat source rapidly using liquid-vapor phase change and then

transfer it to PCM. The use of PCM as a second latent heat sink helps in reducing the size of an otherwise condenser comprising simply of a metal plate closing the vapor chamber (on thermally opposite side of the heat source). For high heat fluxes (on the order of 500 W/cm^2), the size of a condenser plate can be very large increasing the heat sink size. An intermediate sink in the form of PCM significantly helps in reduction of the condenser size.

The key focus of this work is to design and experimentally demonstrate that the proposed integrated vapor chamber – thermal energy storage heat sink is practicable and has a fast charging ability (i.e., can remove and transport pulse heat from a simulated heat source and store the heat in phase change materials so that the heat can be rejected to air over the entire duty cycle via heat spreading).

CHAPTER TWO: LITERATURE REVIEW

Little work has been reported in open literature, which deals with an integrated vapor chamber and thermal energy storage system. Chang et al. [8] studied a similar configuration but comprising of axially grooved heat pipe incorporated with TES to mitigate pulse heat loads. The one-dimensional vapor flow path was along the axis of the heat pipe as against the current study where there will be a distribution of vapor everywhere in the vapor chamber. A three dimensional alternating direct implicit (ADI) scheme was used to numerically simulate the problem and EPCM was used to model TES. They found that such a configuration could be very effective in averaging of pulsated heat loads which otherwise show adverse effects on normal heat pipe operation.

Advanced Cooling Technologies, Inc. (ACT) has developed a high performance thermal storage technology that combines heat pipes with proprietary materials to provide a very effective way to acquire and store large, high heat flux thermal loads [9]. The energy storage density (ESD) of their new materials can be over six times that of a typical PCM. The thermal conductivity of the new materials is approximately fifty times of that of a typical PCM. The materials are operational in a wide temperature range of -20 to 400°C. Figure 5 compares the test results of a PCM device (pink line) and a device using the new material (blue line) for an integrated heat pipe/TES system. The thermal conditions were the same for both devices. As seen, the new material was able to absorb the heat load and maintain the system at a lower temperature than the PCM. No reported numerical or detailed experimental work could be found on the work by ACT in open literature.

Zuo et al. [10] reported a heat pipe having a wick structure made of micro-encapsulated phase change materials sintered together to form the wick. Their configuration is claimed to be able to handle peak excess thermal loads in a duty cycle. Encapsulated phase change materials that form the wick absorb the excess heat. Different variations have been mentioned such as a one containing two heat pipes where the first heat pipe may be a conventional one and the second contains micro-encapsulated PCM wick.

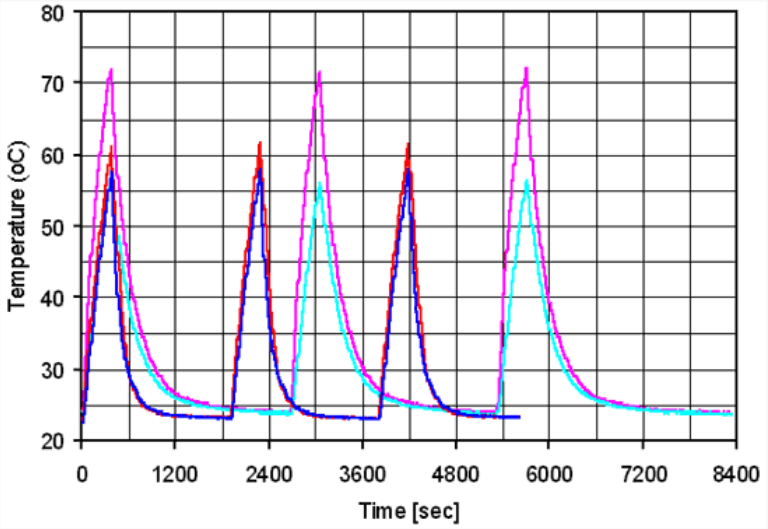

Figure 5: ACT integrated heat pipe/ TES system with a proprietary PCM for TES (blue) – comparison with a normal PCM for TES (pink) [9]

The design of Zuo et al. and the current work are intended for similar applications but the latter has the following advantages as a comparison:

- Compactness (especially because of the comparatively small condenser portion size),

- Can handle high heat fluxes (> 100 W/cm^2) since the heat absorption is not limited to evaporation,
- Good heat conducting path, which implies faster charging,
- More thermal energy storage because of the presence of macro-PCM,
- The design by Zuo et al. may require more PCM to take sudden high heat loads because of which more mass of their system is possible, and
- A lot of PCM exists on the condenser portion and so is not in direct contact with the HTF unlike in the design of the current work.

Some of the prior attempts in dual latent heat sinks were reported in References [11-24]. In Reference [16], a heat pipe is used to transfer heat from a solar panel and then store in PCM for temperature control of buildings. In Reference [17], a unidirectional heat pipe is coupled with PCM lying outside of it and its key motive for using PCM is for temporary absorption of heat during reversal environmental conditions outside the heat sink system. Reference [18] mentions the idea of using a heat pipe to transfer heat from human body to a chunk of PCM lying outside the heat pipe. Reference [19] discusses a concept of using of PCM as an interface between a hot object and a heat pipe. Reference [20] proposes to use a heat pipe as an auxiliary unit for a TES unit or in conjunction with the TES unit by its side for thermal management of electronics in a closed housing. Reference [21] proposes to use PCMs in parallel operation with an oscillating heat pipe to absorb heat from an electromechanical actuator. In Reference [22], PCMs are proposed for use outside a heat pipe to store excess heat emanating from a laptop computer.

The novelty of the current concept lies in using PCM for TES inside a vapor chamber (thereby tremendously increasing the condensation area for vapor) and thus coupling both the

features but not in simply using TES and vapor chamber as separate entities in series or in parallel. In some known heat sinks [10,23], that comprise PCM encapsulated spheres lying inside a heat pipe, a good heat conducting path does not exist between PCM encapsulated spheres (because of point-to-point contacts that exist between clusters of spheres and low thermal conductivity of the sphere materials) during discharging. In addition, no thermal conductivity enhancement mechanism was used in any of the prior similar attempts. Other key improvements in the current design (that have not been attempted before) are elucidated in a detailed manner in Chapter Three under the section on design considerations.

CHAPTER THREE: DESIGN AND OPTIMIZATION TOOL

The goal of developing a design and optimization tool is to optimize the parameters for the selected VCTES system configuration based on design considerations to arrive at a best possible final design that simultaneously meets the requirements of a particular application.

The following sub-section outlines the key design considerations to arrive at a final design for the VCTES system that needs to be optimized.

Key Design Considerations

Shape of the Containers for Thermal Energy Storage

Three types of most common shapes were considered for containers encapsulating the PCM; spherical, cylindrical and rectangular. Table 1 provides a comparison of the three shapes for choosing the best one for TES.

From Table 1 it can be seen that, while spherical TES is available off-the-shelf [25-30] and both spherical and cylindrical shapes provide for low heat flux requirements to the TES (owing to their more surface area to volume ratio compared to rectangular containers), they have a plethora of disadvantages with regards to key thermal performance parameters like heat absorption time, thermal resistance, easiness of using foam, vapor flow resistance, heat discharging path and in aiding the condenser performance by providing fins as extensions of the columns themselves. Though cylindrical shape is reasonably competitive with rectangular shape, the biggest disadvantage of using cylindrical shape for the TES containers is to have the foam cut also in the cylindrical shape. This is hectic and expensive as commercially available graphite foam is mostly in cuboidal shape [31]. In addition, using cylindrical foam pieces in TES will

increase the thermal contact resistance since it is difficult to cut and match the circular contour of foam with the inside of a cylindrical TES container. This is especially true if custom spherical containers are intended to be made. Rectangular containers also provide for a low thermal resistance and low charging time [32] since for the same surface area as a sphere or cylinder, a cuboid has the least distance from its circumference/perimeter to the center. Therefore, a cuboid is the optimum shape for TES storage containers.

Table 1: Comparison of different shapes for TES containers

	Spherical	*Cylindrical*	*Rectangular/Cuboidal*
a) Commercial availability	Yes	Yes	No
b) Manufacturability	Easy	Moderate	Moderate
c) Heat absorption time	High	Moderate	Low
d) Thermal resistance	High	Moderate	Low
e) Incorporation of foam in TES	Difficult	Moderate	Easy
f) Vapor flow resistance	High	Low	Low
g) Improve condenser performance during discharging by providing column extensions as fins	No	Yes	Yes
h) Heat flux on each container	Low	Moderate	Moderate
j) Good heat discharging path	No	Moderate	Yes

Choice of Phase Change Material

A solid-liquid PCM is any material, which absorbs heat when it melts and releases that heat when it solidifies. This phase change enables the PCM to act as heat storage media.

Paraffin wax, metal hydrates, zeolites (because of their hygroscopic property), metal hydrides and fatty acids are examples of PCMs that can be used for latent TES. Paraffins usually change phase over a large temperature range depending on their purity. n-paraffins are generally preferred over iso-paraffins as their solid-liquid transition occurs over a narrow temperature range. A major problem in obtaining pure paraffins is the cost.

PCMs must satisfy the criteria of having a melting point at the required operating temperature, a high ESD so that the overall system is compact, a high thermal conductivity and latent heat so that charging and discharging of TES happens over a very small temperature change and no supercooling (usually happens for zeolites and metal hydrates) during freezing and should be chemically compatible and non-toxic. It also should be commercially available at a low cost.

In addition to the above, an ideal PCM must have a minimal change in volume during phase change. Volume change during phase change happens because of density difference between solid and liquid phases and is directly related to thermal expansion of the PCM. High thermal expansion in a constant volume container requires storing less PCM in its solid form, which means less TES. Another consequence of large density difference between solid and liquid phases occurs during freezing of a molten PCM. During discharging, when a PCM with large thermal expansion coefficient releases the stored energy to solidify, it leaves huge voids because of considerable decrease in the volume. These voids act as thermal barriers to heat conduction and thus affect the performance of a latent TES. Efficient heat transfer and high ESD in any TES system require thin walls for encapsulating PCM. During charging, a large void present adjacent

to the thin wall would create a localized hot spot, leading to possible melting of the PCM containers.

A majority of TES applications demand for isolation of PCM from the outside media, which gave rise to the concept of "Dry PCM". Dry PCM involves two categories – the first type undergoes a solid-to-solid phase transition [6,7] or composites that are engineered so that the liquid phase is not apparent, while the second type is a solid-liquid phase change material enclosed in a capsule (usually a microcapsule [25-30]).

Microencapsulation is a process that separates a selected material from its surroundings or the media in which it is placed. Depending on the size of the final capsule, they are termed as "Micro-encapsulated PCM" or "Macro-encapsulated PCM". Micro-encapsulated PCM are 50-100 μm in diameter with impermeable semi-rigid shell walls of typically less than 1μm thickness. The core PCM comprises 80-85% of the composite mass. An example for macroencapsulated PCM is 2-4 mm sized Encapsulated Phase Change Material (EPCM) capsules – COOLBEADS® [30], which are simply an agglomeration of micro-EPCM further encapsulated with another outer shell.

Table 2 provides a comparison of various available phase change materials and their features and properties. To have a reasonable benefit of using the PCM for temporary energy storage, the sensible heat amount must be limited by limiting the temperature rise (equivalent to a small melting range). The vapor temperature inside the vapor chamber depends on the melting range of the PCM. Smaller melting ranges help the PCM latent heat effect compete with the TES system sensible heat. Other than pure paraffins, most organic phase change materials have

heating history dependent properties with a melting temperature range and undergo incongruent melting. Some of them even exhibit supercooling tendency like inorganic salt hydrates.

Table 2: PCM comparison

	Organic Paraffins	*Metal / Salt Hydrates*	*Fatty Acids*	*Organic-Inorganic Eutectics*	*Glucose Isomers*
Heat of Fusion	220-300	170-340	20-50	200-500	185*
Density (kg/m^3)	800-970	900-2200	800-900	1200-1800	1500-
k (W/m.K)	~ 0.2	0.6-1.2			
Thermal Expansion	Medium to	Low	High	High	
Congruent Melt	Yes	Mostly No	No	No	
Supercooling	No	High		High	Low
Melting Range	Mostly Yes	No			
Corrosiveness	Low	High	Mild	Mild	
Toxicity	No	High	Mild	Mild	No

From Table 2, it can be observed that both salt hydrates and pure paraffin waxes (with a narrow melting range) are the potential candidates for use in the VCTES system. The right choice of PCM depends on the conditions specific to the intended application and the selection of HTF.

Selection of Heat Transfer Fluid

In the current heat sink design, fast heat absorption from a source is possible because of liquid-vapor phase change of a HTF unlike in some prior heat sink designs where the TES itself acts as the primary heat sink. Heat absorption rate would be very slow in such heat sinks because

* Depends on the rate of heating

of poor thermal conductivities of most of the available solid-liquid phase change materials and because of heat transfer by conduction. Therefore, selection of a right HTF in the current heat sink is crucial. Any liquid-vapor phase change material with a high latent heat would be the ideal choice. Water can be used as the working fluid in the system since it has a high value of latent heat of vaporization and will eliminate the risk of working with hazardous fluids in the vapor chamber. It will also reduce the cost.

Optimization Tool

The VCTES system concept is optimized using a network based resistance analysis. This simple model serves as a first design step and is not only useful in arriving at a fast prototype design for the experiments but also useful in filtering out the most important phenomena that need detailed numerical attention. The VCTES system operation broadly includes the following five functioning sub-processes:

- Depending on the application, liquid-vapor phase change of the HTF on heater surface producing vapor,
- Flow and distribution of vapor in a vapor chamber having multiple PCM encapsulated columns/containers,
- Vertical film condensation of vapor on columns and simultaneously, the
- EPCM phase change/melting inside the columns, and
- EPCM freezing by conduction through vapor chamber walls (or column walls depending on the selected configuration) to the condenser.

These processes can be characterized by a group of resistances signifying heat charging and discharging modes as follows,

R1 – liquid-vapor phase change process resistance

R2 – vapor-condensate interfacial resistance

R3 – condensate film resistance

R4 – column wall resistance (lateral direction)

R5 – PCM conduction resistance without foam

R6 – PCM conduction resistance without foam (same as *R5*)

R7 – vapor chamber plate conduction resistance (along the thickness in the lateral direction)

R8 – convective resistance of the condenser

R9 – contact resistance in the air gap between column inside walls and foam

R10 – conduction resistance in the bond between column inside walls and foam

R11 – PCM conduction resistance with foam

The assumption made for this model is that at large times, all the processes can be approximated as steady. Since the time will be a maximum at the end of charging mode, the Fourier number will be large which implies heat conduction in any of the above processes will be large compared to the heat stored. Therefore, the thermal energy storage can be neglected and a resistance can be used to define the process. Similar is the case for processes during discharging mode. In addition, at any time-instant, the system can be assumed to be in an instantaneous

steady state. Even though this is approximate, the model with this approximation reasonably serves as a fast design tool for experiment design purposes. Figure 6 shows the heat sink schematic in terms of the dimensional variables. Figure 7 shows the resistance paths for the two modes of operation of VCTES system. A single column geometry showing the dimensional variables is shown in Figure 8. It must be noted that in defining some of the resistances, the dimension ($z+t_{wall}$) is approximated as z for simplicity. This is true because of the fact in the design that $z >> t_{wall}$ or t_c.

In the model, *R1* is evaluated depending on the intended application and the mode of heat removal at the heater surface, which can be, for example, pool boiling or spray cooling. *R2* is evaluated using the Maxwell velocity distribution for vapor from the kinetic theory of gases, which helps in knowing the flux of molecules passing through the vapor-condensate interface. Knowing the mass flux and latent heat, the heat flux to the interface can be evaluated and this was used to get the interfacial resistance *R2* as,

$$R2 = \left(\left(\frac{2\sigma.x.z}{2-\sigma} \right) \left(\frac{{h_{lv}}^2}{T_{sat} v_{lv}} \right) \left(\frac{M}{2\pi R_u T_{sat}} \right)^{\frac{1}{2}} \left(1 - \frac{P_{sat} v_{lv}}{2h_{lv}} \right) \right)^{-1} \quad (1)$$

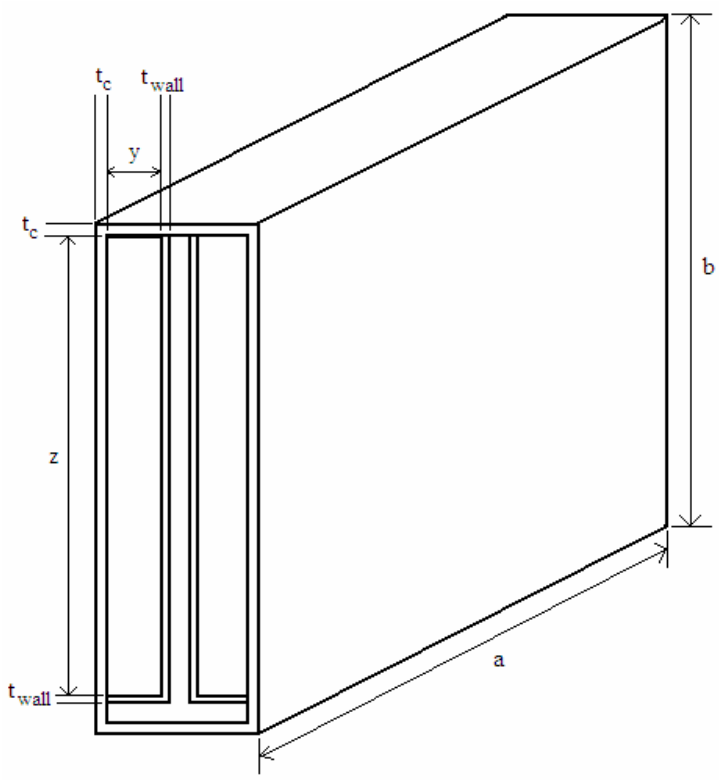

Figure 6: VCTES schematic showing dimensional design variables

Detailed explanation of the above procedure is presented in Reference [33]. An accommodation coefficient of 0.03 was used in the calculations, which is a typical value for water. Knowing *R2* helps in knowing whether the vapor side temperature boundary condition for the film condensation is T_{sat} or if there is a temperature drop at the liquid-vapor interface because of vapor flow.

R3 is calculated from the Nusselt theory [33] for steady laminar film condensation on a vertical wall as follows.

$$R3 = \left(\frac{0.79 x^4 z^3 g \rho_{wl} \left(\rho_{wl} - \rho_{wv} \right) {k_{wl}}^3 h_{lv}}{\mu_l \left(T_{sat} - T_{wall} \right)} \right)^{-0.25} \tag{2}$$

All the resistances *R4 to R11,* except *R8* are calculated assuming pure conduction and were evaluated accordingly as per the geometry as follows.

$$R4 = \frac{t_{wall}}{k_{wall}.x.z};\ R5 = \frac{y}{k_{PCM}.x.z};\ R7 = \frac{t_c}{k_c.x.z};\ R9 = \frac{t_{air}}{k_{air}.x.z};\ R10 = \frac{t_b}{k_b.x.z};\ R11 = \frac{y}{k_{eff}.x.z} \tag{3}$$

$$k_{eff} = k_{foam}.(1-\varepsilon) + k_{PCM}.\varepsilon \tag{4}$$

Natural convection in the melt can be neglected for PCM phase change in foams because of a very low Rayleigh number. This is because of increased capillary effect and hence a reduced gravity effect along with a low temperature difference between foam ligament and PCM for graphite foams. It is shown in Reference [34] that for foams with surface area to volume ratios of more than 1575 (m^2/m^3), a single temperature representative of both foam and PCM can be used. For carbon foams, this ratio is about 20,000 (m^2/m^3) [35] and therefore, it is reasonable to assume foam and PCM as one composite material and use effective properties based on foam porosity to evaluate the conduction resistance *R11*.

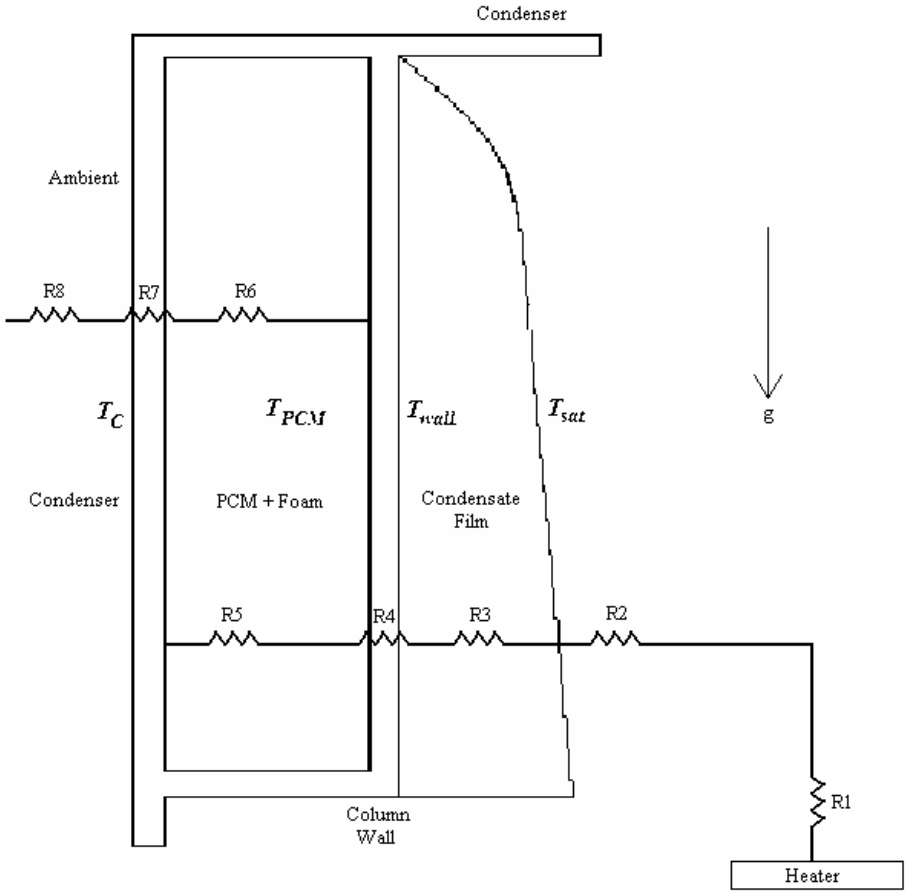

Figure 7: VCTES charging and discharging paths

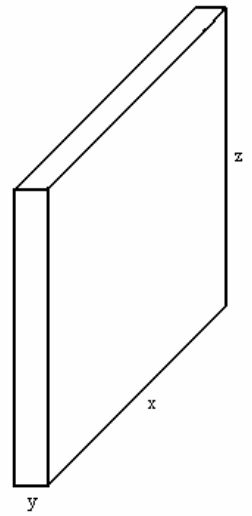

Figure 8: Geometry of a single TES column inside VCTES heat sink

The condenser side thermal resistance *R8* is evaluated from the convective coefficient, which in turn depends on the requirement as dictated by the condenser side heat flux.

$$R8 = \left(\frac{x.z.q_C}{T_C - T_{air}} \right)^{-1} \tag{5}$$

$$q_C = \frac{q_H.D.A_H}{n.x.z} \tag{6}$$

While finding the resistance values, a conservative approach is used wherever applicable. Detailed flow chart for optimization of the mathematical model is shown in Figure 9.

Thermophysical properties for saturated liquid and vapor are updated whenever P_{sat} and T_{sat} are changed in the process of iterative optimization because of varying other variables. At a point in the flow chart where σ_{max} is checked with σ_y, if the condition fails, the first option would be to change/decrease *a* and/or *b* rather than going up all the way to the top of the chart. If vapor chamber size (*a* and *b*) reaches a practical limiting value such that the number of columns of the size assumed in the guess set $\{U\}$ does not fit in it, then the appropriate column size values in $\{U\}$ are guessed again and the optimization is repeated again. A similar methodology is employed at the last step of optimization involving comparing *r* with *rc* and *p* with *pc*.

Even though, a no definitive condition can be employed to stop the iterative optimization, the assumed/provided critical values of ΔTc_{VC}, *rc, pc* and a reasonable value of m_{tot} would break the flow-chart to arrive at a design. It must be noted that higher the value of *p*, higher is the latent advantage in the heat sink design and hence higher storage densities. High value of *r* makes sure that almost all the PCM present in the system gets used in storing heat. Large amounts of unused PCM does not contribute to the latent advantage of the heat sink but results in increasing the mass. Therefore, it is very important to achieve a balance between high *p* and high *r* in the system. It is very tempting to lower the parasitic mass of the heat sink by choosing very thin plates that make up the vapor chamber setup. However, it must be remembered that this leads to undesirable stress and deflection of the plates. If the stress developed in the plates that make up the heat sink exceeds the maximum value that the material with which they are made up of can take, then the plates fail. The reason for the plates to develop stress is high internal pressures desired in the chamber for the working fluid (working fluid at high pressures will have higher heat absorption capacity). Therefore, the failure of the plates will be under tension because of high internal pressures in the chamber. This shows the importance of including the stress and deflection analysis in the optimization flow-chart of Figure 9. The result set $\{V\}$ consists of all the output terms of Figure 9 and is shown later in Table 3.

In Figure 9, the variable and property data set *U* is first assumed and is defined as,

$$\{U\} = [x, y, z, n, T_v, T_{PCM}, \Delta Tc_{VC}, rc, pc, \text{vapor chamber material, column material, foam material and PCM}] \quad (7)$$

and q_{colf} is calculated as,

$$q_{colf} = \left[\frac{(T_{sat} - T_{PCM})}{R2 + R3 + R4 + R10 + R11} \right] . \frac{1}{x.z} \tag{8}$$

The parameter q_{colf} verifies whether a TES column is capable of absorbing the heat flux based on the surface area ratio between itself and the heater surface. If q_{colf} is less than q_i, it implies that the thermal resistance in transferring heat from the vapor to the TES container is large for the design and therefore, the container cannot absorb the heat that it is desired, q_i, to absorb. In that case, the design parameters need to be modified.

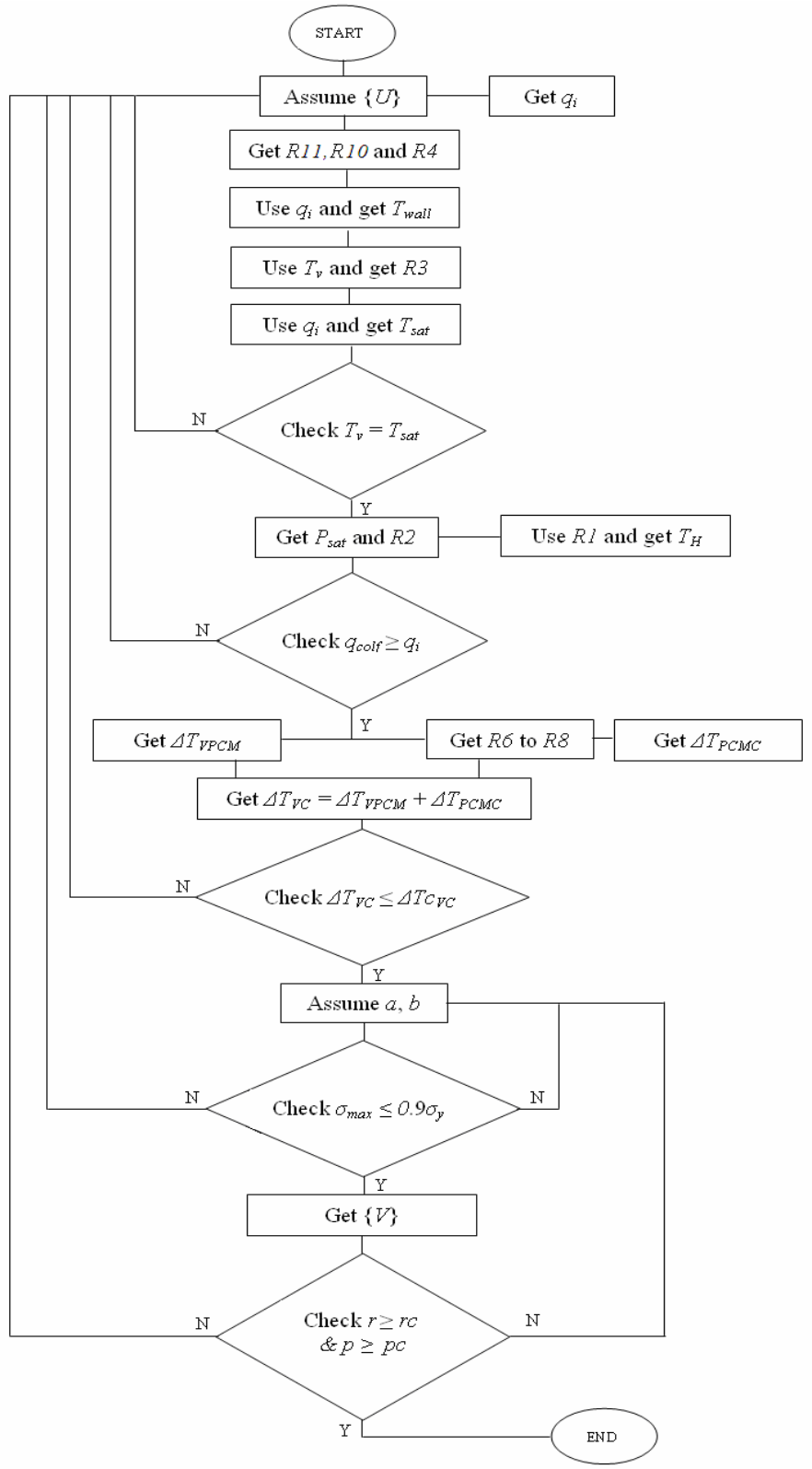

Figure 9: Flow-chart for iterative optimization of the VCTES heat sink

For illustration purposes, a heat source in an example application with a D of 0.05, generating a pulse load of 500 W/cm^2 over an area of 100 cm^2 has been considered. The surface temperature in this particular application is assumed to be constrained to lie always between 100 ^{0}C and 135 ^{0}C.

The preliminary mathematical model is used to optimize and arrive at a best configuration for an example heat sink for the considered application and is assumed to have to meet the following criteria simultaneously.

- Critical temperature difference between vapor and condenser (ΔTc_{VC}) = 10^{0}C
- Critical value for the ratio of used PCM mass to the total PCM mass (rc) = 90%
- Critical value for the ratio of total PCM mass to total VCTES mass (pc) = 45%
- Low heat flux on the condenser portion
- Environment safe operation
- Fast charging ability

Possible solutions to meet the design criteria of an example heat sink

- Minimum possible ΔT_{VC} ensures a narrow temperature range of operation of the VCTES system, which is very important. This is possible by choosing a PCM with as narrow a melting range as possible and decreasing the values of all the resistances during charging and discharging, which in turn is possible by any or some of the following methods:

  i. Keeping the same number of columns, increasing the column height and hence increasing the surface area of each column thereby decreasing the heat flux on each column during charging. But this increases the overall size and mass of the VCTES system. This also increases the used PCM amount and decreases resistance *R8*.

ii. Keeping the same height and amount of PCM, increasing the length of each column decreases the width thereby decreasing the resistance *R11* in foam filled PCM portion of each column. This also decreases the resistance *R8*.

iii. Keeping the same size for columns, increasing the number of columns *n* thereby decreasing the heat flux during charging. However, this increases the overall mass m_{tot} of the VCTES system.

- Though it is good for the VCTES system to have a high PCM mass to the VCTES system mass ratio, it is not appropriate to increase the amount of unused PCM just to increase this ratio. It is important to minimize the amount of excess PCM. Therefore, to achieve an $r \geq rc$ is important and this can be done by decreasing the TES size, which in turn affects all the resistances and mass.
- Having a minimum possible heat flux on the condenser portion of the VCTES system is crucial during discharging mode. A lousy condenser may not dissipate the heat to ambient within the low/no-heat-load time. Because of this, the inside temperatures may increase and the VCTES system may not be ready for the next pulse of the cycle. The heat flux on the condenser can be decreased by increasing its surface area either by increasing the length or height of TES containers both of which increases the mass. Depending on the application if heat flux on the condenser turns out to be very high, fins can be provided on the condenser, which can simply be protrusions of columns inside the vapor chamber.
- Accidental leakage of hazardous vapor chamber fluids can be environmentally unsafe and so water is chosen as the HTF for this example heat sink.
- Since the duty cycle for the example heat sink is low, fast charging is crucial. This can be achieved by minimizing the resistances *R1* to *R4, R10* and *R11*.

Optimized Results

Based on the above constraints, the developed VCTES design and optimization tool was run for multiple times by varying the values of column width, length and height. The results are shown in Tables 3, 4 and 5. For all the runs, the vapor chamber and column material was assumed as Titanium, the bond material (to bond foam to column inside surface) as S-bond® [36] and the PCM as pure POLYWAX® 1000 [37].

From the result set, an optimized case was chosen, which simultaneously satisfies the design criteria considered. For this optimization, since most of the guess values in the set $\{U\}$ are fixed by virtue of the assumed application, the only variable will be column size (x, y, z). Even the column number was fixed apriori. Changing y such that there is always a minimum amount of PCM present in the system to absorb the heat generated will give values for x and z for each case. It can be observed from Figure 10 that y = 20 mm is an optimum value for the width of the TES units since ΔT_{VC} for this case lies below ΔTc_{VC} and it satisfies all the other design criteria considered. The dimensions for the VCTES heat sink are shown in Table 3. Table 4 shows the thermal resistances during charging and discharging modes for the heat sink of Table 3 and Table 5 shows some parameters of the result set $\{\boldsymbol{V}\}$. A parallel optimization was done assuming the columns as cylindrical and observed that by changing the column shape from cylindrical to rectangular; keeping all other parameters the same, there is scope for decreasing the unused PCM mass and even ΔT_{VC}. It can also be observed from Table 3, the importance of using foam inside columns and using a thermal conductive bond between foam and column inside surface (which is otherwise occupied by air or PCM or both).

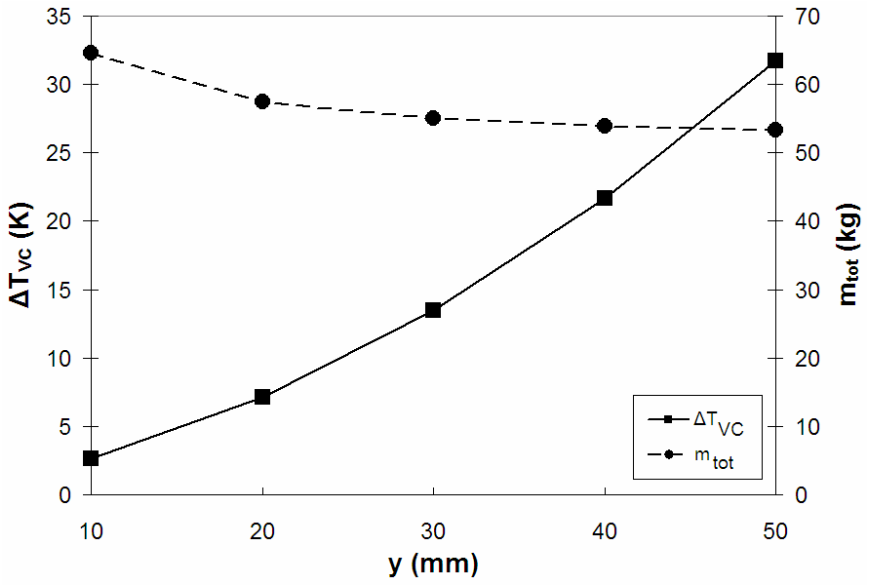

Figure 10: Selection of optimized case for an example heat sink

Table 3: Example VCTES heat sink optimized design parameters

Parameter	*Value*
a (m)	1.006
b (m)	1.001
tc (mm)	0.4
N	2
x (m)	1
z (m)	1
y (mm)	20
t_{wall} (mm)	0.4
q_i (W/cm^2)	2.5
q_{colf} (W/cm^2)	2.5
T_{sat} (K)	393
P_{sat} (atm)	1.95
T_C (K)	385.9
q_C (W/cm^2)	0.1
ΔT_{VPCM} (K)	6.9
ΔT_{PCMC} (K)	0.1
t_p (s)	140

Table 4: Thermal resistances of the example VCTES heat sink

Resistance	*Value*
R1 (K/kW)	0.34
R2 (K/kW)	0
R3 (K/kW)	0.1
R4 (K/kW)	0.03
R5 (K/kW)	133
R8 (K/kW)	79
R9 (K/kW)	1
R10 (K/kW)	0
R11 (K/kW)	0.15

Table 5: Key parameter values of the result set {$\boldsymbol{V}$}

Key Result	*Value*
ΔT_{VC} (K)	7
m_{PCM} (kg)	27
V_{tot} (m^3)	0.072
m_{tot} (kg)	57.5
R	97.5
P	47
Q (MJ)	7
Q_v (MJ/m^3)	97
Q_m (kJ/kg)	122

Discussion

From the results, it can be observed that during charging mode, the dominant resistance to heat transfer is from the PCM (*R5*) unless there is foam. With the presence of foam, *R2* can be neglected compared to *R1*, *R2*, *R3* and *R11*. High value of *R9* suggests that it is essential to use a thermal conductive bond to attach foam to the column inner walls. During the discharging mode, the dominant resistances are again *R6* and *R8* unless there are foam and bond and the conclusion

is same as the charging mode. With the presence of foam, all the resistances can be neglected compared to *R8*. These observations provide good support to the intuitive design features assumed. A point of interest that needs to be mentioned is that, with such low resistance values, the selection of a highly thermal conductive material for the vapor chamber and column plates becomes unimportant. This was verified by using Copper as the material everywhere. It was found that copper increases the weight but does not help in significantly reducing the ΔT_{VC}.

To execute the step in the flow-chart where the design is checked for structural failure, a two dimensional model of the VCTES heat sink is analyzed for stress using a commercial FEM package COMSOL® [38]. The results showed that a σ_{max} of 16 MPa would be developed at the column and vapor chamber wall interface, which is much below the tensile yield strength of pure Titanium or any of its alloys. The stress developed in graphite foam is found to be less than 2 MPa (compressive strength of Pocofoam® [39]) and so foam does not fail/crumble. The maximum deflection of the column walls is found to be 8.3 μm and is a very low number compared to the TES lateral dimension *y*. As assumed before, TES columns are able to provide support to the vapor chamber plates and foam was able to support the TES column plates.

In addition to providing scope for a quick design, the order of magnitude analysis of the resistances in the design tool helps in isolating the key processes of VCTES heat sink operation that require detailed numerical attention. For example, from Table 3 it can be inferred that film condensation on the outside of a column wall coupled with simultaneous phase change of PCM in foam inside the column is a crucial hindrance for fast charging. During discharging, the heat dissipation to ambient causes a delay.

The design described in Table 3 has a volumetric latent heat storage capacity of 97 MJ/m^3. This was possible because of assuming an isothermal melting point for PCM. If PCM melting range is considered (90^0C to 120^0C for POLYWAX® 1000) and if VCTES system operates within the melting range of the PCM, then Q and hence the volumetric heat storage, both reduce. The effect of operating within the PCM melting range on the volumetric heat storage capability as applicable to the current optimized design is shown in Figure 11. It can be seen that for PCM with a melting range, volumetric heat storage capacity is proportional to the operating temperature range of the heat sink within the melting range of the PCM. This is because; the wider the operating temperature range within the melting range of a PCM, more is the latent heat effect, which accounts for more volumetric storage.

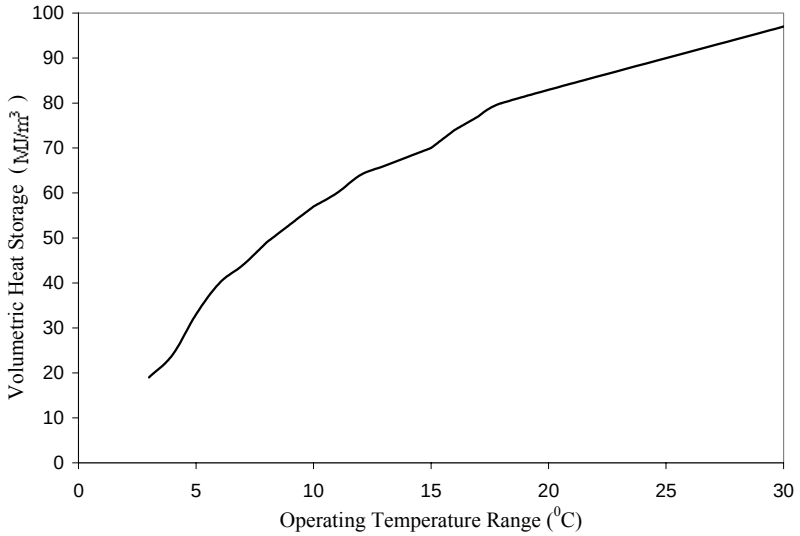

Figure 11: Volumetric heat storage capacity vs. operating temperature range of VCTES system

Prototype design for the experiment

For experimental demonstration of the key objectives of this work i.e., to demonstrate that the VCTES heat sink is practicable and that the temporary use of PCMs can arrest the undue rise in vapor temperature, a reduced size prototype version of the optimized VCTES was selected. This eliminates the huge costs associated with material, fabrication and testing of a 1 m X 1 m heat sink (as mentioned in Table 3) but still captures the required physics qualitatively to show that the key objectives have been met.

For this purpose, two experiment versions were first considered and their performance parameters were compared to pick the best design. As discussed earlier, because of the wide melting range of the available PCM sample, the volumetric storage for the heat sink will be low. It should be additionally observed that, as the heat sink size goes down, the ratio of PCM mass to the parasitic mass decreases. This coupled with the wide melting range effect of the PCM significantly lowers the effect of PCM latent heat. However, to achieve the most important objective of this work, it is enough to show the effect of the presence of PCM in the heat sink qualitatively and so less consideration was given to the values of storage density, heat flux absorption capability and actual temperature rise of an ideal heat sink of Table 3.

Figures 25 and 26 show the two versions of the experiment designs. With a view to reduce the parasitic mass of the columns, the number of columns in the design 1 (Figure 12) was decreased to one in design 2 (Figure 13). The developed thermo-mechanical resistance model was used to optimize the designs for both the versions. Tables 6 and 7 show the results. It was found that design 2 with one column has a bigger overall charging resistance compared to design 1. This is because of a higher heat flux at the column surface (5 W/cm^2) for design 2 (since

design 2 with one column has less surface area for heat distribution compared to design 1 with four columns for which the heat flux at each column face is only 2.4 W/cm^2). In addition to this, design 2 has higher film condensation resistance because of condensation below a flat condenser plate as against film condensation on a vertical wall for which the heat transfer coefficient is about three times higher than in the former case. It can also be observed from Tables 6 and 7 that design 2 has a higher PCM thermal resistance because heat has to penetrate the full width of the foam to melt the PCM completely as against half-width in design 1 (because of symmetry).

Since the key objective of this effort is to demonstrate fast charging with a narrow temperature operation, other advantages of the design 2 like less weight and a high specific heat storage capacity were ignored during comparison. Therefore, design 1 was chosen to perform the experiments.

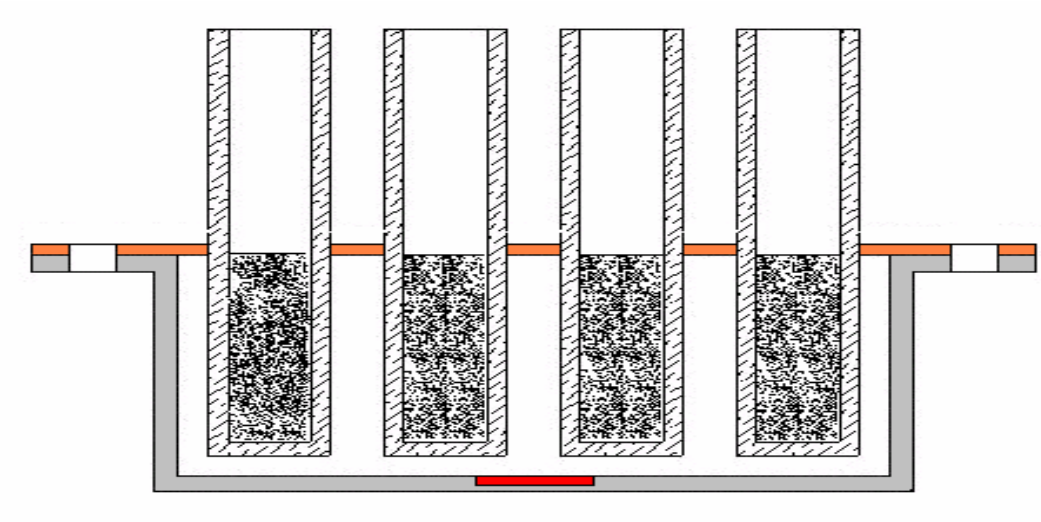

Figure 12: VCTES experiment design version 1

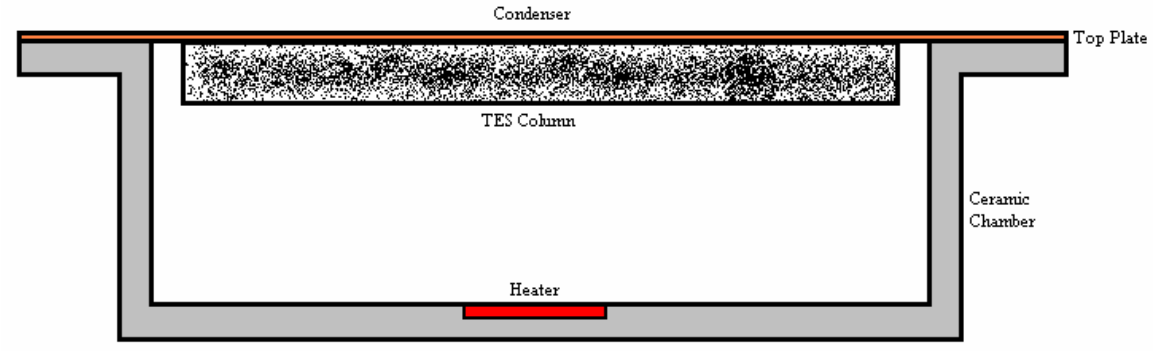

Figure 13: VCTES experiment design version 2

Table 6: Results for VCTES design version 1 (Column and Top Plate Material – Cu)

Parameter	*Value*
VC length (m)	0.14
VC breadth (m)	0.12
VC wall thickness (mm)	7.6
Number of columns	4
Column length (mm)	50.8
Column height (mm)	25.4
Column width (mm)	12.7
Column wall thickness (mm)	1.6
Pulse heat time (s)	16 or 32
Total mass of PCM (gm)	35
Total mass of VCTES (gm)	1600
p = Mass of (PCM / VCTES)%	2.2
Total latent heat storage (kJ)	4.7
Latent storage density (kJ/kg)	2.9

Table 7: Results for VCTES design version 2 (Column and Top Plate Material – Ti)

Parameter	*Value*
VC length (m)	0.14
VC breadth (m)	0.12
VC wall thickness (mm)	7.6
Number of columns	1
Column length (mm)	86.4

Column height (mm)	58.4
Column width (mm)	10.2
Column wall thickness (mm)	0.5
Pulse heat time (s)	16 or 32
Total mass of PCM (gm)	31
Total mass of VCTES (gm)	1000
p = Mass of (PCM / VCTES)%	3
Total latent heat storage (kJ)	4.3
Latent storage density (kJ/kg)	4.3

Similar to the discussion concerning Figure 3, design 1 of Table 6 also suffers from the wide melting range of PCM. This can be illustrated using Figure 14. In Figure 14, x-axis is the PCM melting range (*Tmr*) and y-axis is the ratio (*R*) of PCM latent heat storage to the total thermal energy storage (TES) of the column during PCM melting. From the figure, it is clear that smaller melting ranges help the PCM latent heat effect compete with the system sensible heat (*R* = 1 is the ideal case of PCM with a single melting point where all the TES happens as latent heat storage of PCM). With a melting range of 30 ^{0}C, it can be seen that the latent heat of PCM is not even half of the system TES. This is because of the distribution of the latent heat over a melting range causing a reduction in its peak value, which gives rise to the undesirable combination of reduced latent effect and wide operating temperature range. Therefore, the effect of PCM will be more evident if a pure PCM is used.

The key objective of the experiment is to be able to hold the vapor temperature inside the chamber to within 3 to 5 ^{0}C during the charging time. This can be achieved only if the melting range of the PCM is as small as possible and the PCM has a latent heat of above 200 J/g.

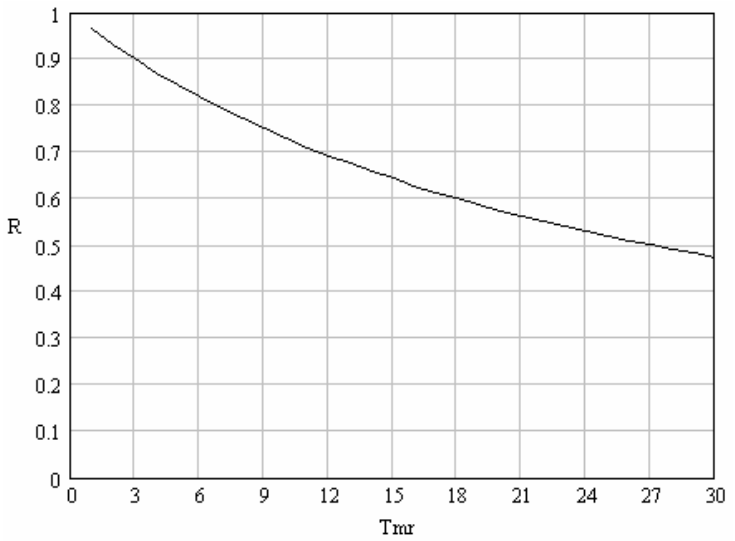

Figure 14: PCM latent heat advantage (R = (PCM latent heat storage)/(total TES during melting)) vs. PCM melting range (Tmr in ^{0}C)

CHAPTER FOUR: NUMERICAL MODEL

The VCTES sink system thermal operation is characterized by the following three processes namely,

- Heat Acquisition (by liquid-vapor phase change inside the vapor chamber)
- Heat Storage (by vapor flow followed by film condensation on containers with simultaneous phase change of a PCM inside those containers) and,
- Heat Rejection (by discharging through the condenser surface of the vapor chamber).

Of these, the most important process is the heat storage or more precisely, the swift temporary storage of waste heat using encapsulated phase change materials in a conductive medium. It is because of this rapid temporary thermal energy storage that this heat sink can be designed for an average heat load rather than for pulsed heat loads. However, as most of the available phase change materials have very low thermal conductivities, the heat storage path evolves as the maximum heat resistance path in heat sinks employing thermal energy storage. But the key feature that enables for a fast heat storage mechanism in this heat sink is a coupled or conjugate heat transfer phenomenon wherein the vapor carries heat from the source and condenses on the outside of thermal energy storage containers and the heat is simultaneously absorbed by phase change materials encapsulated inside those containers in a highly thermally conductive porous graphite foam. Hence, the key focus of this chapter is to numerically analyze the key phenomenon of heat storage as specific to the above-mentioned heat sink.

Most thermal energy storage modeling until date focused only on the heat absorption process with a constant temperature or constant heat flux condition imposed on the surrounding boundary/encapsulation. This kind of analysis can produce different conclusions compared to

actual situation in the integrated VCTES heat sink, where the wall boundary condition for the PCM melting comes from film condensation of vapor on the outer surface of container walls.

There is no available literature until date that focused on the conjugate heat transfer problem of transient laminar film condensation coupled with encapsulated PCM melting in porous graphite foams. Only limited attention was focused on the numerical analysis of conjugate transient heat transfer problem of condensation and melting. Contreras and Thorsen [40] were probably the first to analytically study the transient condensation of a saturated vapor on a solid of same chemical composition coupled with melting of the same solid. They ignored the inertia terms in the momentum equation but included the convective terms in the energy equation and obtained an integral solution using a quadratic temperature profile. Galamba and Dhir [41-43] numerically analyzed the problem of transient condensation of saturated vapor on both normal [41] and subcooled [42] vertical solid walls whose melting temperatures were less than the vapor saturation temperature. The condensing fluid and the melting wall material were assumed immiscible. They used both analytical and numerical techniques for solving the governing equations, which ignored inertia terms in the momentum equation and convective terms in the energy equation. The melt layer physics is treated in a similar way as the condensate film using analogous parameters for melt layer thickness and steady-state time as for film condensation. This kind of treatment for melting does not hold good if melting occurs in porous media like foams, especially in most metal and graphite foams where the pore size is in the order of a few tens to hundreds of microns. The small pore size in foams will provide a capillary effect and lower the effect of gravity. In addition, it was shown in Reference [34] that there would be practically a minimal temperature difference between the ligaments of foam and PCM in the

pores if the surface area to volume ratio *A/V* for the foam were more than 1575 m^2/m^3. For graphite foams, *A/V* is typically of the order of 20,000 (m^2/m^3) [35]. These conditions specific to graphite foams will provide a Rayleigh number smaller than the critical value for natural convection in the melt to become significant. Hence, the PCM melting in graphite foams must be modeled as transient conduction dominated moving melt front problem. Further, the encapsulation of PCM in containers induces wall effects that were not included in any of the prior related work. Chen and Chang [44] studied an analogous conjugate problem of laminar film condensation and natural convection on opposite sides of a vertical wall and included the effect of wall thermal resistance. Char and Lin [45] extended the problem by considering the two media separated by the wall as porous. Both References [44] and [45] were steady state analyses.

Hence, it forms an interesting aspect to numerically solve and understand the transient problem of laminar film condensation coupled with encapsulated solid-liquid PCM phase change inside graphite foam. This would help in better understanding and identifying important parameters that govern the rapidity and efficiency of such temporary heat storage mechanisms in future as in the current VCTES system.

Individual numerical models for PCM melting inside graphite foam and film condensation on the outside of PCM encapsulating containers are given below. Coupling of the two models using heat conduction within the TES container walls is also mentioned.

Encapsulated PCM phase change in a high thermally conductive porous graphite foam

The phase change process of PCM in highly thermally conductive porous graphite foam is solved as a nonlinear transient moving boundary problem. It was observed that the two-temperature model [46] as observed in metal foams could be solved as a one-temperature model

[34] in graphite foams owing to the large *A/V* ratio in graphite foams. The reason for this is explained below.

The actual mode of heat transfer to the PCM in a pore can be assumed as three dimensional through conduction in the foam ligaments. This assumption is equivalent to opening up a cuboid (a hollow rectangular fin) lying in a three dimensional Cartesian coordinate system into a surface (fin) lying in a two-dimensional coordinate system and assuming that the PCM lies above this fin with a uniform thickness. However, when the surface is closed back to form a cuboid, there will be overlapping of PCM volumes. So a two-dimensional model provides for lesser foam surface area for PCM phase change compared to a cuboid fin model. However, this increase in foam surface area in the cuboid fin model can be alternately captured in the two-dimensional fin model by increasing the number of fins per unit inch. On increasing *N* above 20, it was shown in Reference [34] that the PCM phase change in porous foams could be modeled using a one-temperature model. This is also true because of a very low heat flux at the pore level when *N* is a large number. Therefore, it is accurate enough to use a two-dimensional one-temperature model to simulate phase change in foams with high *N*. While $N = 20$ corresponds to a surface area to volume ratio of 1575 (m^2/m^3) in Reference [34], Pocofoam® with a typical surface area to volume ratio of 20,000 (m^2/m^3) [35] leads to a value of *N* much greater than 20. Therefore, a single temperature representative of both the foam and PCM temperatures can be used in the numerical modeling.

Another interesting feature to be noted with respect to heat transfer in graphite foams filled with a PCM is that the heat transfer occurs in series from the column (TES unit) wall to the column center rather than in a lumped manner in all the foam ligaments first and then in parallel

paths in all the pores. This can be better explained by considering an equivalent Biot number (*Bi*) as given by Equation 14 of Lee and Vafai [47].

$$Bi = \frac{h_{\text{int}} \gamma a_s W^2}{4k_{fe}} \tag{9}$$

$\gamma = 1$ for parallel plate / rectangular configurations [47].

For Pocofoam® enclosed in a container as shown in Figure 12, a_s = 20,000, $W/2$ = 0.0064 (refer design 1 of Chapter Three), and k_{fe} = 135 [39] units.

h_{int} can be found from the pore Nusselt number as,

$$Nu_p = (h_{int}.d_p/k_{PCM}) \tag{10}$$

where d_p = 350 micrometers for Pocofoam® and k_{PCM} can be assumed as 0.2 W/m.K (representative of most paraffin waxes). Nu_p can be assumed as 2 [48] by approximating the shape of the PCM interacting with the solid foam as spheres surrounded by Pocofoam®. This gives, h_{int} = 1143 W/m^2.K.

Using the above values in Equation 9, we get Bi ~ 7. With a Bi >> 0.1, it is clear that the conduction resistance in the foam ligaments is much higher compared to the convective heat transfer resistance at the interface of the foam ligaments and PCM, which implies the temperature gradient inside foam ligaments cannot be ignored. Hence, the heat transfer occurs in series from the container wall to the container center portion rather than in the foam ligaments first followed by parallel paths in all the pores.

As far as the effect of film condensation on the dimensions of the phase change problem is concerned, it must be noted that the column wall temperature will have a variation along the height and the temperature drop across the film in the cross-stream direction will be about the same or even more compared to the temperature drop in the PCM filling the foam. Therefore, the heat transfer in PCM will be two-dimensional.

Based on the above conclusions, the model then collapses to solving a phase change problem in the Y-Z plane of the TES column (Figure 15) by considering the effective thermophysical properties of the foam-PCM composite based on the foam porosity. A fixed grid heat capacity formulation [49-51] is used to model this problem. Enthalpy models [52-55] for phase change are attractive in the sense they do not require explicit tracking of the phase change interface unlike in the heat capacity methods. Nevertheless, whereas the heat capacity method provides explicit temperature field in the phase change domain, the temperature field in an enthalpy model has to be implicitly evaluated using the enthalpy-temperature correlation. In addition, liquid fraction field is imbibed in the temperature field in the enthalpy models. It has been traditionally observed that for phase change problems with a melting range and for conjugate heat transfer problems involving adjacent walls, heat capacity method performs better

[51]. Therefore, an easy-to-implement modified effective heat capacity method is used for the current simulation.

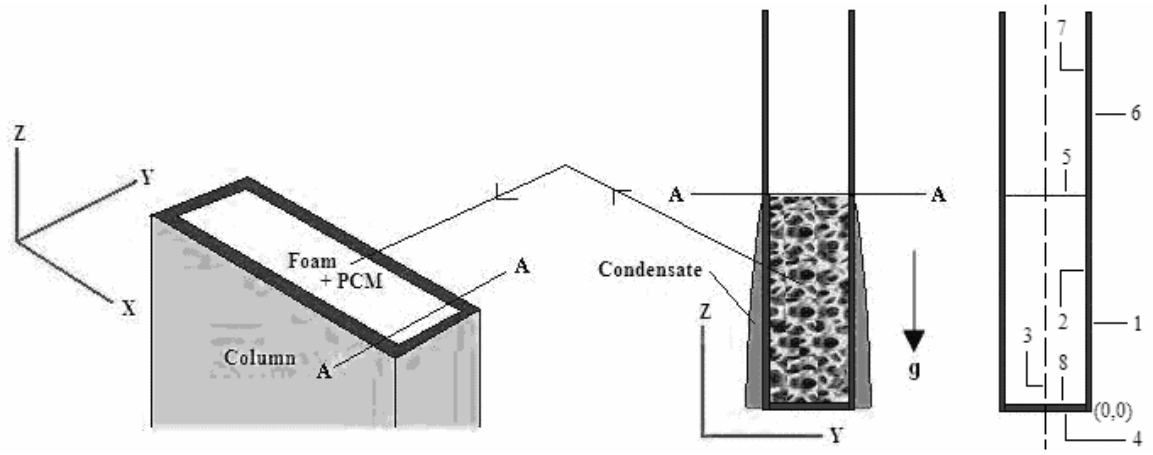

Figure 15: Schematic of the TES unit considered for numerical simulation

The mathematical model is described below and includes the following assumptions:

i. The effects of natural convection within the molten PCM can be ignored as explained earlier. Therefore, the phase change process is conduction dominated.

ii. Temperature gradients in the X-direction can be ignored owing to symmetry of the boundary conditions with respect to that direction. This can be justified since the X-direction boundary conditions for the phase change inside the column come from the condensing film on the outside of the column and the condensate thickness does not vary along the X-direction at any time during the TES unit charging process.

iii. Thermal conductivity of PCM is different for solid and liquid phases but independent of temperature in any one phase. This assumption is reasonable especially for heavy paraffin waxes (number of carbon atoms > 30) as the one assumed in the current work. Paradela et al. [56] exclusively modeled the thermal conductivities of paraffins that are primarily used for TES. From Equation 9 and Table I in Reference [56], it can be seen that the first and second order temperature coefficients for most paraffins are very small compared to their zero order coefficient. In addition, it can be observed that as the value of number of carbon atoms increases, the first and second order temperature coefficients decrease.

iv. Density of PCM is different for solid and liquid phases but independent of temperature in any one phase.

v. PCM is homogeneous and isotropic and has no property degradation with time.

vi. During refreezing of PCM, voids will be created due to a decrease in PCM volume. These voids will be distributed non-uniformly and create a high thermal resistance path to heat transfer. Initiation and growth of such shrinkage voids was thermodynamically studied in detail by Sulfredge et al. [57]. They found that the number and pattern of nucleation centers available for liquid during solidification is a key factor that determines the void arrangement. Techniques such as promoting artificial nucleation sites were also suggested as possible means of dispersing the voids. Using foam provides such nucleation centers for molten PCM, which makes the voids uniformly distributed and thus enhances the conducting path. As far as void formation near the interface of PCM and foam composite and copper wall is concerned, a good contact between the wall and foam ligaments will mitigate the effect of a small void since heat

transfer to the PCM happens by first penetrating from the wall into the foam and then into PCM. If a high thermal conductive epoxy/bond is used to join copper and foam, it can be assumed that there will be a minimum contact resistance at the interface because of void formation. Hence, void formation effects are neglected in the numerical simulation.

For conduction controlled PCM phase change, the transient energy equation in Cartesian coordinate system in general is given by,

$$c_p(T)\frac{\partial T(x,y,z,t)}{\partial t} = \nabla.(\frac{k}{\rho}\nabla T(x,y,z,t)) \tag{11}$$

Since graphite foams exhibit anisotropic thermal conductivity, the numerical model includes the same by defining a two-dimensional tensor for *k* as follows:

$$[k] = \begin{bmatrix} k_{yy} & 0 \\ 0 & k_{zz} \end{bmatrix} \tag{12}$$

As applied to a column as shown in Figure 12, the energy equation then becomes,

$$c_p(T)\frac{\partial T(y,z,t)}{\partial t}=\left(k_{yy}\frac{\partial^2 T(y,z,t)}{\partial y^2}+k_{zz}\frac{\partial^2 T(y,z,t)}{\partial z^2}\right)\frac{1}{\rho} \tag{13}$$

Since melting range is a usual characteristic of paraffin waxes and since they are used in the VCTES experiments of the current work (described in Chapter Five), the specific heat is defined as shown in Equation 14.

$$c_p(T)=\begin{cases}\varepsilon c_{ps}+(1-\varepsilon)c_{pf}\,;T<T_m-(\delta T/2)\\ \varepsilon(c_{pm})+(1-\varepsilon)c_{pf}\,;T_m-(\delta T/2)\le T\le T_m+(\delta T/2)\\ \varepsilon c_{pl}+(1-\varepsilon)c_{pf}\,;T>T_m+(\delta T/2)\end{cases} \tag{14}$$

During melting of PCM, the specific heat is modeled as given in Reference [58].

$$c_{pm}=\frac{h_{sf}}{\delta T} \tag{15}$$

ρ in Equation 13 is given by Equation 16.

$$\rho = \begin{cases} \varepsilon\rho_s + (1-\varepsilon)\rho_f ; T < T_m - (\delta T/2) \\ \varepsilon\left(\dfrac{\rho_s + \rho_l}{2}\right) + (1-\varepsilon)\rho_f ; T_m - (\delta T/2) \le T \le T_m + (\delta T/2) \\ \varepsilon\rho_l + (1-\varepsilon)\rho_f ; T > T_m + (\delta T/2) \end{cases} \quad (16)$$

k_{zz} is defined similarly as in Equation 17.

$$k_{yy} = \begin{cases} \varepsilon k_s + (1-\varepsilon)k_{fy} ; T < T_m - (\delta T/2) \\ \varepsilon\left(\dfrac{k_s + k_l}{2}\right) + (1-\varepsilon)k_{fy} ; T_m - (\delta T/2) \le T \le T_m + (\delta T/2) \\ \varepsilon k_l + (1-\varepsilon)k_{fy} ; T > T_m + (\delta T/2) \end{cases} \quad (17)$$

Laminar film condensation on a flat vertical surface

Analysis of laminar transient film condensation on a vertical plate was done by Sparrow and Siegel [59], Reed et al. [60] and Chung [61]. It was shown in References [59] and [60] that the transient problem could be treated as quasi-steady provided *Ja* and *Ja/Pr* are both << 1. This implies that the temperature profile is linear and the velocity profile is parabolic.

It must be noted that in Reference [60], it was shown that the above condition on *Ja* and *Ja/Pr* holds good for water under atmospheric conditions, while the actual conditions in VCTES need not be usually atmospheric (refer Chapter Three). In addition, *Ja* depends on the temperature difference across the liquid film, which differs from case to case. Hence, appropriate values for thermophysical properties of water for conditions in the vapor chamber (P_{sat} of

approximately 2 atm; refer Chapter Five) were used to evaluate *Ja* and *Pr* for application to the current problem under consideration. Since the film thickness will be small, the temperature difference across the film will be small (~ 1 K). It was found that *Ja* = 0.0019 and *Ja/Pr* = 0.0014. Even for a temperature difference across the film of 10 K (which is usually unlikely), *Ja* and *Pr* are 0.019 and 0.014, respectively with both much smaller than unity. Therefore, a quasi-steady approach can be used.

The film thickness in any given time-step can be reasonably approximated using Equation 18 as shown below, where the variation in the wall temperature in the column height direction is also included.

$$\delta(z,t) = \left[\frac{4k_c\mu_c \int_0^L (T_v - T_{wall}(z,t))dz}{h_{lv} g(\rho_c - \rho_v)\rho_c} \right]^{0.25} \tag{18}$$

Heat conduction in the solid wall encapsulating the PCM

A two-dimensional energy equation in Cartesian coordinates is solved in the solid wall as shown in Equation 19.

$$c_{pw} \frac{\partial T_w(y,z,t)}{\partial t} = \left(\frac{\partial^2 T_w(y,z,t)}{\partial y^2} + \frac{\partial^2 T_w(y,z,t)}{\partial z^2} \right) \frac{k_w}{\rho_w} \tag{19}$$

Initial Condition:

$$T_w(y,z,0) = T_0 \tag{20}$$

Boundary Conditions:

$$q.\boldsymbol{n} = 0 \text{ on boundary 4}$$

$$T(0,z,t) = T_{wall}(z,t) \text{ on boundary 1} \tag{21}$$

Numerical coupling

In the numerical problem, coupling is required at two junctions, between condensing film and the column outer wall (boundary 1 in Figure 15) and between the column inner wall (boundary 2 in Figure 15) and the composite region of graphite foam and PCM. Coupling is done using the temperature and heat flux continuity at both the interfaces.

The assumptions made for the numerical coupling are:

i. The vapor temperature 'T_v' is a constant. This was assumed because the goal of this simulation is to approximately model and qualitatively study the use of having a heat storage mechanism in the heat sink system.

ii. The heat transfer coefficients for heat removal on the column boundaries 6 and 7 (Figure 15) were chosen to be 50 W/m^2K and 5 W/m^2K for column outside and inside faces respectively assuming the modes of heat removal from those faces as forced and natural convection respectively [48]. This is reasonable since forced convection can only be used on the outside surfaces of columns and not on the inside surfaces as shown in Figure 15.

The following solution procedure is implemented in each time-step:

i. Solve the PCM and graphite foam composite phase change problem.

ii. Solve for $\delta(z,t)$.

iii. Get $T_{wall}(z,t)$ using temperature and heat flux continuity at the column wall and condensate interface.

iv. Go to the next time-step.

v. Repeat steps 1 through 4 until the end of the VCTES charging period.

Finite element method is used to solve the above system of equations. A commercial finite element code, COMSOL® along with MATLAB® [62] is used and user-defined modules for solving PCM phase change in graphite foam and condensate film thickness are incorporated.

Results and Discussion

The PCM phase change model is first verified with one of the experimental results as described in Reference [63], wherein, a cylindrical copper block was attached to a cylindrical piece of POCO graphite foam. The copper block was made to act as a heat source by using an external heater attached to its top surface. The entire assembly was then immersed into a Teflon enclosure serving as thermal insulation. The graphite foam was a priori filled with paraffin wax.

Schematic of the setup is shown in Figure 16. Experiments were performed for different heat inputs and the transient temperature distribution of the PCM at the locations 2, 3, 4 of the foam and PCM composite are plotted in Figure 8 of Reference [63]. A case where the heat input was 11.63 W is selected to validate the current model. The same setup and boundary conditions are implemented and the thermocouple locations 2, 3, 4 are picked to be exactly at the same locations as described in Reference [63] and bear the same numbering. For a better comparison, the results are overlapped onto Figure 8 in Reference [63] and are shown in Figure 17. It can be observed that the results of the current model with assumptions mostly overlapped those in Figure 8 of Reference [63] and so can reasonably simulate PCM phase change in graphite foams. Since in Reference [63], individual details of thermophysical properties of PCM, foam and heat transfer coefficient for natural convection were not mentioned, typical values for those as mentioned in literature were taken (5 W/m^2K for the heat transfer coefficient [48]).

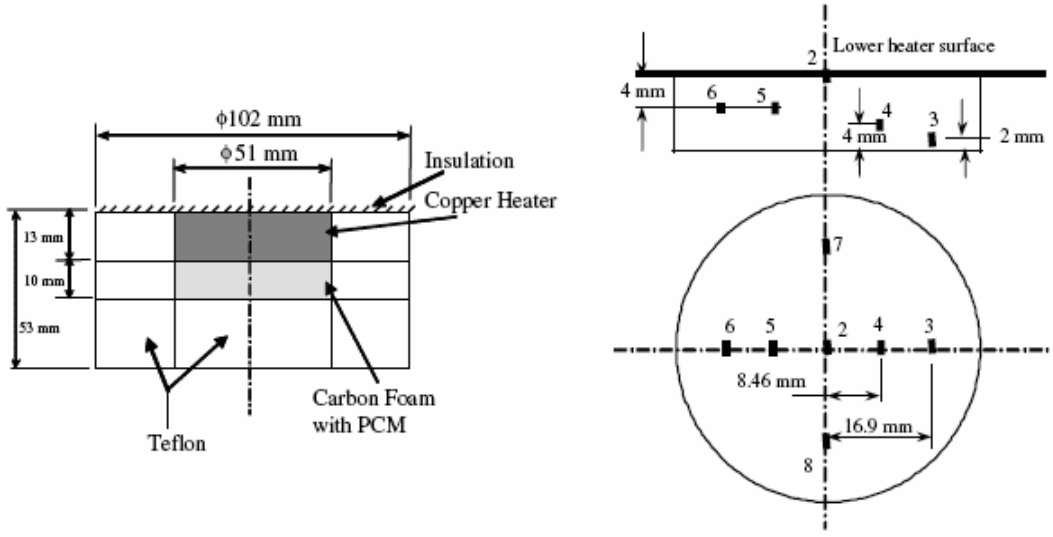

Figure 16: Schematic of thermal protection cell as given in Reference [63] with thermocouple locations

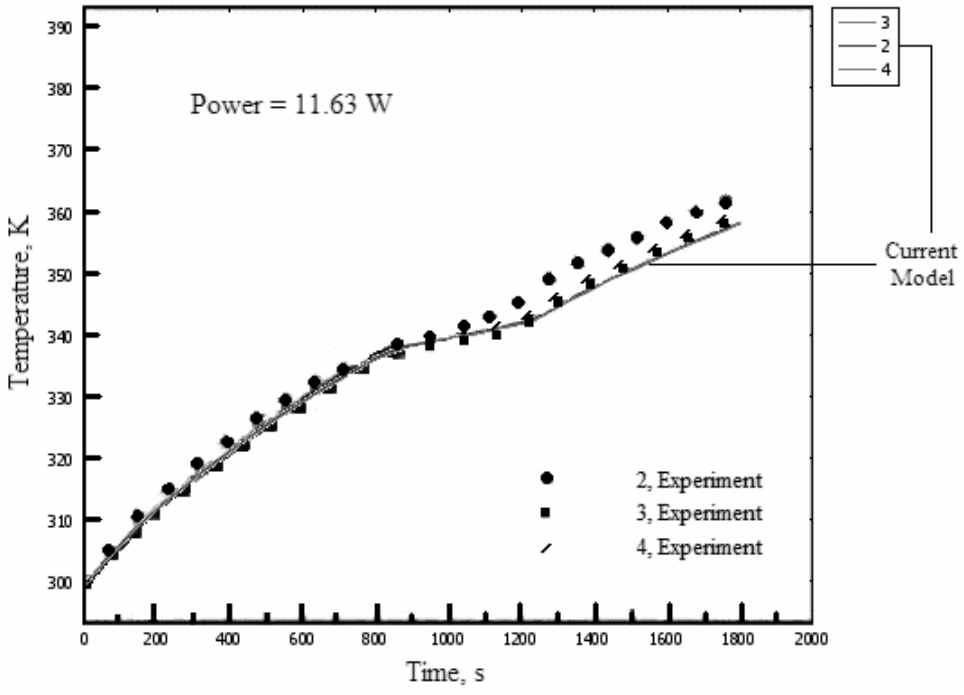

Figure 17: Comparison of current model with experimental results of Reference [63]

The dimensions of the TES columns as designed for experiments (refer Chapter Three); L ~ 0.023 m, W ~ 0.01 m and t_w ~ 0.00163 m, and the same material (copper) are used for current numerical simulation.

The PCM is assumed as POLYWAX® 1000 and the DSC curve for the PCM is shown in Figure 18. The following thermophysical properties are used in the numerical simulation: c_{ps} = 2900 J/kg.K, c_{pl} = 3500 J/kg.K, h_{sf} = 266 kJ/kg, ρ_s = 970 kg/m^3 and ρ_l = 900 kg/m^3. Since, thermal conductivities of solid and liquid phases of the wax are not known/measured, typical values of thermal conductivities (k_s = 0.20 W/m.K, k_l = 0.18 W/m.K) available in literature for most paraffin waxes are used. It must be noted that small inaccuracies in the thermal conductivity values of PCM does not affect the results as the foam conductivity dominates the negligible PCM conductivity in any phase. Corresponding thermophysical property values for graphite foam are taken as c_{pf} = 1730 J/kg.K, ρ_f = 2200 J/kg.K, k_{fy} = 135 W/m.K (out-of-plane) and k_{fz} = 45 W/m.K (in-plane). The porosity for graphite foam is taken as 0.75.

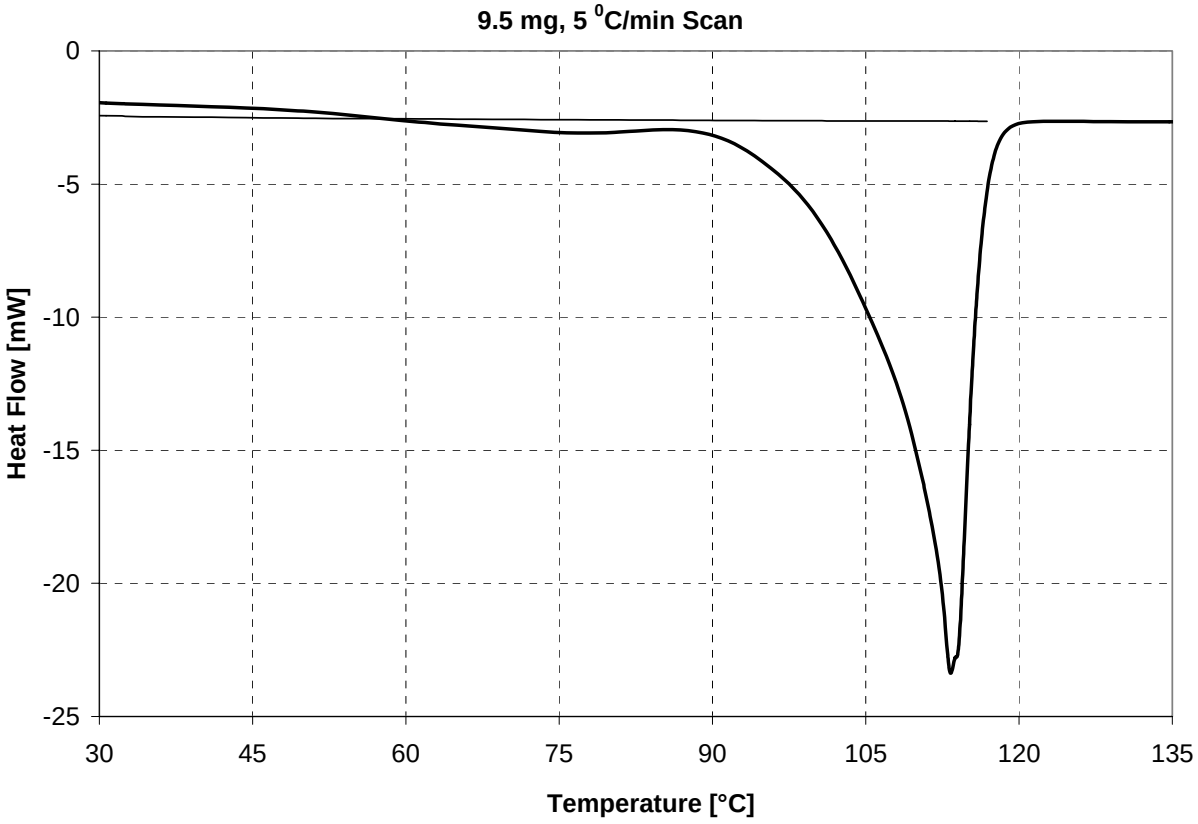

Figure 18: DSC curve of PCM

The chosen PCM has a wide range of melting and so to use the latent heat of PCM effectively by simultaneously not sacrificing the narrow temperature operation of the device, an operating temperature range within the melting range of PCM is chosen where the latent heat is a maximum. Figure 19 shows the heat of fusion against the operating temperature range starting from a specific temperature and is obtained from Figure 18 by integrating the DSC curve over an operating range to obtain the area and hence the heat of fusion for that range of temperature. For example, if an operating range of 10 ^{0}C is chosen, then there will be multiple options within the melting range (363 K – 393 K) but only one of them corresponds to a maximum heat of fusion.

The best ranges of operation for all the possibilities are chosen from Figure 19 and are shown in Table 8, where *T1* and *T2* are the starting and ending points respectively of the operating temperature range T_{or} and δh_{fs} is the heat of fusion within that range. An operating range of 8 K from 380 K to 388 K is chosen, where the latent heat is, h_{sfo} = 138 kJ/kg.

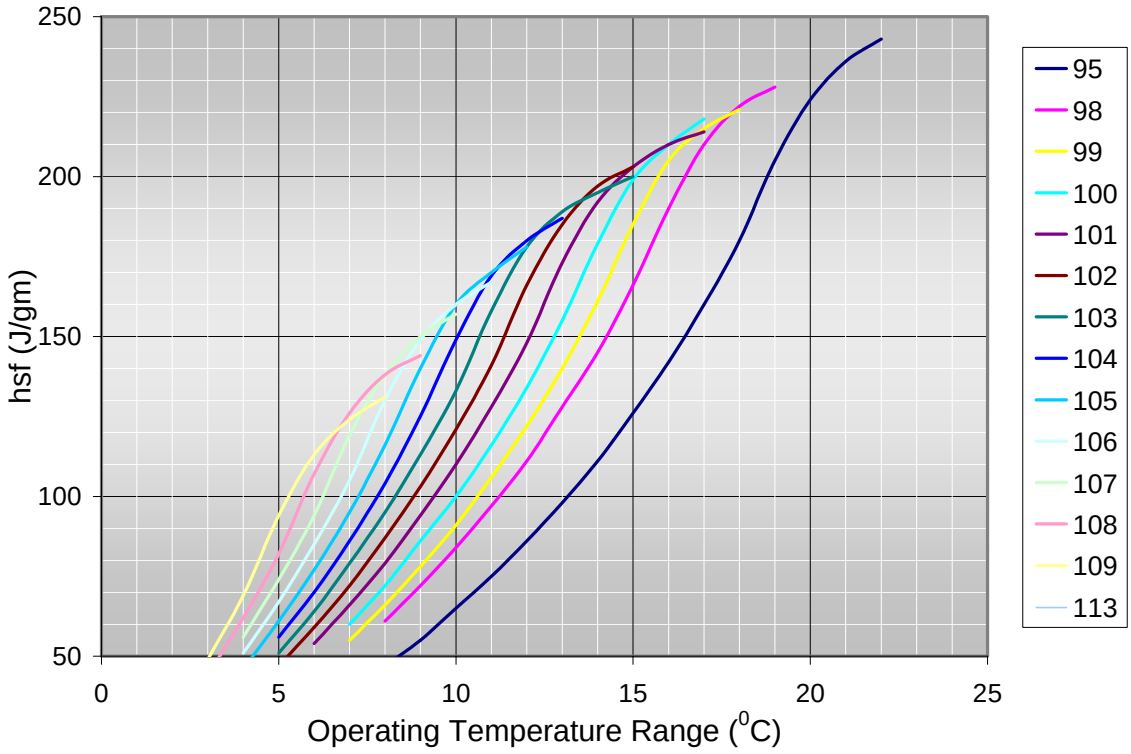

Figure 19: Heat of fusion vs. operating temperature range starting from an initial temperature

Table 8: Best operating temperature ranges for POLYWAX® 1000 within melting range

T1 (^{0}C)	*T2* (^{0}C)	T_{or} (^{0}C)	Δh_{fs}
90	120	30	266
98	116	18	222
100	117	17	218

100	116	16	210
101	117	16	210
101	116	15	203
102	117	15	203
102	116	14	197
103	116	13	189
104	116	12	180
105	116	11	170
105	115	10	160
106	116	10	160
107	116	9	150
107	115	8	138
108	116	8	138
108	115	7	126
109	115	6	113
109	114	5	94
109	113	4	69
113	116	3	55

Based on the above, c_{pm} is redefined for this particular simulation as,

$$c_{pm} = \frac{h_{sfo}}{\delta T_o} \tag{22}$$

Default unstructured meshing option available in the software program was used to mesh the geometry. This avoided the matching constraints on the node number on different length boundaries that needed to be taken care of during manual structured meshing. Three unstructured meshes consisting of 13404, 53616 and 214464 triangular elements were used to perform grid independency check on the final solution. The minimum mesh element quality was 0.62 and the average mesh quality was more than 0.8 for all the three meshes. It was found that the final

solution on an average improved by less than 0.15 K as the mesh is refined to contain more than 13404 elements. Therefore, the same mesh was used for all the simulations. In addition, for all the simulations, a relative tolerance of 1e-4 was used to check for convergence of the solution in any single time-step.

TC3, TC6 and TC7 in Figure 20 are the points of temperature measurement locations in the foam and PCM composite. Two more thermocouple locations TC1 and TC2 were chosen for the numerical simulation to monitor the outside wall temperature of the TES column. In Figure 20, TC7 is located at 6 mm and TC2, TC3 and TC6 are located at 12 mm, all in the vertical direction from the top surface of the foam (boundary 5 in Figure 15). TC1 is chosen to be any point very close to the foam top surface. In the horizontal direction, TC1 and TC2 lie on the column wall outside, whereas TC3 lies on the boundary 2 in Figure 15. TC6 lies at a distance of *W/4* and TC7 lies at a distance of *3W/8* both from the column inside wall.

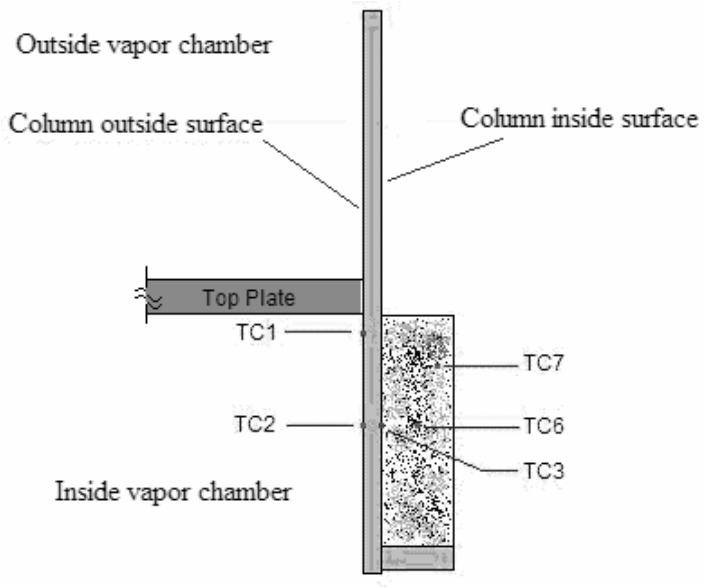

Figure 20: Temperature measurement locations in the numerical model

A T_v of 390 K, T_0 of 380 K and a charging time of 15.5 s are chosen for all the simulations. Figure 21 shows the simulated time history of temperature at various thermocouple locations of Figure 20.

The following observations and conclusions can be drawn from Figure 21:

- The wall temperature drops rapidly from an initial value of chosen vapor temperature because of the presence of a heat sink (PCM) and then begins to rise slowly.
- The dominant resistance during charging is from the condensate film. Once a steady state is reached (a long time after the end of charging), the film and PCM resistances become comparable (refer Chapter Three).
- The presence of a varying thickness condensate film makes the PCM phase change problem two-dimensional as expected.
- The PCM temperature governs all other parameters like 'T_{wall}' and 'δ'.
- Heat penetration into PCM is mostly from the top portion of the column wall where the film thickness is small because of a small thermal penetration resistance. This can be verified by comparing TC7 with TC6.
- The initial temperature choice 'T_0' of the PCM is appropriate since on an average, the PCM temperature rose from 380 K (107 ^{0}C) to 384.5 K (111.5 ^{0}C), where the latent heat h_{sfo} is a maximum within the PCM's entire melting range as discussed before.
- PCM temperature at the end of charging time is still less than 'T_v' implies the vapor temperature will not rise before the end of charging period. This means that all the PCM present has not participated in TES implying that there is scope for PCM to absorb more heat for longer charging times before the heat sink system temperature starts to rise.

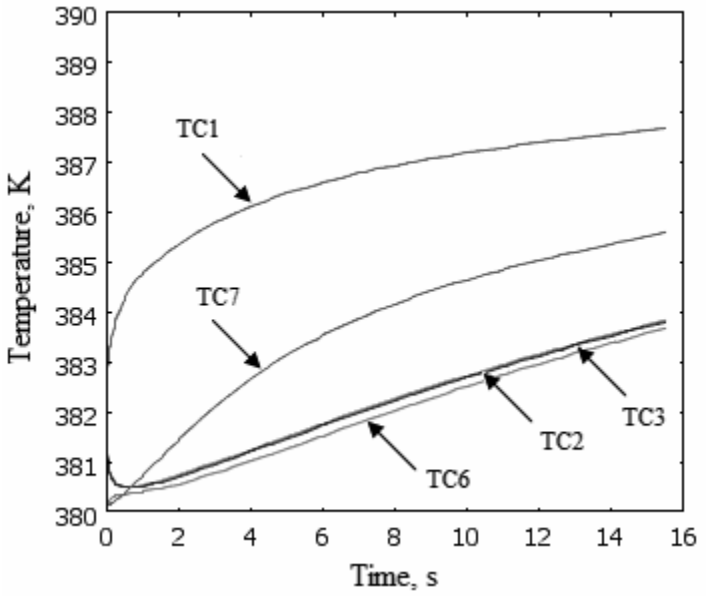

Figure 21: Temperature vs. time for PCM with a melting range

The temporal temperature distribution history for the current case under study can be seen in Figure 22. Some of the conclusions of Figure 21 can be clearly observed in Figure 22. Figure 23 shows the time evolution of the condensate film during the charging time. The variable *Time* spans from 0 to 15.5 s and is the same in both the figures. In Figure 23, it can be observed that the average film thickness at *Time* = 0 is zero while at *Time* = 0.001 s, it is about 81 μm and at *Time* = 0.5 s, δ on an average increases to 226 μm. This corresponds to the initial rapid cooling of the wall from 'T_v' at *Time* = 0 to a much lower value at *Time* = 0.5 s as can be seen in Figure 21. As T_{wall} starts to rise again, the film thickness starts going down until the end of charging time to an average value of 190 μm.

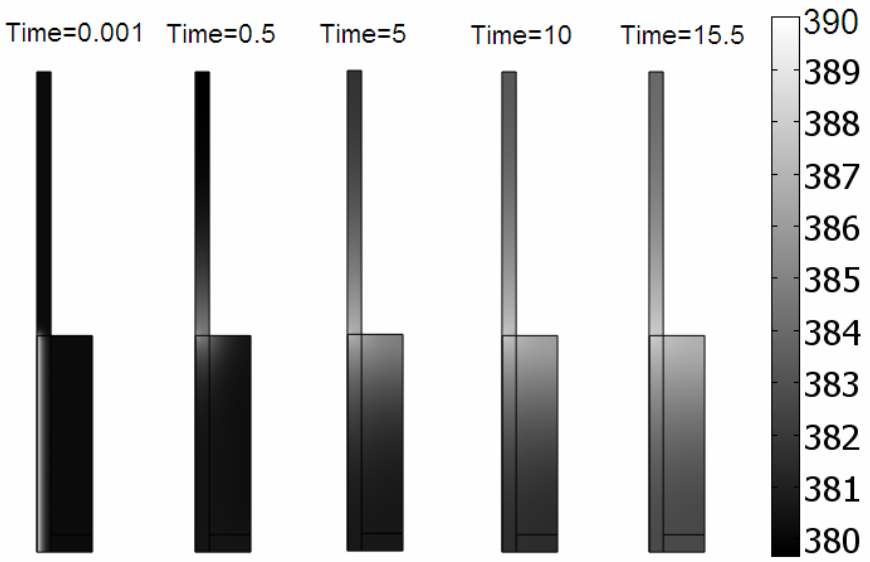

Figure 22: Temperature distribution in TES at various Time during charging

Using Figure 21, it is found that 81% of the total absorbed heat is by the PCM and foam composite, while the remaining 19% is by encapsulating column walls. This shows the importance of including the column wall inertia effects in the simulation of conjugate problem for the chosen boundary conditions. In addition, inclusion of column walls in the model facilitates for simulating simultaneous heat removal on the condenser side (extended portion of the columns i.e., boundaries 6 and 7 in Figure 15 that protrude outside of the vapor chamber as shown in Figure 20).

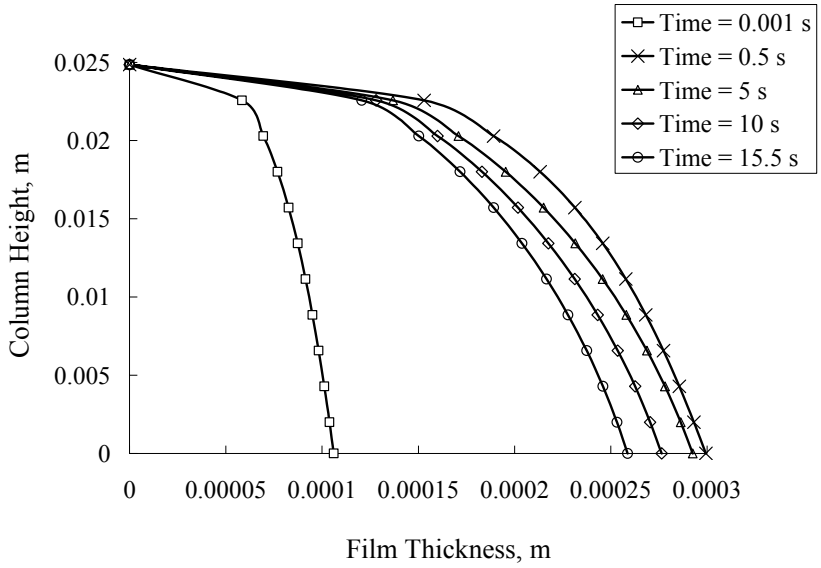

Figure 23: Transient film profile history (film thickness at Time = 0 is zero)

Importance of having TES in the VCTES heat sink

The effect of presence of PCM on charging of the VCTES heat sink can be observed in Figure 24, where the PCM was replaced with air for comparison with Figure 21. It can be seen that the wall temperature drops down initially. However, because the sink in this case is not as effective as in Figure 21, the wall temperature starts to rise rapidly and catches up with the vapor temperature even before the end of charging time.

If the vapor temperature was not fixed as in the current model, this will cause a continuous increase in the vapor temperature and hence the pressure inside the chamber. It can also be observed by comparing Figures 21 and 24 that in Figure 24, the temperature rise is purely characteristic of transient heat conduction as in a solid but in Figure 21, the temperature rise is in a more linear fashion because of PCM phase change.

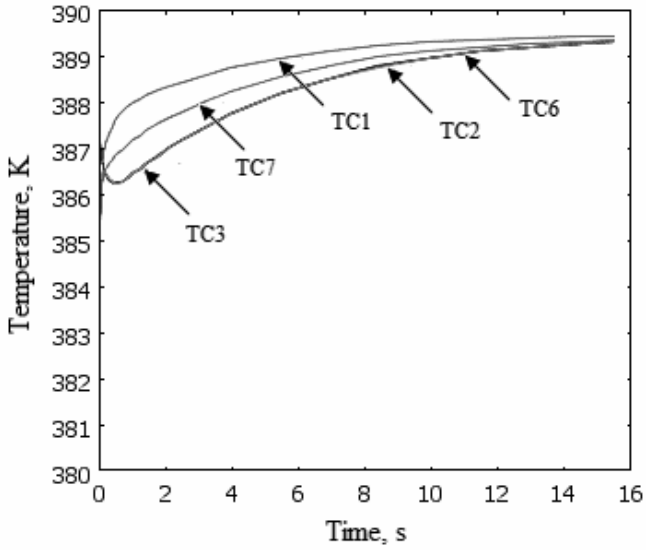

Figure 24: Temperature vs. time for TES columns with air (without PCM)

Importance of pure PCM

In Figure 25, the effect of using a pure PCM is analyzed and plotted. Pure PCMs are characterized by isothermal melting (here, 386 K) and hence the effect of full latent heat can be felt on the heat sink system. PCMs like the one used to simulate the case of Figure 21, will have a reduction in the latent heat peak owing to its distribution over a melting range (shown in Figure 18). The effect of melting range on the TES performance was studied and mentioned in Chapter Three. Heat capacity methods exhibit problems in simulating ideal isothermal melting and so usually enthalpy methods are used. Therefore, a δT of 0.001 K is used to approximately model the phase change process for this case and the entire h_{sf} of 266 kJ/kg is assumed to be distributed over this δT. Three more cases for a δT of 0.01 K, 0.0001 K and 0.00001 K were run. It was found that the time taken to reach a converged solution at each time-step almost doubled as δT became smaller. A difference of less than 0.01 K on an average was found to contain between

final solutions for δT of 0.001 K and 0.0001 K and this difference became less than 0.005 K as δT went down. Therefore, a δT of 0.001 K was selected for the simulation as achieving an accuracy of the final solution to more than two significant digits is not the goal of this simulation but to broadly see the effect of using pure PCM. The temperature-time history of PCM in Figure 25 is typical of pure PCMs. An initial cooling down of the wall temperature can be observed because of the presence of an effective heat sink (just like in Figure 21). The wall temperature begins to rise again but remains almost a constant when the PCM reaches its melting point and continues to stay there even until the end of charging time.

The same initial temperature as chosen in the simulation of Figure 21 was used even in the simulation of Figure 25 and so we could observe rapid initial temperature rise in the beginning (the period of no PCM phase change). The advantage of pure PCMs can be very clearly seen if an initial temperature is chosen such that it is slightly less than the PCM melting temperature. For example, in the case of Figure 25, if an initial temperature of 385.9 K were chosen, the entire operating temperature of PCM during charging period would have remained at 386 K and the wall temperature would have remained almost the same between 386.5 K and 387.5 K. In Figure 21, since the PCM has a melting range, it is inevitable to pick an initial temperature much less than the melting point peak to allow for the PCM temperature rise during melting.

Thus, it is evident that pure PCMs provide for better performance and near isothermal operation of the VCTES heat sink. It is interesting to note that the developed numerical model has little convergence problems even in solving an isothermal phase change problem, which is highly nonlinear compared to phase change problems with a melting range.

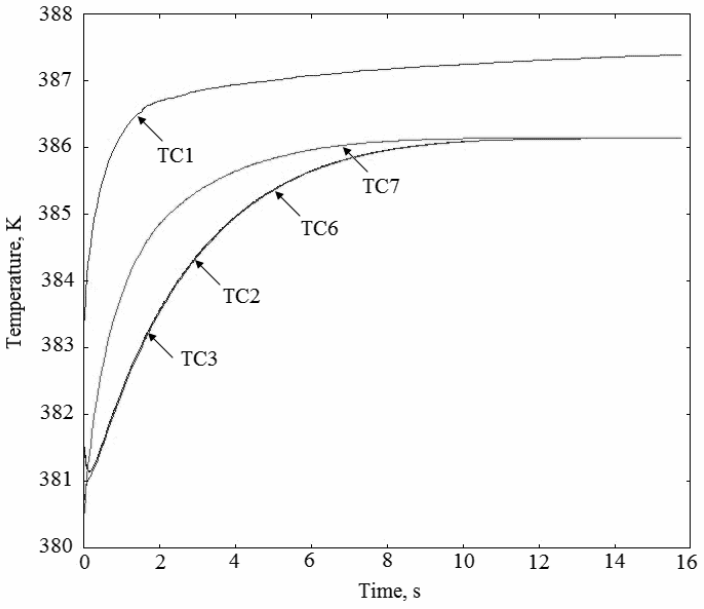

Figure 25: Temperature vs. time for pure PCM (with near-isothermal melting point)

Importance of graphite foam in TES

The developed numerical model was also used to study the importance of using foam in TES units. Accordingly, only PCM was assumed present in the columns without any thermal conduction-enhancing medium (graphite foam). The results are shown in Figure 26. The wall temperature drops initially because of the presence of a sink in the form of copper walls and PCM but this drop is not quite as much as in Figure 21. This is because in Figure 26, the majority of the heat sink comprises only of copper walls because of the poor penetration of heat in the PCM sans graphite foam. This could be clearly observed in Figure 26, where TC6 and TC7 are still at the initial temperature at the end of charging time indicating that no melting of PCM has taken place at those locations. Therefore, owing to its poor thermal conductivity, the resistance to heat transfer in PCM without graphite foam dominates the film condensation resistance during the transient charging process.

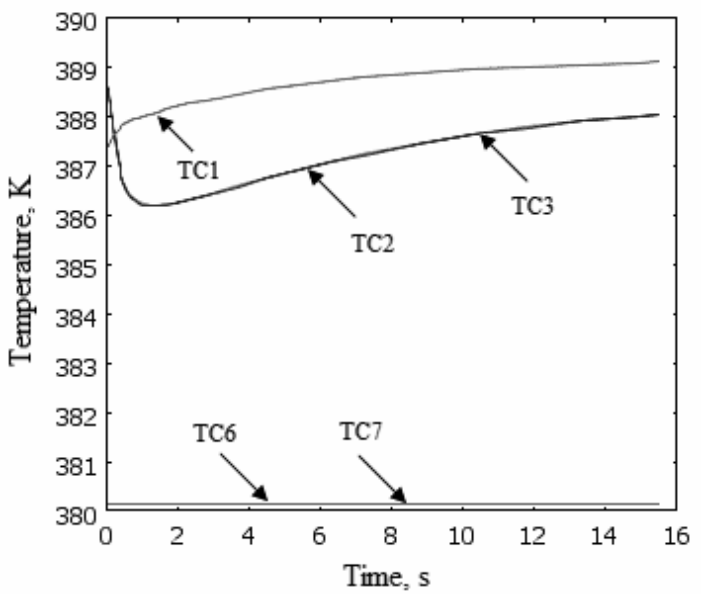

Figure 26: Temperature vs. time for TES columns without graphite foam

Importance of condenser on the performance

In the assumptions for the numerical simulation, it was assumed that heat removal from the outside surfaces of TES columns in Figure 15 is by forced convection. To see the effect of condenser on the performance of the storage feature in the heat sink, natural convection was assumed even on the outside surfaces of the TES columns and the results for this case are shown in Figure 27. It can be observed that the system temperature on an average is greater by about 0.5 K for this case compared to Figure 21 as expected. This shows that an efficient condenser plays a crucial role in controlling the temperature rise for fixed charging period conditions.

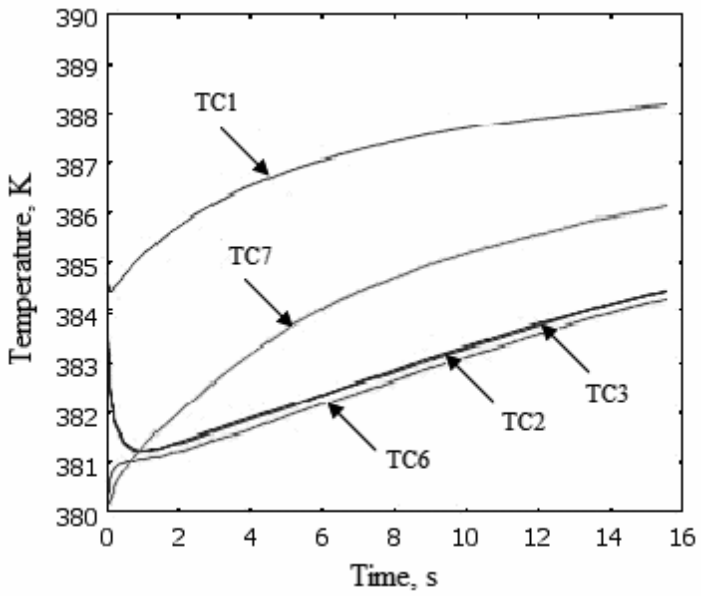

Figure 27: Temperature vs. time for TES columns with natural convection heat removal on the condenser

CHAPTER FIVE: EXPERIMENT

The primary objective of performing experiments with the VCTES heat sink is to show that using PCM columns inside the vapor chamber prevents in undue temperature rise of the system. There is no available open literature until date that focused on experimentation of a dual latent phase change system except for a similar work by Weislogel and Chung [11,12]. They experimentally studied the condensation phenomenon on packed bed of closely spaced spheres filled with a PCM. However, their work differs from the current effort in that their focus was not on observing the effect of having PCM in a vapor chamber with specific heat sink application as a heat spreader, which is the key focus of this work. Also, the flow effects of vapor on TES does not apply to the current concept, since vapor always occupies the chamber and does not flow through densely packed TES units unlike in Reference [12]. This will induce a different boundary condition for heat transfer to the TES. In addition, variety of improvements were made in the TES setup of this heat sink compared to the setup described in Reference [12] and have been detailed in Chapter Three. Therefore, it is interesting to perform experiments on integrated vapor chamber thermal energy storage (VCTES) heat sink to verify the implementation feasibility and understand the major impediments to its efficient thermal performance. The focus of this work is to verify the effectiveness of the concept during charging through experimentation.

Component acquisition and integration

A prototype integrated vapor chamber/TES system was built based on design 1 (detailed in Chapter Three) to validate the concept. The vapor chamber and top plate were machined using CNC mill. The 3D models and the machined parts are shown in Figures 28 to 34. A material with

a high tensile strength, lightweight, easy-to-machine and compatible with the HTF would be an ideal choice for the vapor chamber and TES columns. For experiment purposes, an easy-to-machine, low thermal diffusivity glass-mica ceramic material, Macor®, was selected for the vapor chamber along with its sidewalls to prevent parasitic heat loss in the experiments. For the top plate to the vapor chamber and for making custom TES containers, Copper was selected as the appropriate material as it is compatible with water. Copper also has high strength and so can withstand high internal pressures.

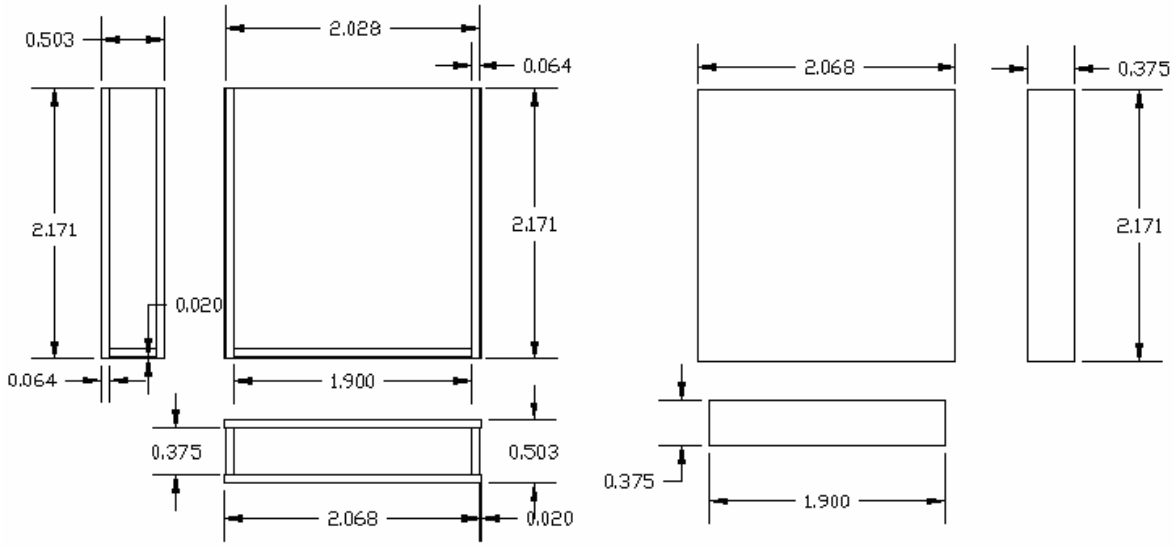

Figure 28: A single TES column – CAD drawing

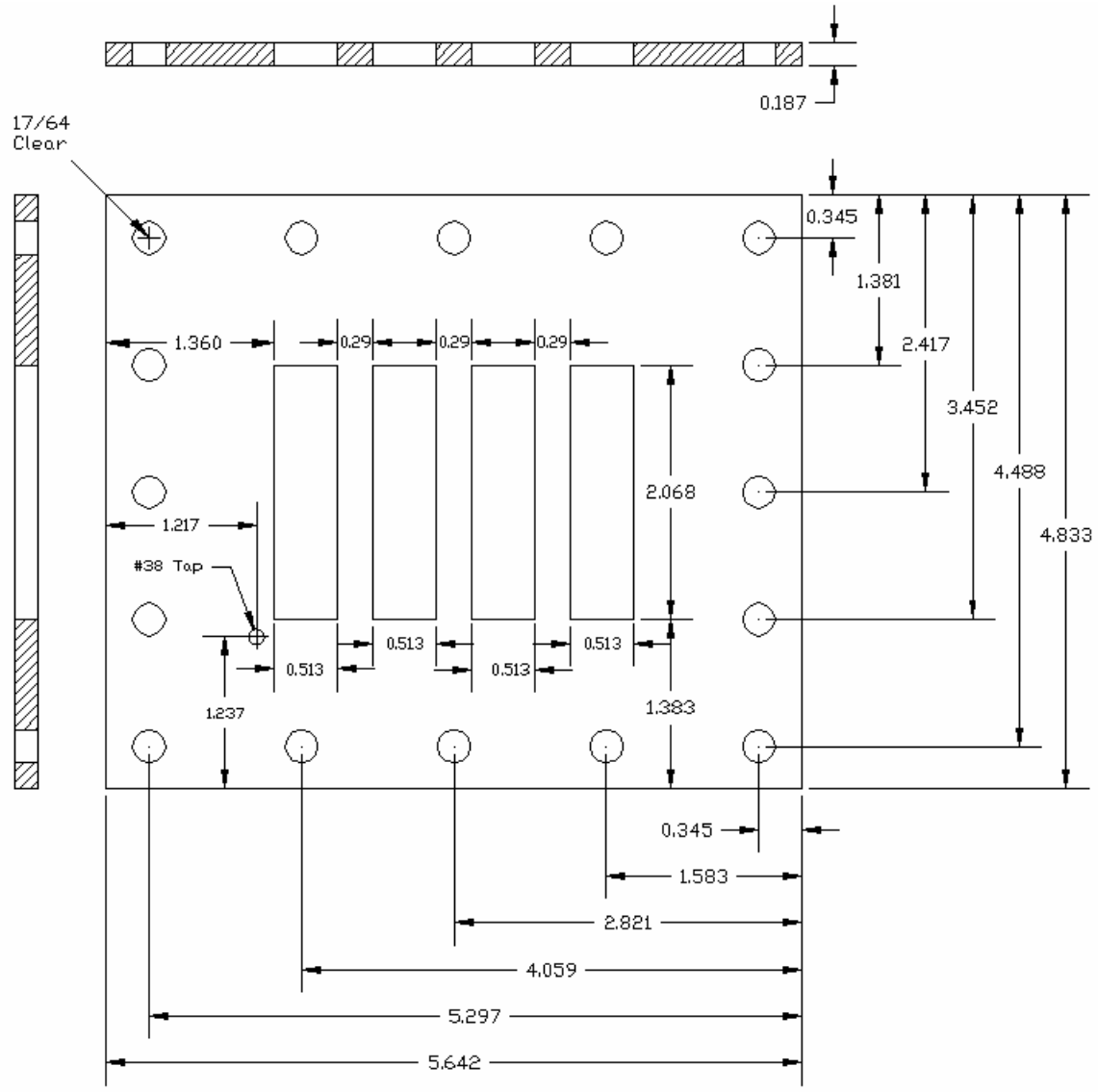

Figure 29: Top plate – CAD drawing

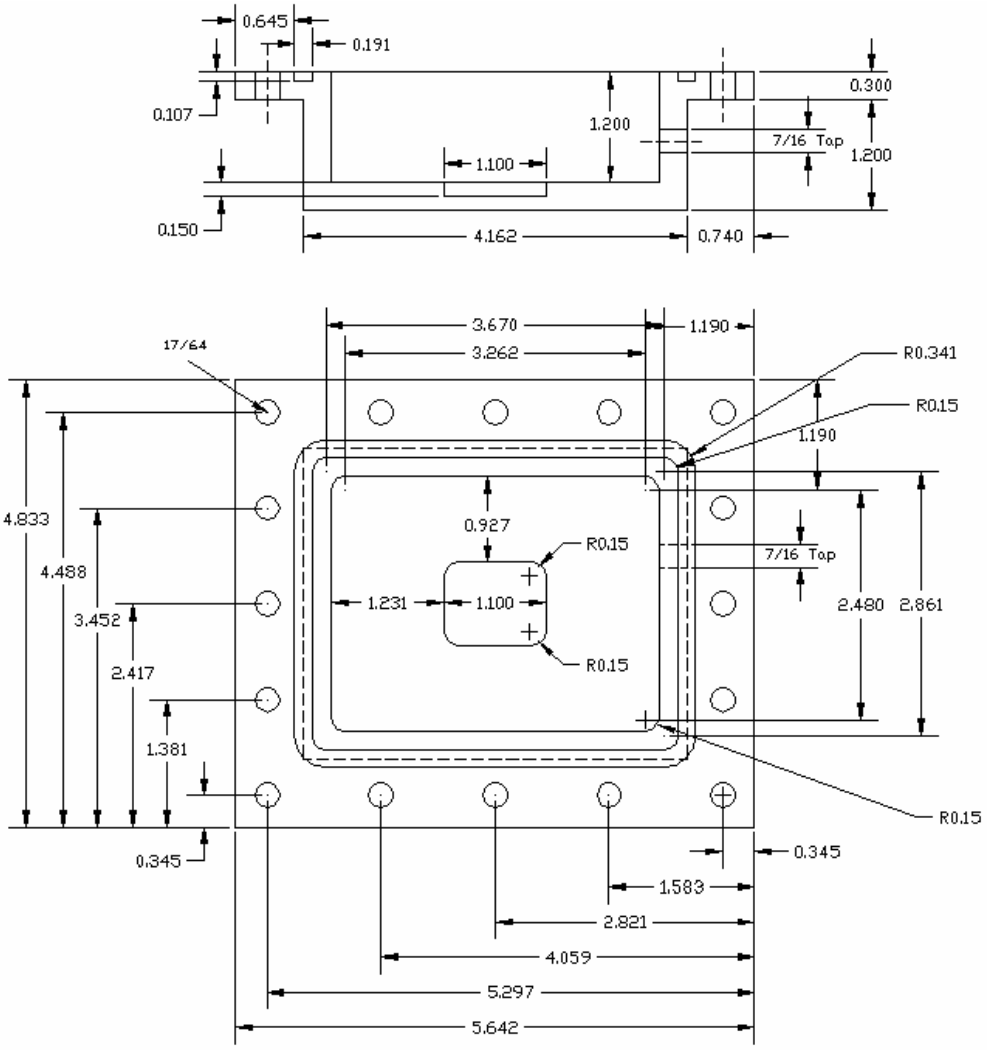

Figure 30: Vapor chamber bottom portion – CAD drawing

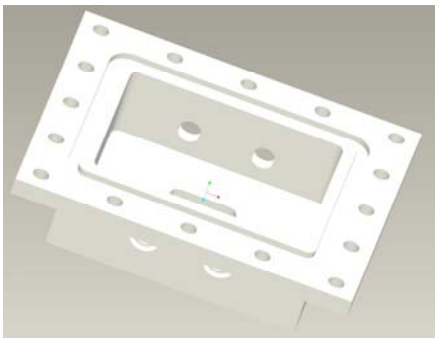

Figure 31: Vapor chamber bottom portion – 3D model

Figure 32: Vapor chamber bottom portion – manufactured part

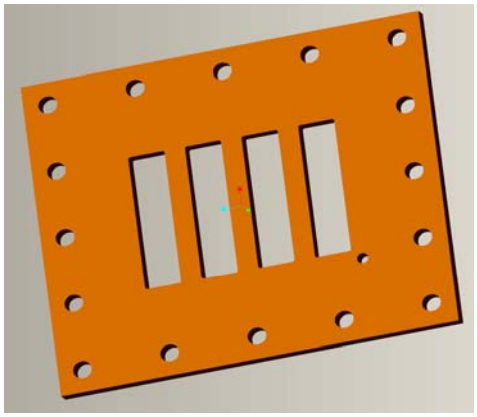

Figure 33: Top plate – 3D model

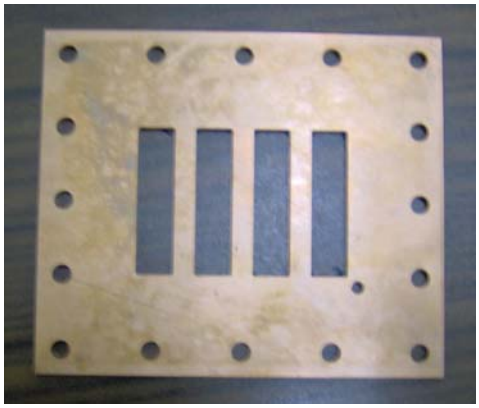

Figure 34: Top plate – manufactured part

The TES columns were integrated from the parts shown in Figure 28. Figure 35 shows various steps of integration of a single column and filling PCM by dipping the column in an oil bath and raising the oil temperature above the PCM melting temperature. A high thermal conductive bond, PyroDuct 597A® [64] (thermal conductivity of 9.1 W/m.K), was used to bond foam pieces to the copper plates of the TES columns. PyroDuct 597A® has a maximum operating temperature of 960 ^{0}C and so was not subjected to any damage during soldering of the column plates. Holes were drilled in the foam samples for inserting thermocouple wires. AWG 36, T-type thermocouples were used. Each column contained five thermocouples. Locations of the four thermocouple tips are shown in Figure 36. The fifth thermocouple tip lied on the center of the foam sample large face and was used for measurement of temperature in the heat transfer direction along with the one at the center of the sample.

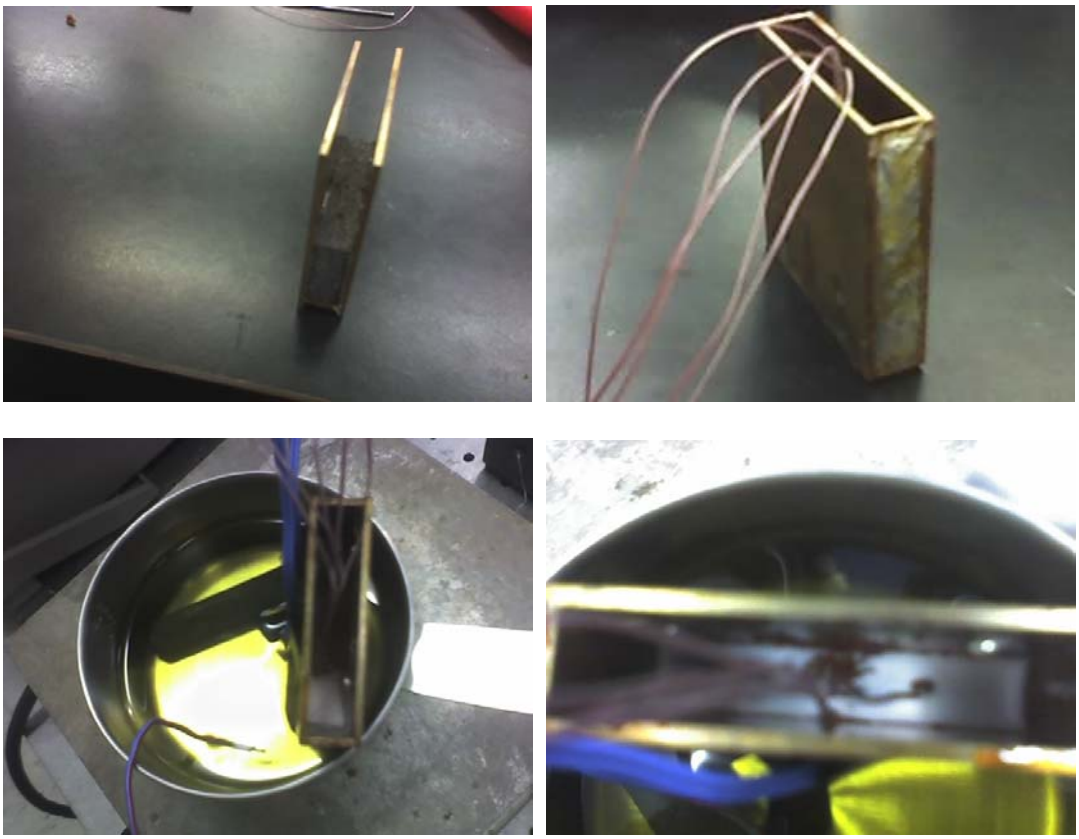

Figure 35: Column with two flat plates bonded together with foam in between (top left); Column with all the plates bonded by soldering and thermocouple wires inserted into the foam piece (top right); Tilted column in oil bath during PCM filling (bottom left); Top view of the setup for PCM filling (bottom right)

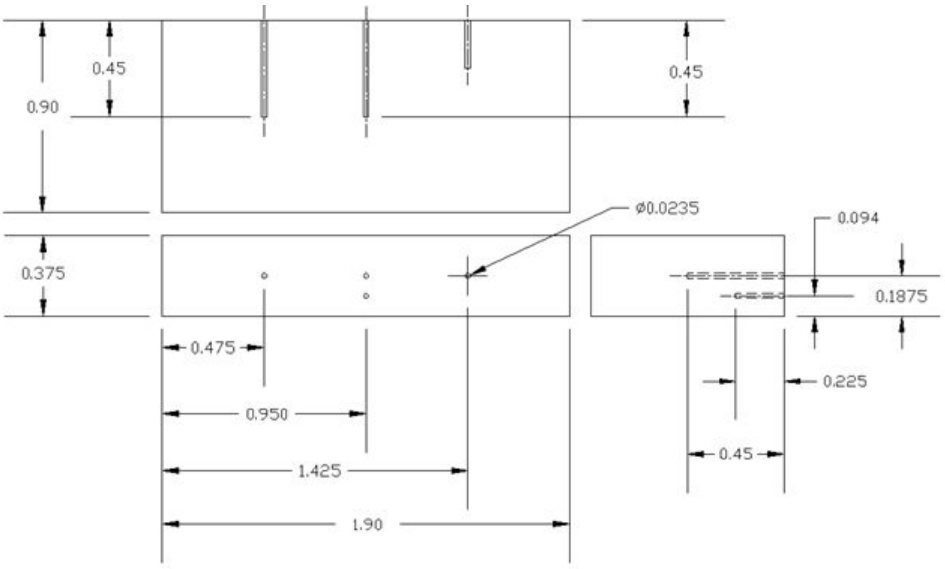

Figure 36: Thermocouple locations in Pocofoam for single column experiments

(all dimensions are in inches)

After assembling the TES columns, the condenser (top plate with TES columns) was assembled by attaching the sealed columns to the top plate and is shown in Figure 37. A special epoxy H74 from Epotek® [65] was used for this purpose.

While attaching the columns to the top plate, the entire setup and individual columns were all checked for horizontal orientation using a spirit level. Figures 38 and 39 show that the top plate and the combined span of the four columns are in the horizontal position after the joining epoxy is completely cured. Similarly, each of the four columns (when mounted in the top plate) was checked for correct horizontal positioning. Figure 40 shows the sealing mechanism employed at the inside junctions of the top plate assembly.

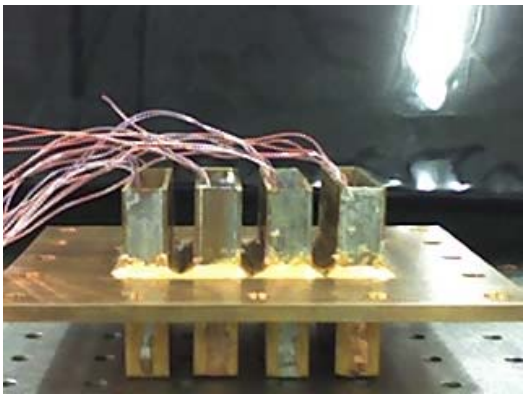

Figure 37: Condenser assembly

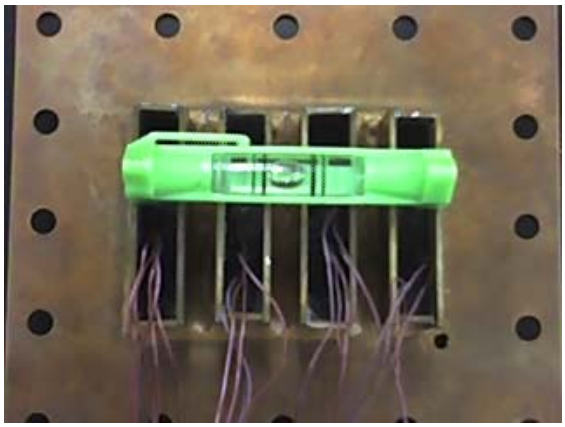

Figure 38: Levelled column span

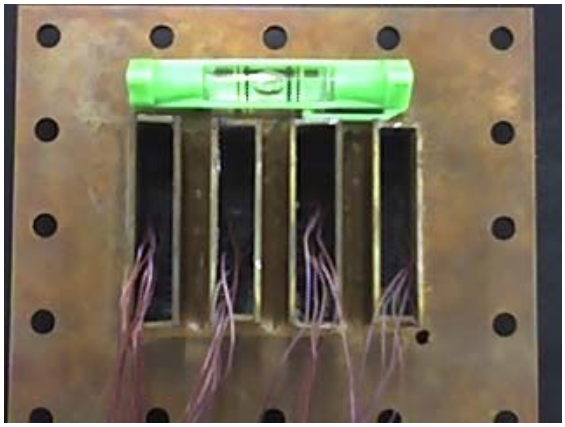

Figure 39: Levelled top plate

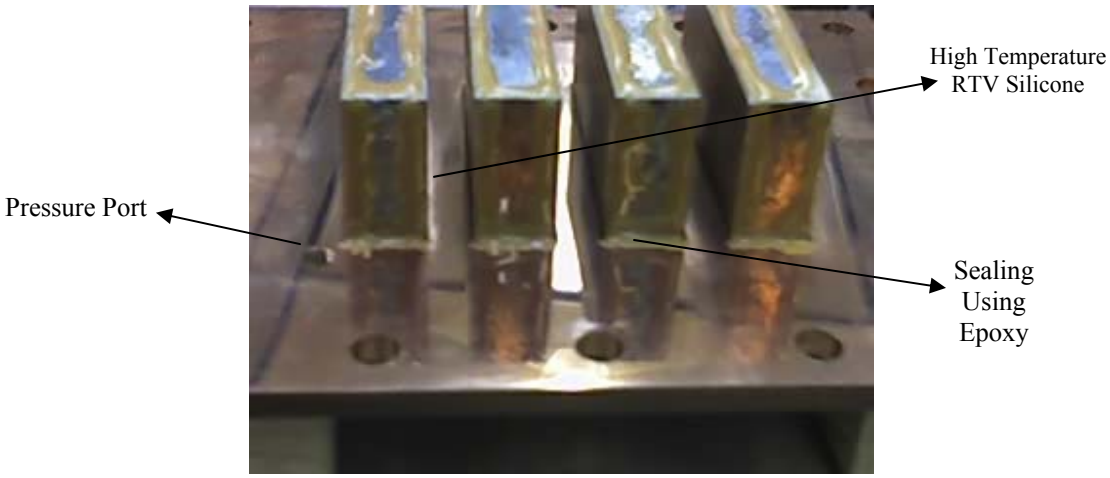

Figure 40: Sealing at the condenser bottom surface

A manually controlled pulsed power supply was built and checked for proper operation. The power supply circuit consisted of two different DC power supplies connected in parallel to a switch, one power supply with high voltage and current capability to produce pulse loads and the other with low voltage and current rating to simulate the low heat period loads. The switch used was of single-pole double-throw (SPDT) type with break-before-make integrated circuit. It was found that manual switching with the procured switch can be performed in less than a second and so the same was used during experiments to switch between pulse heat and low heat times, which were in the order of tens of seconds. Since the switch was of break-before-make type, no short-circuiting was found to occur during switching between the two power supplies. Figure 41 shows the power supply circuit diagram. The power supply system was integrated with the data acquisition (DAQ) system to measure current and voltage.

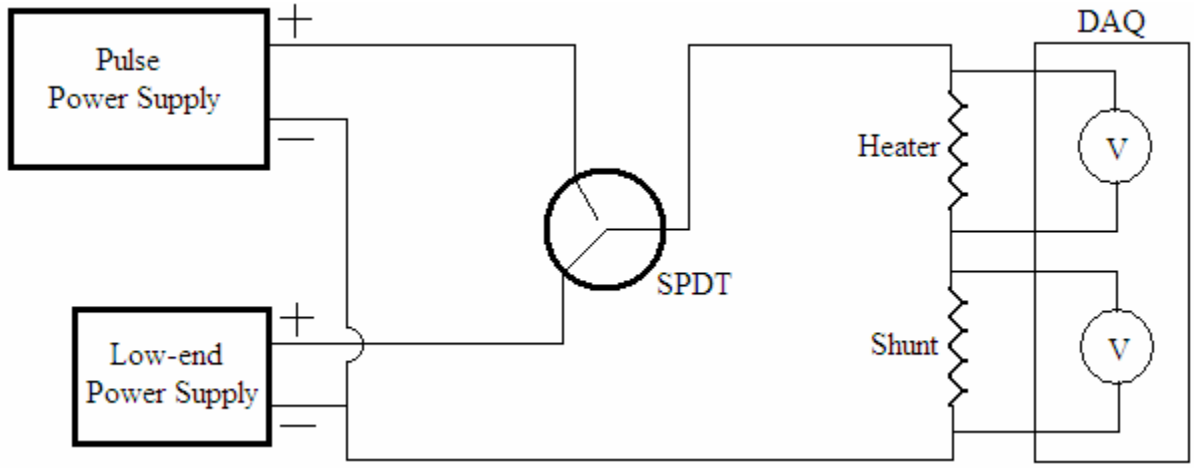

Figure 41: Power supply circuit diagram

Custom feedthroughs were designed for instrumentation of the VCTES system and are shown in Figure 42. Figure 43 shows the details of a feedthrough. Thermocouple wires were passed through a commercially available adapter with an o-ring and the empty space was filled with the high-temperature RTV silicone.

To prevent steam leakage through the gap between the bare wire and the insulation, the wires were stripped such that it exposed the bare wire in the middle. Silicone was then used to surround the bare wire. To prevent touching of two thermocouple wires at the stripped portions, they were separated using a shirt button. The internal details of a feedthrough are shown in Figure 44.

Five feedthroughs were used in the VCTES experiments for temperature monitoring and hosted ten thermocouples (AWG 24, T-type) in total for measurement of vapor temperature at different places inside the chamber. One feedthrough was used to pass power supply wires.

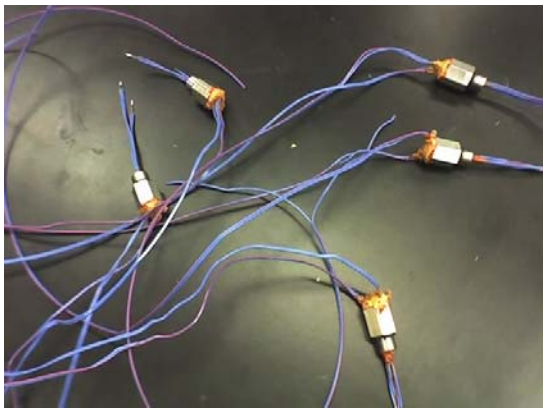

Figure 42: Custom made feedthroughs

Figure 43: Feedthrough with silicone and o-ring

Figure 44: Feedthrough internal details

Two different types of PCM were considered for use in the experiments (based on the discussion in Chapter Three). Magnesium Chloride HexaHydrate ($MgCl_2.6H_2O$ = MCHH) was considered first to be used as the energy storage material. It is attractive in terms of cost and material compatibility.

The exact melting temperature of a dry salt of magnesium chloride is 714 ^{0}C. For hydrates when being used as latent thermal energy storage materials, melting temperature is often used for dehydration temperature. Dehydration temperature is where the salt hydrate loses its water by absorbing heat (equal to the heat of hydration). The dry salt and water will be two separate compounds. When the same amount of heat is released from an encapsulated salt hydrate-water system, the water molecules coagulate back into the lattice of the alkaline metal salt molecules forming a crystalline structure. This is a result of the hygroscopic property of most alkaline earth metal salts like magnesium chloride and calcium chloride. This phenomenon enables salt hydrates to be used as thermal energy storage materials.

MCHH has low thermal expansion. This coupled with a high value for the density in either state enables for an efficient TES. The thermal conductivity compares with other PCMs on the high side both in its solid and liquid phases. It has reasonably high values of latent and specific heats. MCHH usually has the problems of incongruent melting, corrosiveness and supercooling but provide the advantage of using water as the HTF since the boiling point of water (100 ^{0}C) is close to the melting point of MCHH (116.7 ^{0}C). In addition, water is highly non-toxic and is cheaply available for the experiment. MCHH has a single melting point, which makes it ideal for use as TES in the current setup.

A >99% pure MCHH sample was heated in an open container to temperatures above its melting point. Upon solidification, it formed a dry salt ($MgCl_2$) but not the crystalline hexahydrate. This showed that all the moisture is evaporated and there is no chemical bonding in molten/dehydrated salt between salt and water molecules. This puts a limitation of putting solid MCHH by melting and pouring it into foam filled TES columns. Wax would be easy to handle in such cases as it undergoes exactly a phase change but not a dehydration reaction like MCHH. Therefore, a paraffin wax that melts at close to the boiling point of water was searched. POLYWAX® 1000 from Baker Petrolite Polymers Division was found to have a melting peak at 113 ^{0}C (386 K) and so it was selected for use in the experiments.

Different configurations were considered for a heater like using a heater with a threaded base that can be screwed to the bottom of the vapor chamber base, a detachable plate heater etc. An assembly of thick film resistors of BeO [66] attached/soldered to a thin 20 mm X 20 mm copper plate fixed in a slot to the bottom of inside surface of vapor chamber (see Figure 12) was used as the heat source. Care was taken to match the level of the copper plate surface of the heater with vapor chamber bottom surface so that there is always water on the heater surface. The heater setup is shown in Figure 45.

Figure 45: Heater assembly

Accuracy of all the thermocouples used in the experiments was checked by comparing with ice and steam points. Uncertainty of temperatures measured was ±0.5 ^{0}C. The temperature measurements were obtained by fitting a fifth-order polynomial to the sensed voltage readings and incorporated into the DAQ.

Integration of the experimental setup and testing

Two different types of experiments were performed, one with a single TES column dipped in oil and one with an integrated VCTES setup. Experiments with a single column dipped in oil (up to the height of foam inside the columns) undergoing transient heating helped to measure temperatures at various locations of the PCM inside foam-filled columns and thereby to check the possibility of using such a configuration in an integrated VCTES system for TES. These experiments were also useful to observe the melting and solidification behavior of PCM in the columns for transient temperature boundary condition, the effectiveness of filling of pores of foam by PCM, formation of voids and possibility of supercooling of PCM inside pocofoam. In addition, these experiments proved the fabrication feasibility of leak-proof TES columns and thus simplify the path for performing integrated VCTES setup experiments.

The results of the single column experiments for different heat rates are shown in Figures 46, 47 and 48.

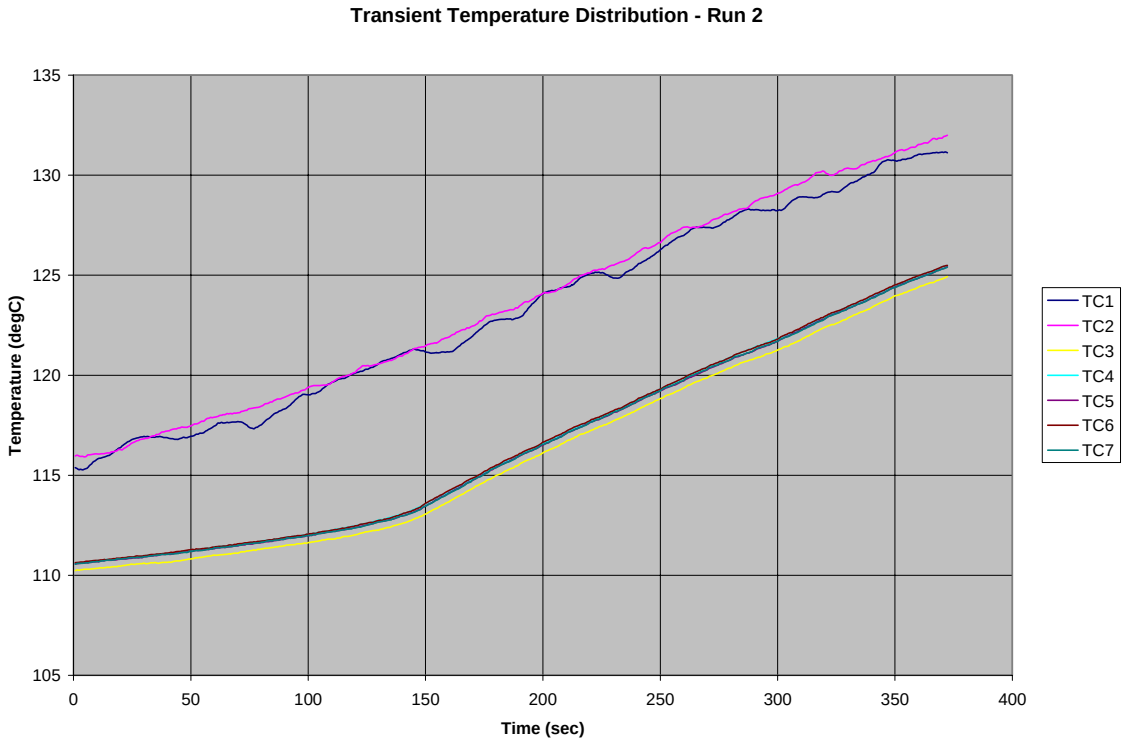

Figure 46: Transient temperature distribution for a temperature rise rate of 0.039 ^{0}C/s

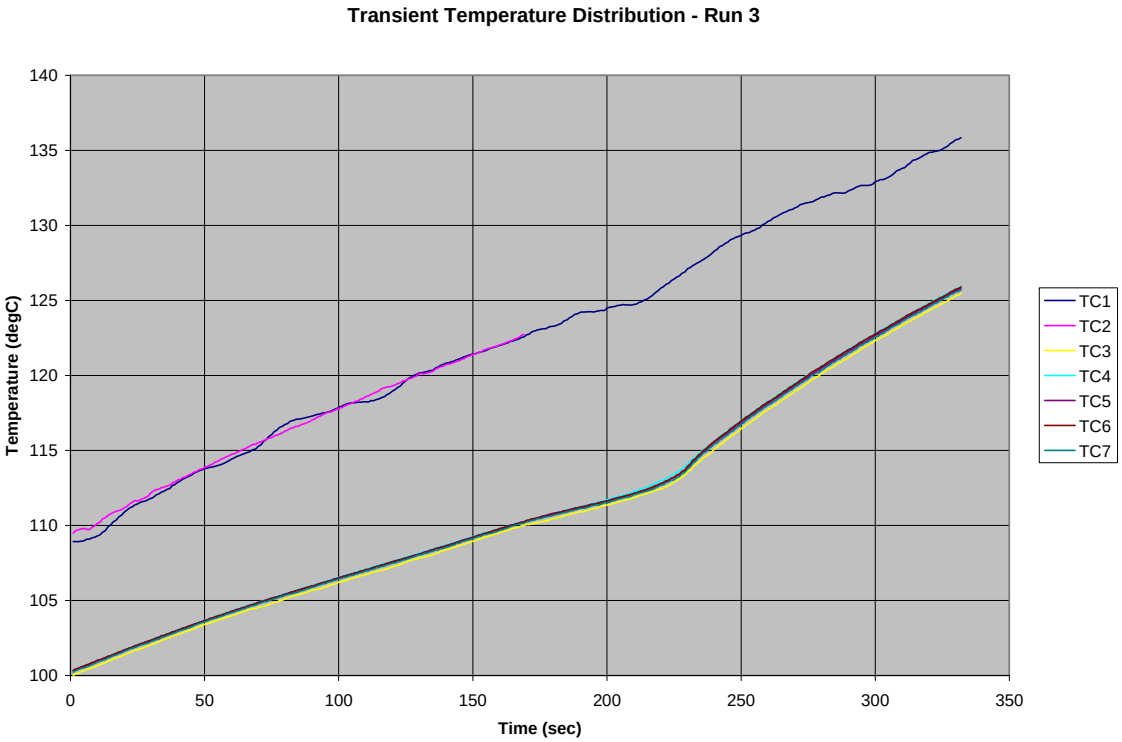

Figure 47: Transient temperature distribution for a temperature rise rate of 0.071 ^{0}C/s

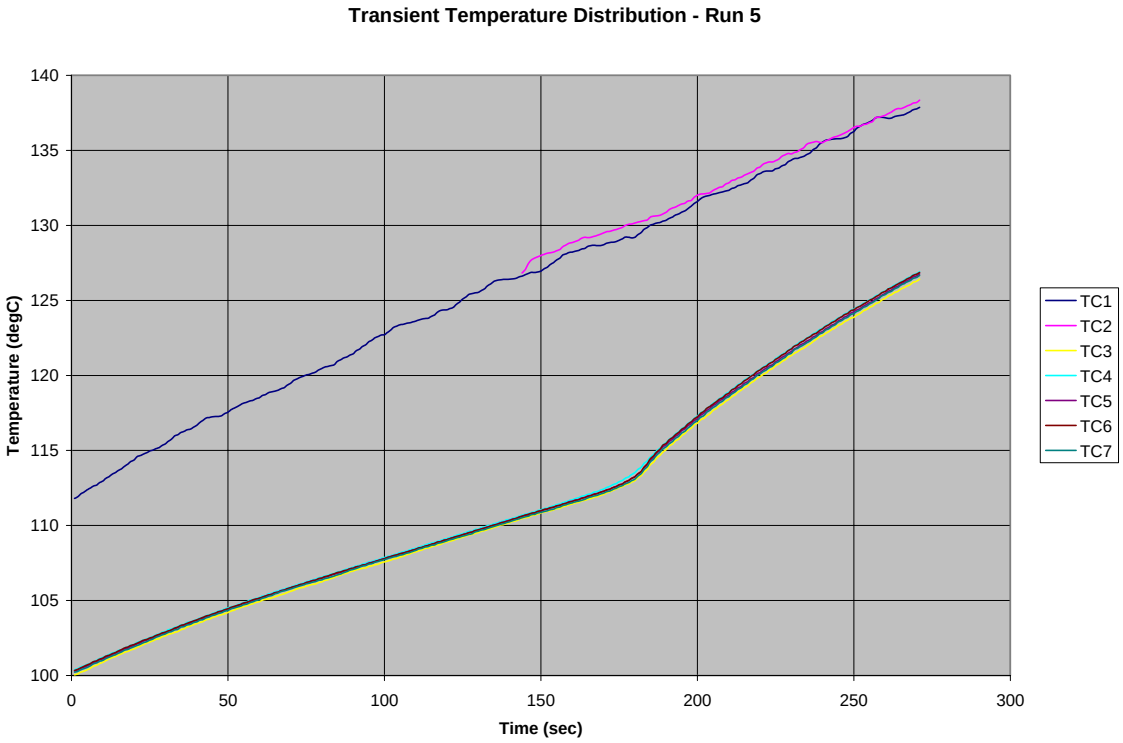

Figure 48: Transient temperature distribution for a temperature rise rate of 0.093 ^{0}C/s

During the experiments, thermocouples TC1 and TC2 were not soldered to the column outside surfaces since those columns were intended for use in integrated VCTES experiments. From the plot, this can be clearly observed with TC1 and TC2 lying much above the other thermocouples.

A key conclusion can be made from the results that for a transient temperature rise of the column outside surface at a constant or variable rate, all the thermocouples inside the foam and PCM composite were found to maintain nearly a same temperature. Therefore, this kind of behavior was expected even during the integrated VCTES experiments. These experiments also

showed the importance of having a good thermal contact between foam and copper walls of TES columns.

The complete VCTES setup was then integrated. A high temperature o-ring made of Ethylene-Propylene material (has a very low steam permeability rate) was smeared with a thin layer of high vacuum grease and was used to perfectly seal the junction between the top plate and the chamber. A support wooden plate was used at the bottom of the VCTES heat sink for holding against stress due to internal pressures. The experiment setup and the integrated system are shown in Figures 49 and 50. All the pipes (made of high temperature Teflon), pressure and vacuum gauges, flow control and pressure relief valves were thoroughly insulated.

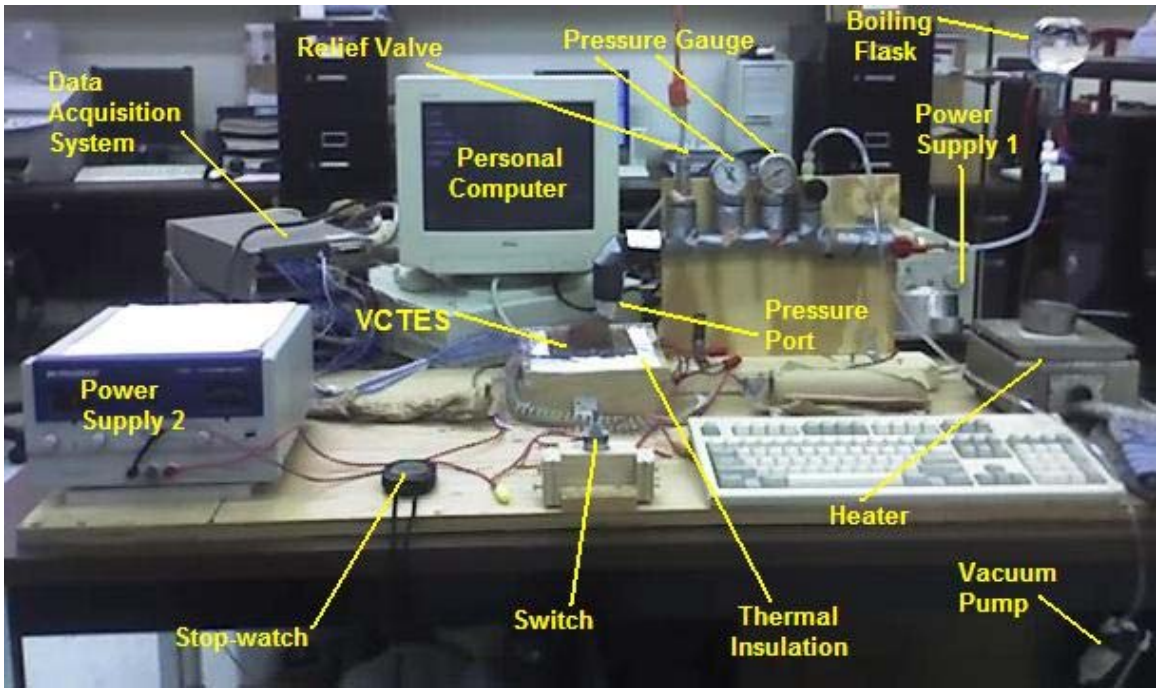

Figure 49: Integrated VCTES experimental setup

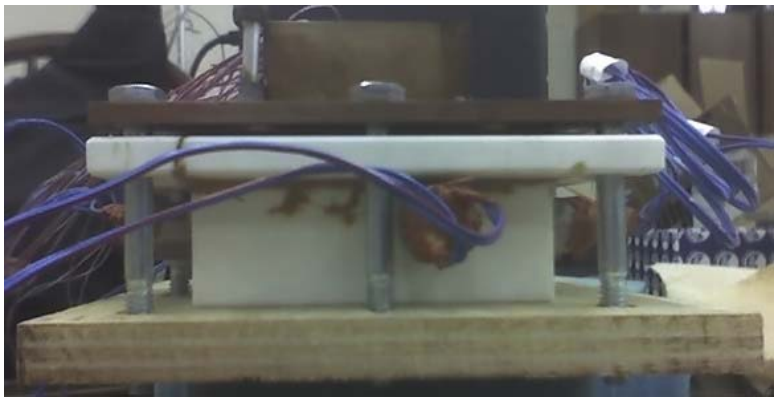

Figure 50: Integrated VCTES setup with a support wooden plate at the bottom

A pulse heat flux of 40 W/cm^2 was used in all the experiments. The low–end heat flux was found to be ~11 W/cm^2 to get the system to a steady-state temperature of 107 ^{0}C. To observe the difference between the pulse heat and low heat periods clearly, no forced convection was used on the condenser portion. A pressure relief valve rated for 50 psig was used for safety. The VCTES setup was insulated by surrounding it with glass wool. All the thermocouples were instrumented to a programmable DAQ system. A pressure and a vacuum gauge were used to monitor pressure and vacuum respectively inside the chamber. Two control valves were used, one attached to the vacuum pump and the other attached to the boiling flask. The boiling flask consisted of distilled water boiled continuously for more than five hours.

The vacuum pump valve was first opened and the boiling flask valve was closed. This created vacuum inside the chamber. The boiling flask valve was then opened with the vacuum pump valve closed, which sucked water into the chamber. 35 mL of water was sent in for all the experiments. This prevented the submerging of TES columns in the water below them. In

accordance with the height of water level above the heater that corresponds to 35 mL, a pulse heat flux of 40 W/cm^2 was found to be suitable to prevent heater dry-out.

A series of experiments were then performed all without PCM in the columns. These served as baseline experiments for comparison with experiments with PCM in the columns. For all the experiments, the TES columns were numbered as shown in Figure 51. It must be noted that columns 1 and 4 lie outside the heater while columns 2 and 3 lie directly above the heater in the assembled VCTES setup. In all the experiments, thermocouples TC12 and TC14 lie in column 1, TC17 and TC21 lie in column 2, TC22, TC23, TC24 and TC25 lie in column 3, TC27 and TC28 lies in column 4, and TC 29 and TC 30 lie in the vapor space.

The chamber was opened after each experiment to drain out the used water and exactly the same measured volume of freshly boiled distilled water was again sent in through the flow setup. Water droplets were also thoroughly cleaned from the TES columns' outside surfaces for each new experiment. This process was repeated to ensure identical conditions for all the experiments. Uncleaned water droplets on TES column surfaces will cause thermal resistance to heat transfer from vapor, each time a new experiment is started.

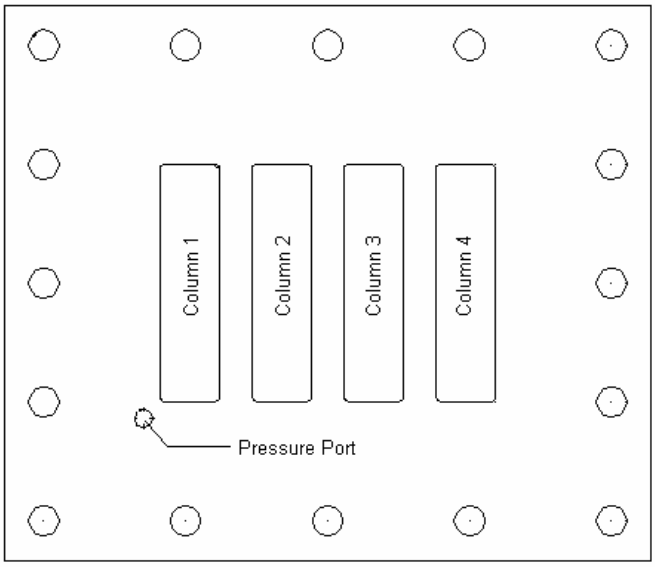

Figure 51: Numbering of TES columns

Results and discussion

Experiment case 1 consisted of allowing the system to reach a steady state at 107 ^{0}C (heat flux of 11 W/cm^2), providing a pulse of 40 W/cm^2 for 16 seconds and then giving the system a discharge time sufficient enough for it to reach back to the steady state. This was followed by another pulse of 16 seconds to check the repeatability. The results for this case are shown in Figures 52 and 53. In Figure 53, data values for only those thermocouples in TES columns are plotted along with the heat flux for simplicity. It was found that the system on an average returned back almost close to initial state at the end of discharging period. The slope *dT/dt* was found to be the same (~ 0.18 ^{0}C/s) for both the pulses. This confirms the repeatability aspect.

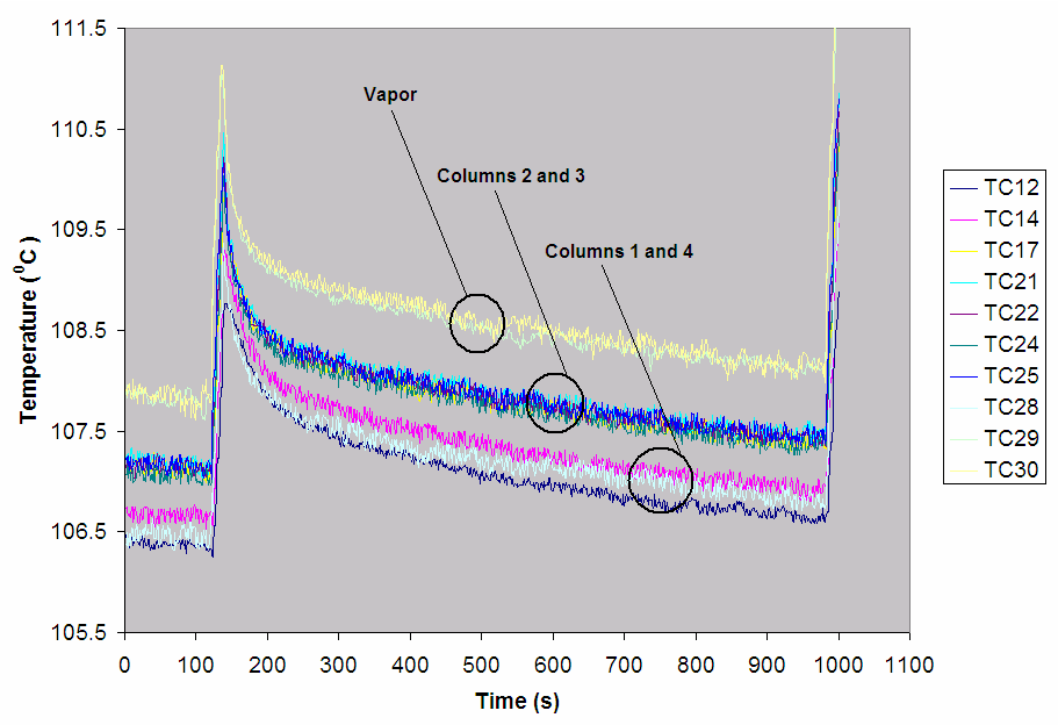

Figure 52: Temperature vs. time plot for case 1 without PCM

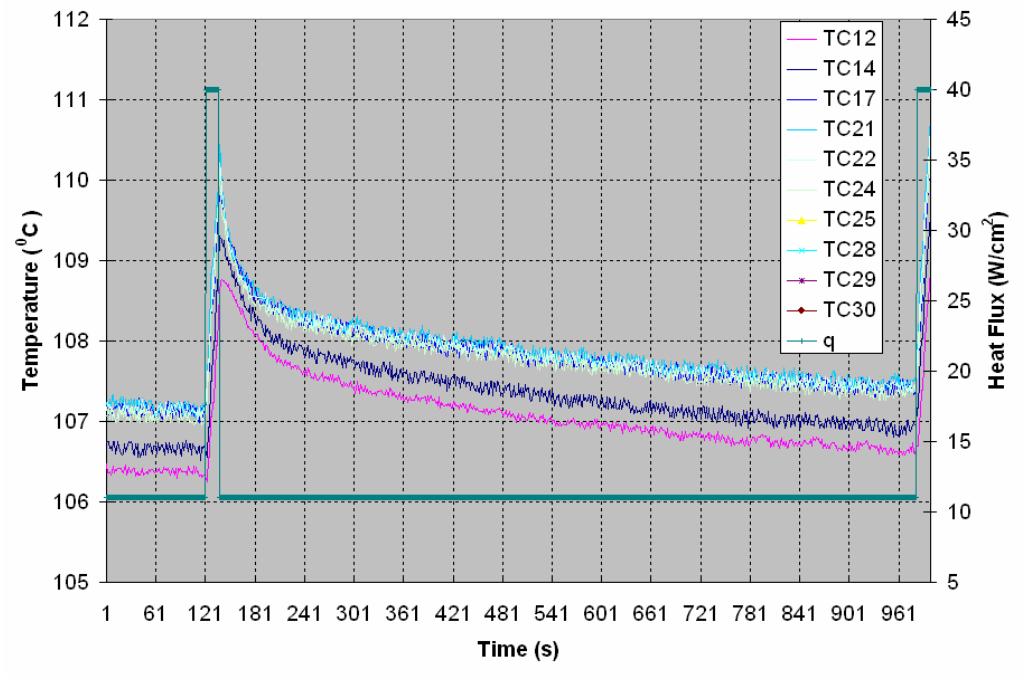

Figure 53: Temperature, heat flux vs. time plot for case 1 without PCM

To verify the VCTES heat sink behavior for high heat loads without PCM, case 2 experiments were performed, where a pulse of 32 seconds is provided instead of 16 seconds like in case 1. The results are shown in Figure 54. It is clear that the system temperature rose more than in case 1 as expected.

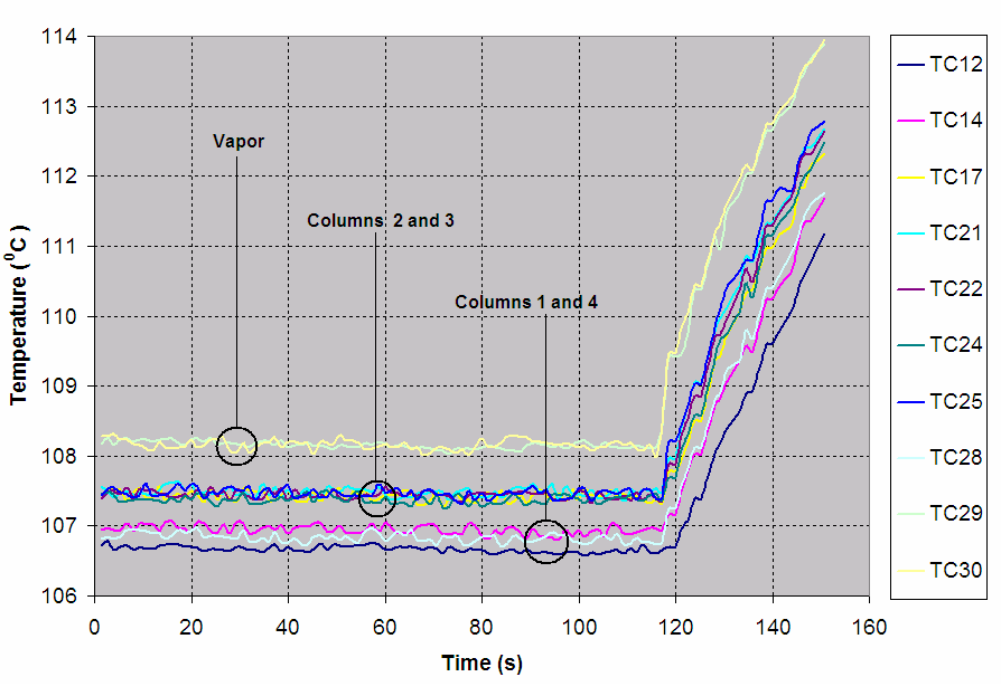

Figure 54: Temperature vs. time plot for case 2 without PCM

The same cases were repeated with PCM inside columns and the results are shown in Figures 55 and 56. A fan was used for case 1 with PCM to get the system back to the steady-state.

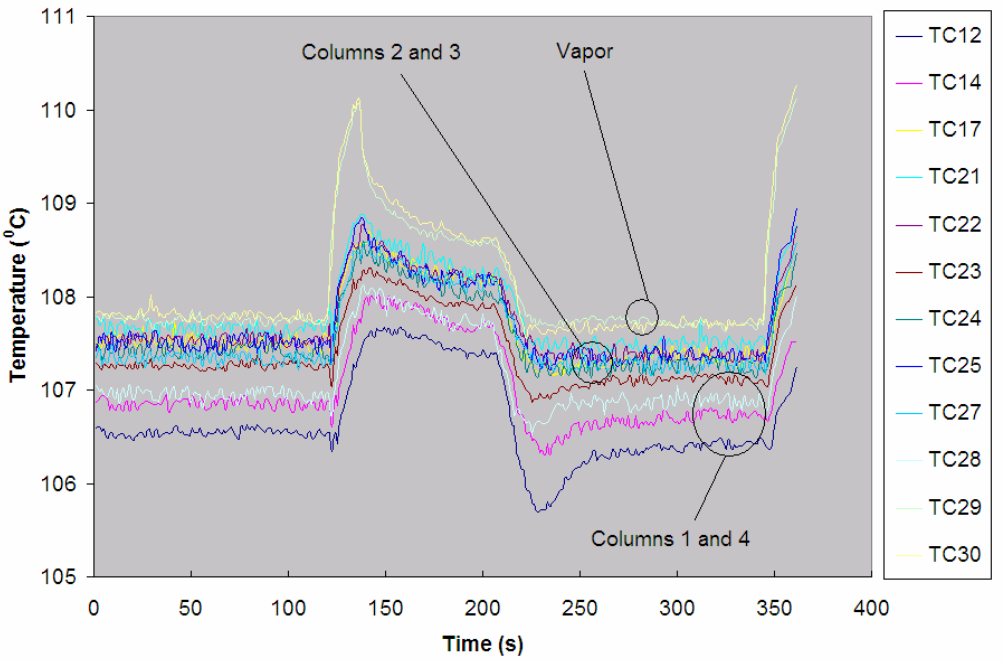

Figure 55: Temperature vs. time plot for case 1 with PCM

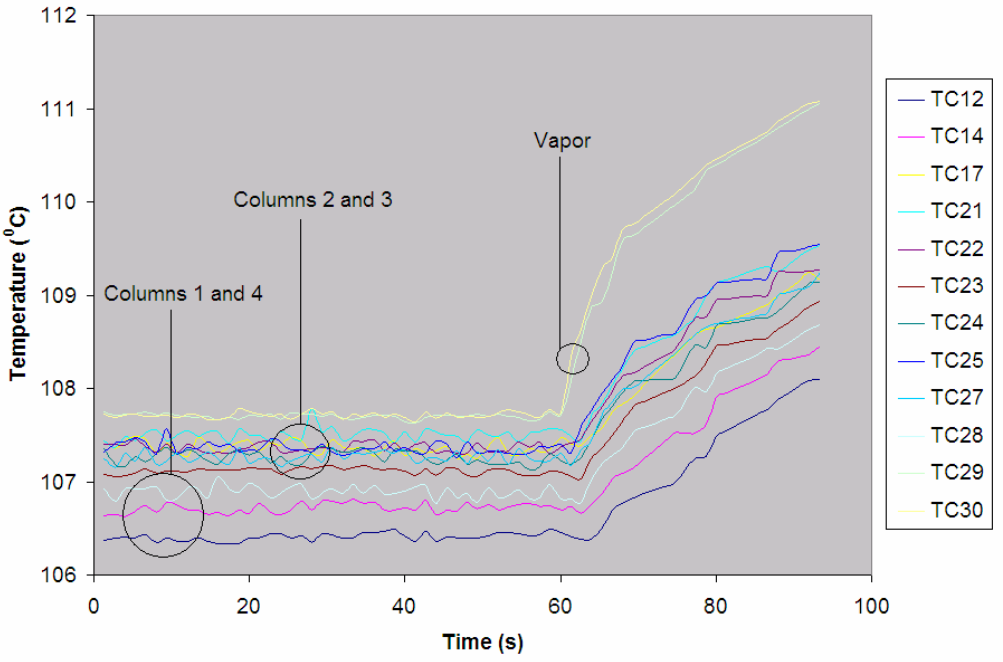

Figure 56: Temperature vs. time plot for case 2 with PCM

For clearly comparing the effect of using PCM in the heat sink, the vapor temperature TC30 for cases 1 and 2 for different initial steady state temperatures are plotted in Figures 57 to 60. Figures 61 and 62 show the vapor temperature for various experiments performed, all with PCM, for cases 1 and 2 respectively, for different initial steady state temperatures.

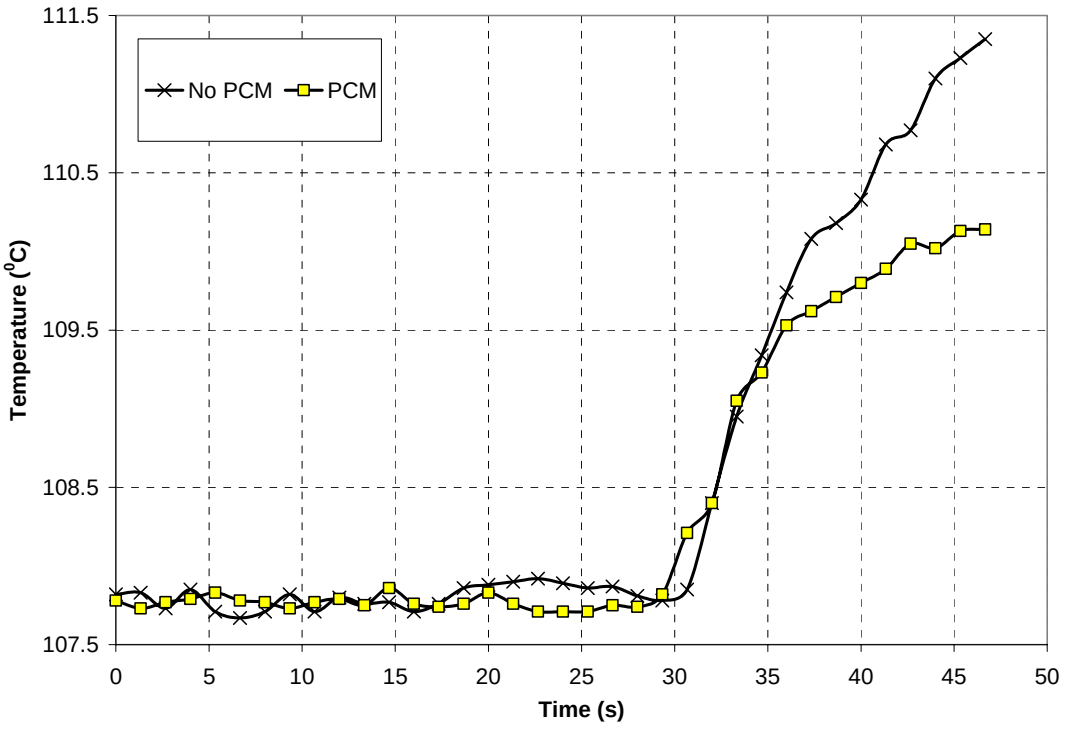

Figure 57: Comparison of vapor temperature rise for case 1 with and without PCM – steady state of 107.80 ^{0}C

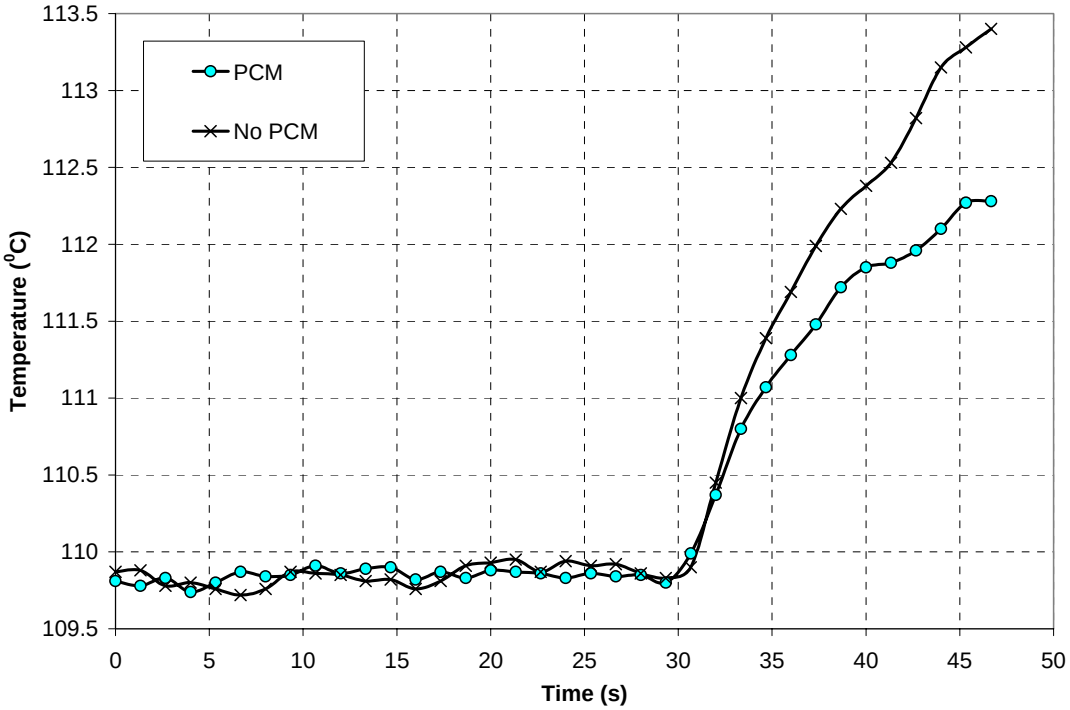

Figure 58: Comparison of vapor temperature rise for case 1 with and without PCM – steady state of 109.85 ^{0}C

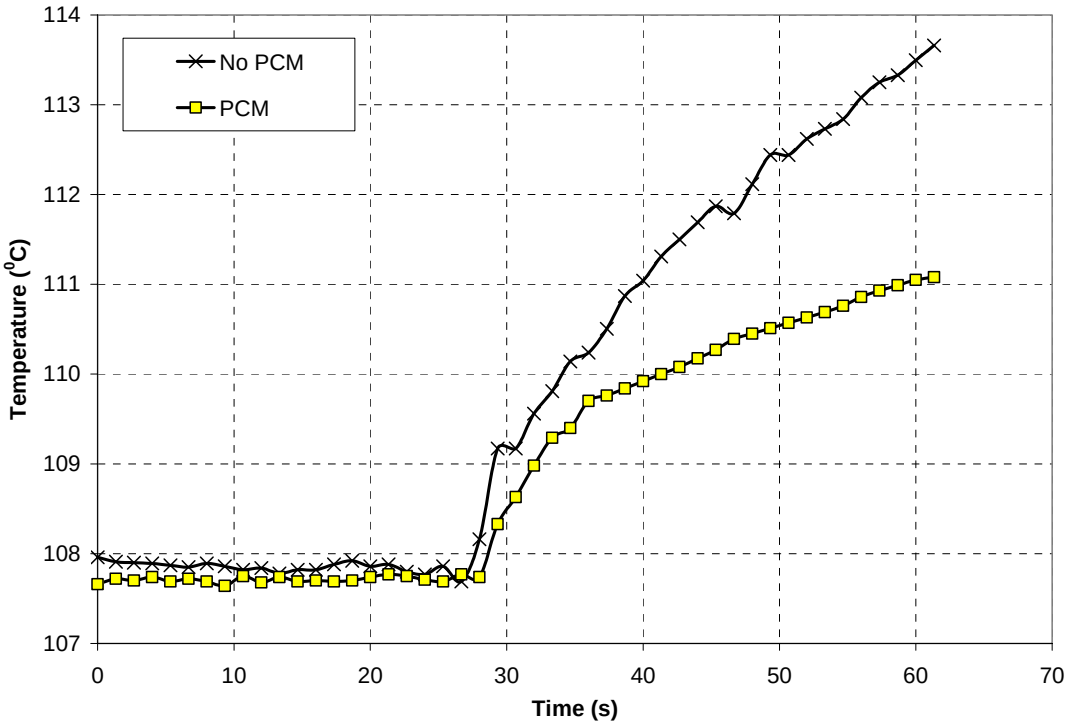

Figure 59: Comparison of vapor temperature rise for case 2 with and without PCM – steady state of 107.87 ^{0}C

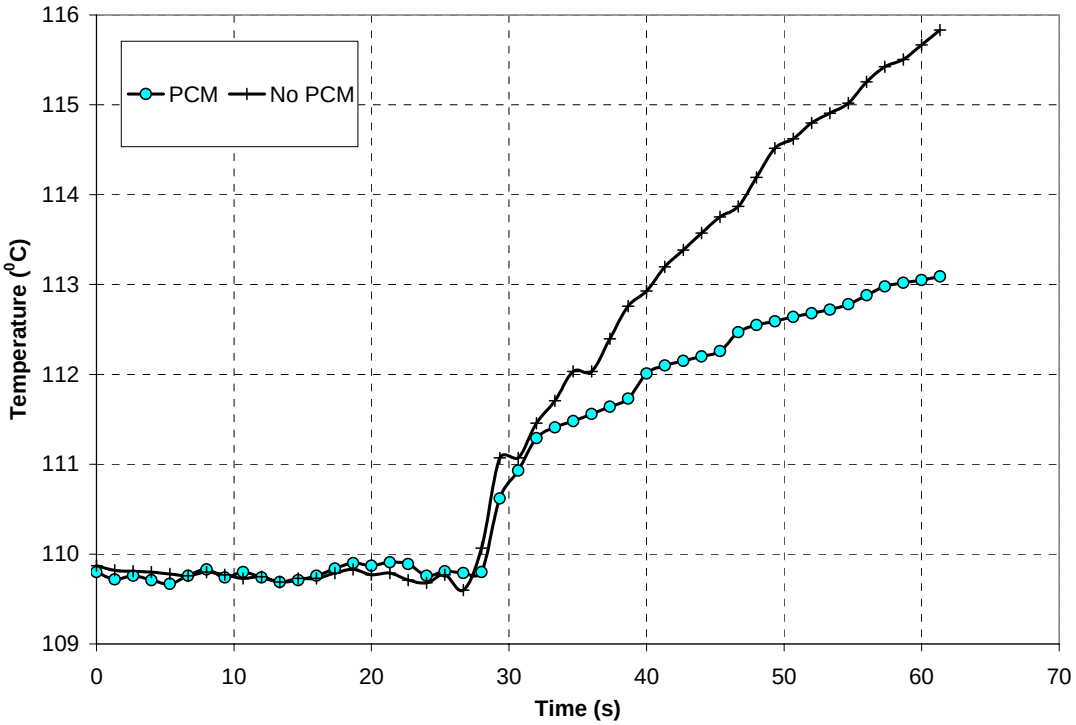

Figure 60: Comparison of vapor temperature rise for case 2 with and without PCM – steady state of 109.76 ^{0}C

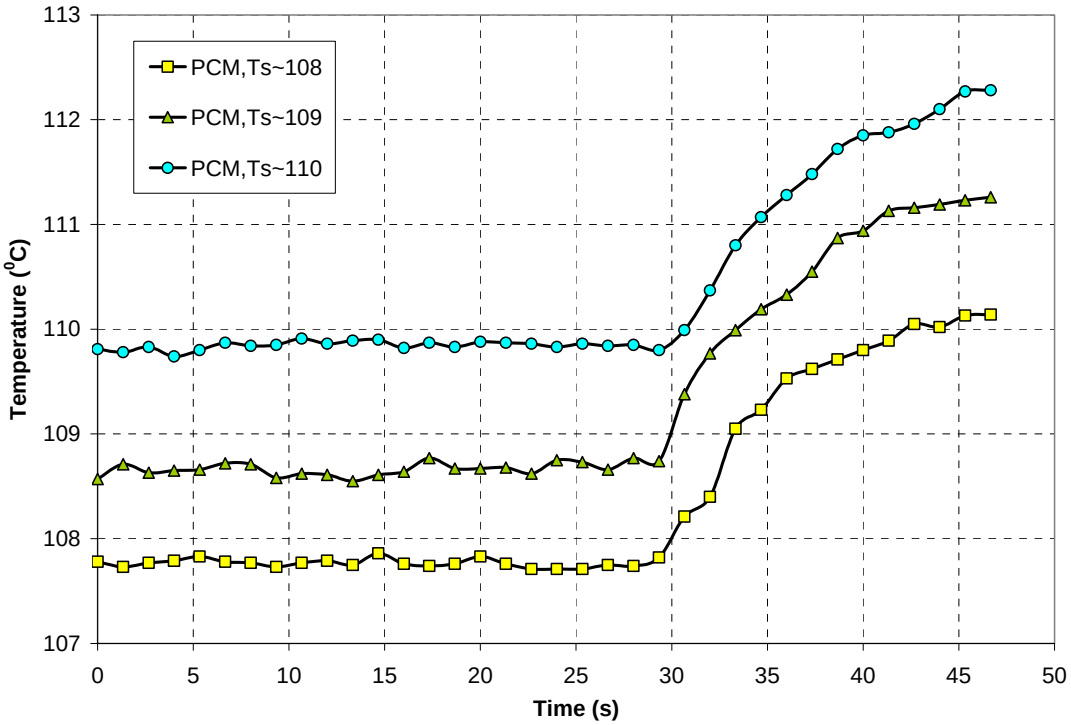

Figure 61: Case 1 experiments with PCM for different steady state temperatures ($T_s = T_0$)

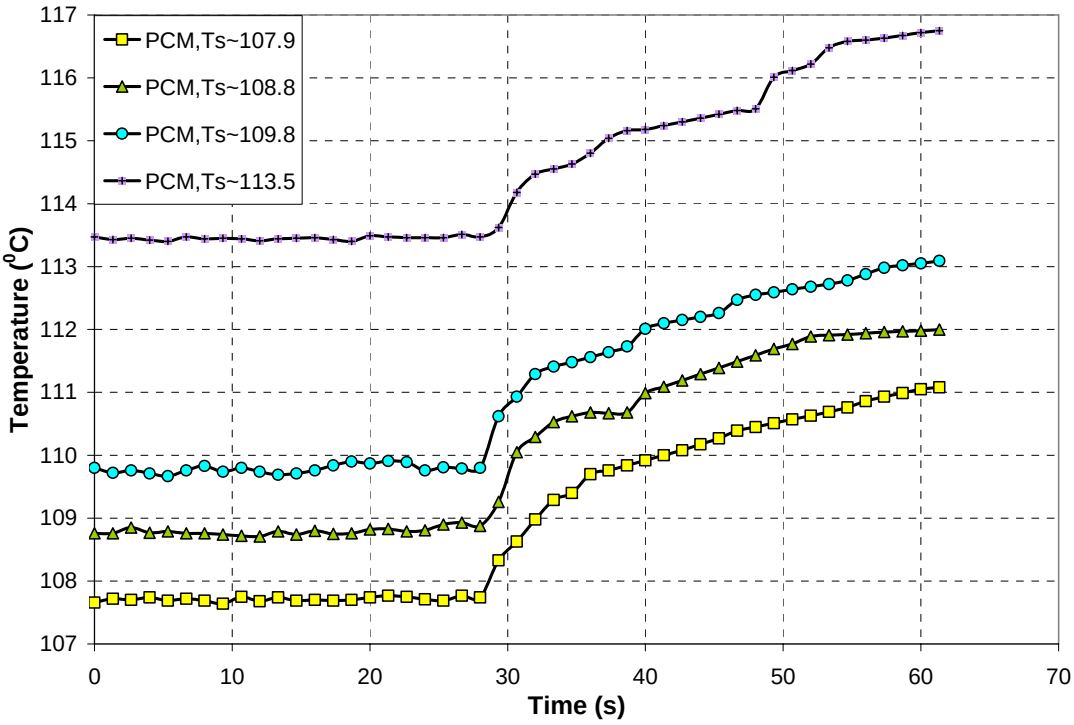

Figure 62: Case 2 experiments with PCM for different steady state temperatures ($T_s = T_0$)

All the experiments were found to be reasonably repeatable. Figure 63 shows the charging curves for two different case 2 experiments starting from same steady state temperatures. Similarly, repeatability was checked by comparing charging curves of case 1 experiments and the first half portion of the charging curves of case 2 experiments that were started from a same steady state temperature (for example, by comparing appropriate portion of curves in Figures 55 and 56). They were found to reasonably overlap confirming the repeatability of the experiments. Repeatability for a single experiment over two charging periods was also observed (Figure 55).

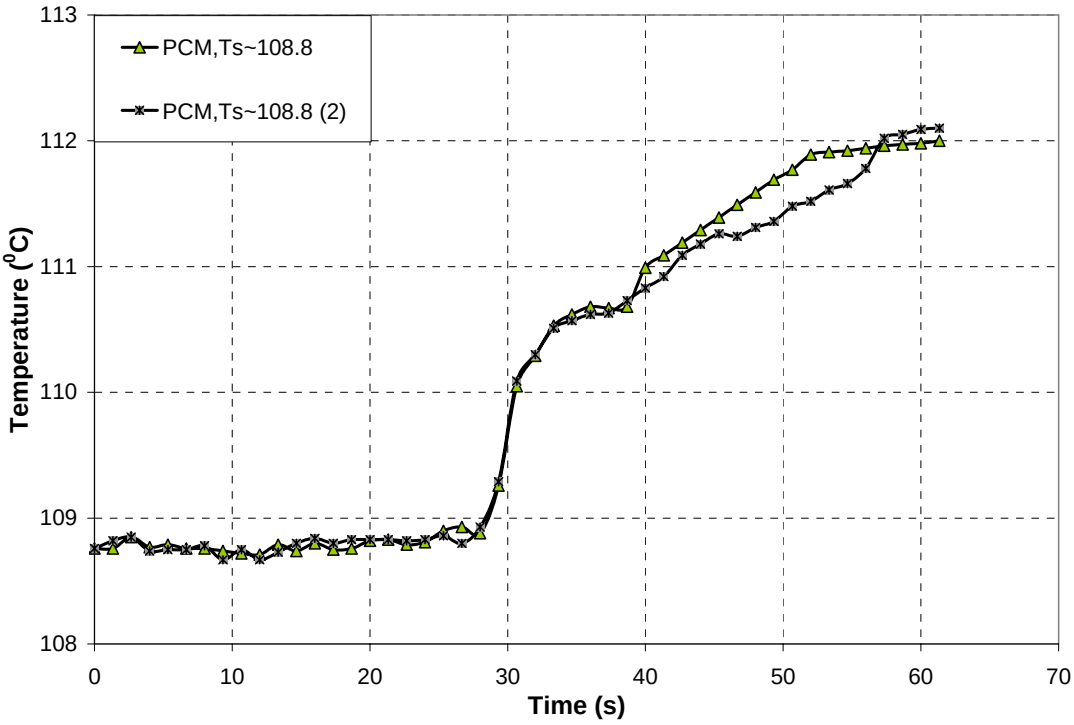

Figure 63: Repeatability of charging experiments

The following important conclusions can be drawn from the above experiments:

- The vapor temperature always exists above all other thermocouple readings as expected. All the temperatures in any single column are almost the same as observed in the single column experiments (within thermocouple measurement errors). This shows that there will be a very low resistance in the foam and PCM composite in any direction if the temperature on the encapsulating boundary is transient and depends on the PCM temperature.
- The temperature of columns lying directly above the heater surface (columns 2 and 3) is always slightly more than the other two columns (columns 1 and 4). This is because of splashing of water and the gushing stream of vapor generated during boiling hitting the

columns directly above providing some heat from their bottom surfaces. Columns 1 and 4 receive a slightly low amount of heat compared to columns 2 and 3 because of their off-location from the heater. This would not have happened in a bigger chamber where if all the columns can be placed at an offset from the heater surface or at a height sufficiently distant from the heater surface.

- It can be seen that the system temperature rises rapidly as soon as the pulse heat flux is provided and reaches a maximum value at the end of the charging period and then begins to drop down as expected.
- All the experiments were found to be reasonably repeatable.
- The slope of the charging curves without PCM is reminiscent of typical transient heat conduction process for heating. The temperature during the pulse is found to rise very rapidly, resulting in a more non-isothermal operation. With PCM, on providing the pulse heat, the vapor temperature initially begins to rise but PCM immediately starts arresting the rise and the slope of the charging curve changes to a more linear fashion symbolizing PCM phase change. This shows that using PCM helps in preventing undue temperature rise of the heat sink. It must be noted that in all the experiments with PCM, there is a delay time before the effect of PCM on the vapor temperature rise could be felt. The vapor temperature rose quickly during the delay times in all the experiments. This might be because of the high thermal inertia of the TES column plates (encapsulation copper plates) coupled with simultaneous discharging through TES column extensions/fins causing a time delay effect to heat transfer to PCM. Time delay might also be occurring because of thermal resistance between the TES units and vapor. The key factors responsible for this resistance are the condensate and the interface contact between PCM and foam composite and the copper walls of the TES units. This resistance can

be reduced by providing efficient means of condensate disposal from the TES units' outside walls (like providing tiny vertical grooves along the height) and by employing a high thermal conductivity bond (for example, like S-bond® [36]) with better bonding properties to join foam and copper plates when making a TES column.

Uncertainty analysis of the experiment results

Uncertainty analysis was performed to know the accuracy of test measurements and to confirm that the measurement uncertainty does not affect the key conclusions. A maximum sample size of three was available for any of the considered parameters. A 95% confidence level was used to specify the uncertainty. Appropriate quotient, difference and power formulae were used to estimate uncertainties wherever applicable, for example, in evaluating the error in heat flux estimation. In-depth details of the uncertainty analysis can be found in Reference [67]. The following are the uncertainties in the key parameters measured in the experiments.

Amount of water sent in: 35 (+ 2) mL

Pulse heat flux: 40 (± 0.03) W/cm^2

Low-end heat flux: 11 (± 0.01) W/cm^2 for a steady-state of 107 ^{0}C

Thermocouple uncertainty: ± 0.5 ^{0}C

Total amount of PCM in all TES units combined: 35 (± 0.025) gm

Pulse heat time: 32 (± 0.14) s

It must be noted, especially in the case of temperature measurements, that the uncertainty is large because of the very small sample size. This is because of the fact that only a maximum number of three different experiments could be repeated with the setup under the available constraints. For large sample sizes, the uncertainties would be small. The current errors in measurements are within acceptable limits in the sense they do not change the key conclusion of the experiments that using PCM helps in a narrow temperature operation of the heat sink.

CHAPTER SIX: CONCLUSION

A novel concept for a heat sink is proposed. Key design considerations for selecting the best features for the concept are mentioned. A design tool based on thermal resistance concept is developed and is useful in isolating the important processes that need detailed numerical attention. The model also helps in arriving at a quick design for prototype development and experimentation.

It is shown that it is possible to have a TES heat sink with attractive features like high heat storage ability (7 MJ), compactness (0.072 m^3, 57.5 kg), low vapor-to-condenser temperature difference (7 ^{0}C), and fast charging ability, environment safe operation, high heat flux capability (500 W/cm^2 over an area of 100 cm^2) and high energy storage density (97 MJ/m^3, 0.122 MJ/kg) including added features of a vapor chamber like self-acting and quiet operation.

The promising aspects that make this concept feasible include using carbon foam in the TES columns (which help the thermal conductivity of TES to increase from ~0.2 W/(m.K) to 135 W/(m.K) for Pocofoam® and 245 W/(m.K) for PocoHTC®); a large surface area for TES (which helps in fast charging/heat absorption and a low heat flux at each column thus reducing the temperature gradients); and placing of PCM containers inside the vapor space of the chamber to ensure rapid transport of pulse heat loads to the PCM containers. The design tool described is an approximate theoretical model and is only a guideline to estimate the thermal performance and feasibility of the concept but is not a thorough final design criterion. Complicated in-depth numerical analyses and experiments are to be performed to understand and very accurately quantify the key processes that govern the VCTES heat sink performance during transient operation.

By integrating the DSC curve of the PCM in the temperature ranges of most of the experiments performed (107-110 ^{0}C, 108-111 ^{0}C etc.), it was found that the PCM has a latent heat of approximately 30 kJ/kg. A total of 35 gm of PCM was present in the four TES units. This implies that, out of about 4500 J of heat supplied during charging, for example, for case 2 experiments, PCM was able to absorb only 1050 J (35 gm X 30 J/gm). If we consider using one of the highly pure grades of the same PCM and assume that its entire latent heat of 266 kJ/kg is distributed within the same operating range as the current experiments, then the PCM would be capable to absorb 9310 J (35 gm X 266 J/gm) of heat during pulse. This facilitates for providing the pulse flux for a much longer time, still having the same temperature rise as the current experiments. However, for experiments without PCM, longer pulse times could increase the system temperature by a much larger value compared to the current experiments without PCM, which is close to 6 ^{0}C for case 2 runs. Therefore, the effect of PCM will be more evident if a pure PCM is used.

In addition, by comparing the value of p in Table 5, which is 47%, with p for the prototype version tested, which is 2.2% (Table 6), it is very clear that the performance of the VCTES heat sink would be best if the system is large (since the parasitic mass effect would go down and the latent advantage R increases as the system becomes large). This can also be illustrated by comparing the latent storage density of the heat sink in Table 6, which is 2.9 kJ/kg, with the latent heat of PCM itself, which is 266 kJ/kg (Figure 11).

Therefore, the effect of PCM will be more evident if a pure PCM is used, if the system is large (like the original optimized design of Chapter Three, which is capable of absorbing 500 W/cm^2 heat flux and 7 MJ of total pulse heat, thus facilitating a high R) or if the final application

demands stringent operating temperature limitations. The reduced size experiment version is intended simply to show that PCM can arrest the system temperature rise and it is successfully demonstrated.

In addition to showing the effectiveness of the concept through experimental demonstration, it is qualitatively shown through approximate numerical analysis that using PCM as a second latent sink helps the VCTES system to have a narrow temperature operation. Also, some cases that could not be verified by experiments are analyzed numerically to give an idea of some of the important features of the heat sink like using foam (which are mentioned in Chapter Three), which otherwise consume too much experimental time.

The results of the developed numerical model showed that the concept is effective in preventing undue temperature rise of the heat sink. The advantage of having a second latent phase change phenomenon in the heat sink in the form of PCM phase change is shown by assuming the lack of PCM in the design. It is also numerically shown that pure PCM exhibits a better performance. The significance of having a thermal conductivity enhancing medium for PCM is also shown. As expected, graphite foam plays a very crucial role in transferring heat to the PCM and thus helps in rapid charging.

It is found that for a constant vapor temperature boundary condition during transient melting driven by film condensation, the key impediment to rapid heat absorption comes from the condensate film. Because of the condensate profile, the PCM phase change problem becomes two-dimensional and the temperature gradient in the interfacial solid wall in the height direction is large. It is also observed that for PCMs with a melting range, selection of a right operating range and initial temperature are crucial. The fundamental science of the developed numerical

model is also useful for other applications involving melting driven by film condensation. The thermo-mechanical resistance model is also a useful tool for a quick design of future similar applications, especially for testing purposes.

REFERENCES

1. Chow, L. C., Zhong, J. K., and Beam, J. E., "Thermal Conductivity Enhancement for Phase Change Storage Media," *International Communications in Heat and Mass Transfer*, Vol. 23, No. 1, 1996, pp. 91-100.
2. Gallego, N. C., and Klett, J. W., "Carbon Foams for Thermal Management," *Carbon*, Vol. 41, 2003, pp. 1461-1466.
3. http://www.enertron-inc.com
4. Vafai, K., Wang, W., "Analysis of Flow and Heat Transfer Characteristics of an Asymmetrical Flat Plate Heat Pipe," *International Journal of Heat and Mass Transfer*, Vol. 35, 1992, pp. 2087-2099.
5. Dincer, I., Rosen, M. A., *Thermal Energy Storage – Systems and Applications*, John Wiley & Sons, Ltd., London, 2002.
6. Wirtz, R. A., Peng, S., and Fuchs, A., "A Polymer-Based Thermal Energy Storage Composite for Temperature Control of Sensors and Electronics", The 6th ASME-JSME Thermal Engineering Joint Conference, March 16-20, 2003.
7. Wirtz, R. A., Zheng, N., and Chandra, D., "Thermal Management Using "Dry" Phase Change Materials", Proceedings of the Fifteenth IEEE Semiconductor Thermal Measurement and Management Symposium, San Diego, California, March 9-11, 1999.
8. Chang, M., Chow, L. C., Chang, W. S., and Morgan, M. J., "Transient Behavior of Axially Grooved Heat Pipes with Thermal Energy Storage", *Journal of Thermophysics and Heat Transfer*, Vol. 6, No. 2, pp. 364-370, 1992.
9. http://www.1-act.com/thermstore.html

10. Zuo, J., and Ernst, D. M., "Heat Pipe Having a Wick Structure Containing Phase Change Materials", US Pat # 6,889, 755 B2.

11. Weislogel, M. M., "Heat and Mass Transfer in a Dual-Latent Thermal Energy Storage System," M. S. Thesis, Department of Mechanical and Materials Engineering, Washington State University, 1988.

12. Weislogel, M. M., and Chung, J. N., "Experimental Investigation of Condensation Heat Transfer in Small Arrays of PCM-Filled Spheres," *International Journal of Heat and Mass Transfer*, Vol. 34, No. 1, 1991, pp. 31-45.

13. Horbaniuc, B., Dumitrascu, G., and Popescu, A., "Mathematical Models for the study of Solidification within a Longitudinally Finned Heat Pipe Latent Heat Thermal Storage System," *Energy Conversion and Management*, Vol. 40, 1999, pp. 1765-1774.

14. Liu, Z., Wang, Z., and Ma, C., "An Experimental Study on Heat Transfer Characteristics of Heat Pipe Heat Exchanger with Latent Heat Storage. Part I: Charging Only and Discharging Only Modes," *Energy Conversion and Management*, Vol. 47, 2006, pp. 944-966.

15. Liu, Z., Wang, Z., and Ma, C., "An Experimental Study on Heat Transfer Characteristics of Heat Pipe Heat Exchanger with Latent Heat Storage. Part II: Simultaneous Charging/Discharging Modes," *Energy Conversion and Management*, Vol. 47, 2006, pp. 967-991.

16. Cogliano, J. A., W.R. Grace & Co., New York, NY, U.S. Patent for a "Passive Solar Heating and Cooling Panels," Patent No. 4,273,100, 16 Jun. 1981.

17. Basiulis, A., Hughes Aircraft Company, Los Angeles, CA, U.S. Patent for a "Rechargeable Thermal Control System," Patent No. 4,673,030, 16 Jun. 1987.

18. Cao, Y., Miami, FL, U.S. Patent for a "Human Body Cooling Suit with Heat Pipe Transfer," Patent No. 5,386,701, 7 Feb. 1995.

19. Giammaruti, R. J., Hudson Products Corporation, Houston, TX, U.S. Patent for a "Passive Cooling of Enclosures using Heat Pipes," Patent No. 5,579,830, 3 Dec. 1996.

20. Glover, R. J., Bishop, M. R., and Tenser, M. S., Nortel Networks Corporation, Montreal, Canada, U.S. Patent for a "Packaging System for Thermally Controlling the Temperature of Electronic Equipment," Patent No. 6,104,611, 15 Aug. 2000.

21. Lin, L., Leland, J. E., and Ponnappan, R., The United States of America as represented by the Secretary of the Air Force, Washington, DC, U.S. Patent for a "Cooling of Electro Mechanical Actuator with Phase Change Material and Thermosyphons Containing Working Fluid," Patent No. 6,294,853 B1, 25 Sep. 2001.

22. Kung, S., and Liu, C., Compal Electronics, Inc., Taipei, Taiwan, U.S. Patent for a "Thermal Module with Temporary Heat Storage," Patent No. 6,971,443 B2, 6 Dec. 2005.

23. Zuo, J., and Ernst, D. M., Duane Morris LLP, Philadelphia, PA, U.S. Patent for a "Heat Pipe having a Wick Structure containing Phase Change Materials," Patent No. US2005/0269063 A1, 8 Dec. 2005.

24. Liu, Z., Wang, Z., Sun, X., Li, J., and Ma, C., Chinese Patent for "A Multi-functional Heat Pipe Exchanger with Latent Heat Storage," Patent No. 03242284.9, 2006.

25. Colvin, D. P., Bryant, Y. G., and Mulligan, J. C., "Twenty Years of Encapsulated PCM Development in the United States: Coolants, Composites, Powders, Coatings, Foams, Fibers and Apparel", Presented at the First World Congress on Phase Change Materials, Yverdon, Switzerland, 2003.

26. Colvin, D. P., Bryant, Y. G., Duncan, J. D., and Gravely, B. G., "Microencapsulated PCM Slurries for Heat Transfer and Energy Storage Systems", Transactions of The Sixth Symposium on Space Nuclear Power Systems, Albuquerque, New Mexico, January, 1989.

27. Colvin, D. P., Bryant, Y. G., "Microencapsulated Phase-Change Material Suspensions for Heat Transfer in Spacecraft Thermal Systems", *Spacecraft and Rockets*, Vol. 83, No. 3, 1996.

28. Colvin, D. P., "Protective Clothing Containing Encapsulated Phase Change Materials", *Advances in Heat and Mass Transfer in Biotechnology,* ASME HTD Vol. 362/BED Vol. 40, November, 1998.

29. Colvin, D. P., Colvin, V. S., Bryant, Y. G., Hayes L. G., and Spieker, M. A., "Development of a Cooling Garment with Encapsulated PCM." *Advances in Heat and Mass Transfer in Biotechnology*, ICEME Proceedings, ASME HTD Vol. 368/BED Vol. 47, November, 2000.

30. http://www.deltathermal.com/technology.htm

31. http://www.pocographiteonline.com/servlet/Categories?category=Thermal+Materials

32. Zivkovic, B., Fujii, I., "An Analysis of Isothermal Phase Change of Phase Change Material within Rectangular and Cylindrical Containers," *Solar Energy*, Vol. 70, No. 1, 2001, pp. 51-61.

33. Carey, V. P., *Liquid-Vapor Phase-Change Phenomena*, 1st ed., Taylor & Francis, Oxford, UK, 1992.

34. Du, J., Chow, L., and Leland, Q., "Optimization of High Heat Flux Thermal Energy Storage with Phase Change Materials", Proceedings of 2005 ASME International Mechanical Engineering Congress and Exposition, Orlando, FL, 5-11 November 2005.
35. Klett, J., "High Thermal Conductivity Graphite Foam", URL: www.ms.ornl.gov/researchgroups/cmt/foam/foams.htm.
36. http://www.s-bond.com
37. http://www.bakerpetrolite.com
38. COMSOL Multiphysics, Modeling Package, Ver. 3.3, COMSOL, Inc., Burlington, MA, 1997–2007.
39. http://www.poco.com
40. Contreras, W., and Thorsen, R. S., "Transient Melting of a Solid Heated by a Condensing Saturated Vapor – Case 1: Negligible Interface Curvature," *Journal of Heat Transfer*, Vol. 97, 1975, pp. 570-575.
41. Galamba, D., "Some Aspects of Simultaneous Melting-Condensation on Vertical Surfaces," Ph. D. Dissertation, Department of Mechanical and Aerospace Engineering, University of California, Los Angeles, CA, 1985.
42. Galamba, D. and Dhir, V. K., "Transient Simultaneous Condensation and Melting of a Vertical Surface," *ASME Journal of Heat Transfer*, Vol. 107, No. 4, 1985, pp. 812-818.
43. Galamba, D. and Dhir, V. K., "Transient Condensation - Melting of a Subcooled Vertical Surface," *Numerical Heat Transfer*, Vol. 15, 1988, pp. 33-65.
44. Chen, H., and Chang, S., "Coupling Between Laminar Film Condensation and Natural Convection on Opposite Sides of a Vertical Plate," *International Journal for Numerical Methods in Fluids*, Vol. 24, 1997, pp. 319-336.

45. Char, M., and Lin, J., "Conjugate Film Condensation and Natural Convection Between Two Porous Media Separated by a Vertical Plate," *Acta Mechanica*, Vol. 148, 2001, pp. 1-15.

46. Krishnan, S., Murthy, J., Garimella, S., "A Two-Temperature Model for the Analysis of Passive Thermal Control Systems," *Journal of Heat Transfer*, Vol. 126, 2004, pp. 628-637.

47. Lee, D., and Vafai, K., "Analytical Characterization and Conceptual Assessment of Solid and Fluid Temperature Differentials in Porous Media," *International Journal of Heat and Mass Transfer*, Vol. 42, 1999, pp. 423-435.

48. Incropera, F. P., DeWitt, D. P., Bergman, T. L., Lavine, A. S., *Fundamentals of Heat and Mass Transfer*, 6th ed., John Wiley & Sons, Inc., NJ, 2007.

49. Morgan, K., "A Numerical Analysis of Freezing and Melting With Convection," *Computer Methods in Applied Mechanics and Engineering*, Vol. 28, No. 3, 1981, pp. 275-284.

50. Hsiao, J. S. and Chung, B. T. F., "An Efficient Algorithm for Finite Element Solution to Two-Dimensional Heat Transfer With Melting and Freezing," *Proceedings of 22nd ASME National Heat Transfer Conference*, ASME, New York, NY, 1984.

51. Cao, Y. and Faghri, A., "A Numerical Analysis of Phase-Change Problems Including Natural Convection," *ASME Journal of Heat Transfer*, Vol. 112, No. 3, 1990, pp. 812-816.

52. Voller, V. R. and Cross, M., "Accurate Solutions of Moving Boundary Problems Using the Enthalpy Method," *International Journal of Heat and Mass Transfer*, Vol. 24, 1981, pp. 545-556.

53. Voller, V. R., "Implicit Finite Difference Solutions of the Enthalpy Formulation of Stefan Problems," *IMA Journal of Numerical Analysis*, Vol. 5, 1985, pp. 201-214.

54. Voller, V. R., Cross, M. and Markatos, N. C., “An Enthalpy Method for Convection/Diffusion Phase Change,” *International Journal for Numerical Methods in Engineering*, Vol. 24, 1987, pp. 271-284.

55. Voller, V. R., “Fast Implicit Finite Difference Method for the Analysis of Phase Change Problems,” *Numerical Heat Transfer B*, Vol. 17, 1990, pp. 155-169.

56. Paradela, F., Queimada, A., Marrucho, I., Neto, C., and Coutinho, J., “Modeling the Thermal Conductivity of Pure and Mixed Heavy n-Alkanes Suitable for the Design of Phase Change Materials,” *International Journal of Thermophysics*, Vol. 26, No. 5, 2005, pp. 1461-1475.

57. Sulfredge, D. C., Chow, L. C., Tagavi, K. A., "Initiation and Growth of Solidification Shrinkage Voids", Annual Review of Heat Transfer, Vol. 10, Ed. Chang-Lin Tien, Begell House, Inc., 1999.

58. Bart, G. C. J. and van der Laag, P. C., “Modeling of Arbitrary-shaped Specific and Latent Heat Curves in Phase Change Storage Simulation Routines,” *ASME Journal of Solar Energy Engineering,* Vol. 112, 1990, pp. 29–33.

59. Sparrow, E. M. and Siegel, R., “Transient Film Condensation”, *Journal of Applied Mechanics*, Vol. 26, 1959, pp. 120-121.

60. Reed, J. G., Gerner, F. M., Tien, C. L., “Transient Laminar-Film Condensation on a Vertical Plate”, *Journal of Thermophysics and Heat Transfer*, Vol. 2, No. 3, 1988, pp. 257-263.

61. Chung, P. M., “Unsteady Laminar Film Condensation on Vertical Plate”, ASME Journal of Heat Transfer, 1963, pp. 63-70.

62. http://www.matlab.com

63. Mesalhy, O., Lafdi, K., Elgafy, A., "Carbon Foam Matrices Saturated with PCM for Thermal Protection Purposes," *Carbon*, Vol. 44, 2006, pp. 2080-2088.

64. http://www.aremco.com

65. http://www.epotek.com

66. http://www.barryind.com

67. Coleman, H. W., Steele Jr., W. G., *Experimentation and Uncertainty Analysis for Engineers*, John Wiley & Sons, Inc., NJ, 1989.